The Dissertation Committee for Wen-Yueh Yu certifies that this is the approved version of the following dissertation:

Catalytic Chemistry of Pd−Au Bimetallic Surfaces

Committee:

C. Buddie Mullins, Supervisor

Graeme Henkelman

Gyeong S. Hwang

Brian A. Korgel

Greg O. Sitz

Catalytic Chemistry of Pd−Au Bimetallic Surfaces

by

Wen-Yueh Yu, B.S.; M.S.

Dissertation

Presented to the Faculty of the Graduate School of

The University of Texas at Austin

in Partial Fulfillment

of the Requirements

for the Degree of

Doctor of Philosophy

The University of Texas at Austin

August 2015

Dedication

To my family, Yu-Tang, and our baby Austin

Acknowledgements

I would like to express my sincere gratitude to my supervisor, Prof. C. Buddie Mullins, for his guidance and support over the past six years. Buddie's expertise and humor always make me really enjoy the time discussing with him about the research in his office. I am so grateful that Buddie gave me the chance to join this group six years ago so I can explore the world of model catalyst studies.

I would like to acknowledge Prof. Graeme Henkelman, Prof. Gyeong S. Hwang, Prof. Brian A. Korgel and Prof. Greg O. Sitz for their valuable time serving on my committee. I also appreciate the insightful suggestions and ideas from Prof. Henkelman, Prof. Hwang and Dr. Liang Zhang on our collaboration projects.

I am so pleased to work with many talented students in Buddie's group. Dr. Dave Flaherty is the first one teaching me how to conduct model catalyst experiments and I really appreciate this opportunity to work with him in his last year in UT. I also thank Dr. Ming Pan and Dr. Ting Yan for their teaching and help so I can have more confidence on using/maintaining UHV chambers. I would like to thank Greg Mullen for helping me start Pd−Au catalyst studies and providing many useful suggestions for paper writing. I would like to thank Adrian Brush and Edward Evans for their help and bringing lots of joy to our subgroup. I am grateful to Dr. Nathan Hahn, Dr. Son Hoang,

Dr. Paul Abel, Dr. Sean Berglund, Will Chemelewski, Alex Rettie, Kyle Klavetter and Sean Wood for letting me "borrow" much useful lab stuff. I appreciate the friendship with Dr. Yong-Mao Lin and Hoang Dang. I also enjoy working with all of the other members in Buddie's group. I would like to acknowledge all of our department staff, particularly Kate Baird, Jason Barborka, Randy Rife, Eddie Ibarra, Kevin Haynes, Shallaco "Shak" McDonald, Butch Cunningham and Jim Smitherman.

Being a TA has been an important part in my PhD life. I would like to thank Dr. Donna Lyon, Eric Wigdahl and Chris Johnson in general chemistry lab, Dr. Conrad Fjetland, Adriel Salazar, Zachary McCarty and Shao-An Wang in organic chemistry lab, as well as Dr. Keith Friedman and Dr. Tuo Wang in senior lab for their kindly help.

I am fortunate to have many great friends in Austin. I would like to thank Dr. Yu-Sheng Su, Dr. Chih-Liang Wang, Dr. Yi-Der Lin, Dr. Chun-Hsien Wu, Dr. Kevin Tung, Chen-Hsun Tsai, Chun-Cheng Chou, Yu-Hao Tsai, Ying-Chieh Weng, Rena Huang, and Jessie Chen. I also thank all of my friends in Taiwanese Student Association at UT Austin.

Finally, I would like to express my deepest appreciation to my family. I would like to thank my mom for her love and support from Taiwan. To my beloved wife, Yu-Tang, thank you so much for completing me. To our baby, Austin, we are looking forward to seeing you.

Catalytic Chemistry of Pd−Au Bimetallic Surfaces

Wen-Yueh Yu, Ph.D.

The University of Texas at Austin, 2015

Supervisor: Charles Buddie Mullins

Catalyst development is important to the contemporary world as suitable catalysts can allow chemical processes to proceed with reduced energy consumption and waste production. In order to design catalysts with improved performance, the fundamental studies that correlate catalytic properties with surface structures are essential as they can provide mechanistic insights into the reaction mechanism. Pd−Au bimetallic catalysts have shown exceptional performance for a number of chemical reactions, however, the interplay between the reactive species and surface properties are still unclear at the molecular level. In this dissertation, the catalytic chemistry of Pd−Au surfaces was investigated via model catalyst studies under ultrahigh vacuum conditions. A range of Pd−Au model surfaces were generated by annealing Pd/Au(111) surfaces and characterized/tested by surface science techniques. The findings in this dissertation may prove useful to enhance the fundamental understanding of structure-reactivity relation of Pd−Au catalysts in associated reactions.

Table of Contents

List of Tables

List of Figures

List of Schemes

Chapter 1: Introduction

1.1 Model Catalyst Studies

Heterogeneous catalysts have been widely used in chemical processes including hydrocarbon refining, production of bulk chemicals, automobile pollution control, and fuel cell technologies.[1-2] Around 85−90% of industrial products are made in catalytic processes, and the sales of process catalysts is around $13 billion/year worldwide, which contributes to products with a value of around $500−600 billion/year.[1]

Although the use of heterogeneous catalysts increased rapidly since the early 20th century, fundamental knowledge for associated reaction mechanisms was accumulated much more slowly at the same period until the advent of spectroscopy and other catalyst characterization techniques in the late 1950s (Figure 1.1).[3]

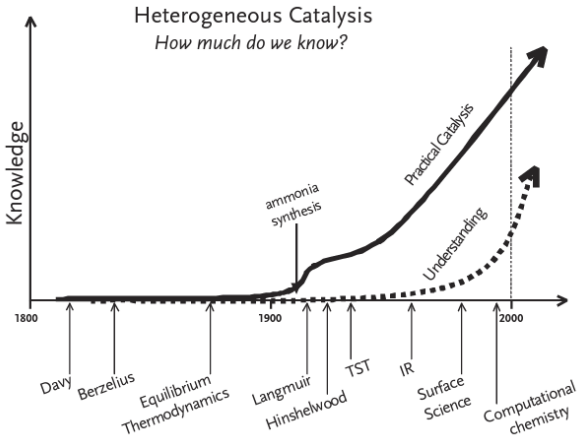

Figure 1.1. The development history of heterogeneous catalysts.[3]

A molecular-level understanding of catalytic mechanisms was significantly advanced by the development of surface science combined with model catalyst studies. The comparison between classic catalyst and model catalyst systems is shown in Figure 1.2. Classical catalysts are typically constructed of active metal nanoparticles uniformly dispersed on a high-surface-area oxide support and operated at high pressures and temperatures. Such material complexity and harsh environments increase the level of difficulty to investigate the reaction on the catalyst surface microscopically. On the other hand, in model catalyst studies, reactions are normally investigated on well-defined single-crystal surfaces under ultrahigh vacuum (UHV) conditions, which enable the correlation of catalytic properties to surface structures at the molecular level.[4-11]

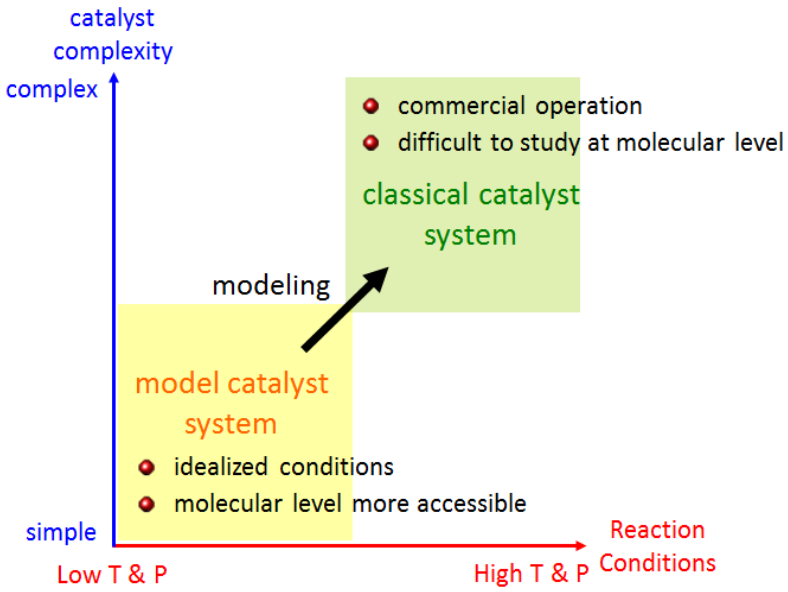

Figure 1.2. The comparison between classical catalyst and model catalyst systems.

Although model catalyst studies are performed under idealized conditions, many researchers have demonstrated that model catalyst studies can be useful for improving the understanding of chemical processes catalyzed by real catalysts. One of the well-known examples is the pioneering work of Professor Gerhard Ertl, whose team clarified the molecular events of the Haber-Bosch process via model catalyst studies using a host of surface science methodologies.[12]

1.2 Palladium-Gold Bimetallic Catalysts

1.2.1 Classical Pd−Au Catalysts

Bimetallic catalysts are a class of important heterogeneous catalysts as they often exhibit physicochemical properties that are distinctly different from those of their parent metals. These unique properties offer the opportunity to design catalysts that possess better catalytic properties, e.g., enhanced activity, selectivity and stability.[4-5]

As one of the most studied bimetallic systems, Pd−Au catalysts have displayed promising performance for a broad range of catalytic reactions such as CO oxidation,[13-15] acetoxylation of ethylene to vinyl acetate,[16-17] selective oxidation of alcohols,[18-21] selective hydrogenation of unsaturated hydrocarbons,[22-25] hydrodechlorination of chlorinated compounds,[26-28] hydrodesulfurization of sulfur-containing molecules,[29-30] decomposition of liquid hydrocarbons for H_2 production,[31-32] and the direct synthesis of H_2O_2 from H_2 and O_2.[33-38]

Although it has been demonstrated that Pd−Au catalysts exhibit enhanced activity, selectivity, and stability in these reactions, the key factors governing the catalytic properties of Pd−Au catalysts remain topics of debate. The vast diversity of preparation methods, catalyst supports, and reaction conditions employed could make the comparison between different classical catalysts more difficult.

1.2.2 Model Pd−Au Catalysts

The promising performance of Pd−Au catalysts has motivated many researchers to conduct model catalyst studies to examine these chemical processes. Table 1.2 lists the Pd−Au model catalyst surface and catalytic reaction investigated in a number of selected Pd−Au model catalyst studies.

Table 1.1. Selective Pd−Au model catalyst studies in the literature.

Model surfaces	Reactions
Type I	
AuPd(100)	CO oxidation[39-40]
	CO/NO and CO/NO/O_2[41]
PdAu(111)	CO oxidation[42]
Type II	
Pd/Au(111)	Coupling of acetylene to benzene[43-44]
	Acetoxylation of ethylene to vinyl acetate[17]
Pd/Au(100)	Acetoxylation of ethylene to vinyl acetate[17]
Au/Pd(111)	Coupling of acetylene to benzene[45]
	Selective oxidation of alcohol[46]
Au/Pd(100)	CO oxidation[47]
Type III	
Au-Pd/Mo(110)	CO oxidation[13]
Au-Pd/TiO_2/Mo(110)	CO oxidation[13]

To date three types of Pd−Au bimetallic model surface have been developed: (I) Pd−Au single crystals, e.g., AuPd(100) alloys[39-41] and PdAu(111);[42] (II) Pd–Au thin films generated by depositing one metal onto another metal single crystal surface, e.g., depositing Pd on Au single crystals, e.g., Pd/Au(111),[17, 43-44] or depositing Au on Pd single crystals, e.g., Au/Pd(111)[45-46]; (III) Pd–Au thin films generated by depositing Au and Pd onto refractory or other surfaces, e.g., Au-Pd/Mo(110).[13]

In this dissertation, Pd−Au bimetallic surfaces were prepared by depositing Pd atoms from a homemade thermal evaporator onto a single crystal surface of Au(111) at 77 K. A variety of Pd−Au surfaces were generated by controlling the amount of Pd deposited onto the surface and the annealing temperature with which the surface was prepared. The physicochemical properties of these Pd−Au surfaces such as composition and site structures were characterized and correlated with their interactions with small molecules such as H_2, CO, O_2 and HCOOH. The goals of our studies include advancing the fundamental understanding of interactions of these molecules with Pd−Au surfaces and providing mechanistic insights into the associated catalytic reactions.

1.3 DISSERTATION OVERVIEW

This dissertation consists of seven chapters. Chapter 1 provides general background information for the research conducted in this dissertation. In the following five chapters, each chapter represents an independent study which has been published

(Chapters 2−5) or to be submitted (Chapter 6) in peer-reviewed journals. Finally, Chapter 7 covers some concluding remarks and recommendations for future studies.

Chapter 2 describes our work of hydrogen interaction with Pd−Au model catalyst surfaces, which has been published in *Journal of Physical Chemistry C* authored by Yu, W.-Y.; Mullen, G. M.; Mullins, C. B.[48] In this study, various Pd−Au surfaces were generated by annealing Pd/Au(111) surfaces to various temperatures in UHV. These annealed Pd/Au(111) surfaces were characterized by Auger electron spectroscopy (AES) and reflection-absorption infrared spectroscopy using CO as a probe molecule (CO-RAIRS). The interaction (i.e., adsorption, absorption, diffusion and desorption) of hydrogen with these characterized surfaces was studied by temperature-programmed desorption (TPD).

Chapter 3 depicts our study of interactions of hydrogen and carbon monoxide on Pd−Au model catalyst surfaces, which has been published in *Journal of Physical Chemistry C* authored by Yu, W.-Y.; Mullen, G. M.; Mullins, C. B.[49] The coadsorption of hydrogen and carbon monoxide was achieved by exposing CO to the hydrogen-precovered Pd/Au(111) surfaces that was previously annealed in UHV. TPD was conducted to study the interactions of hydrogen and carbon monoxide coadsorbed on the annealed Pd/Au(111) surface. The processes for adsorption and desorption of hydrogen and CO were explored by molecular beam scattering (MBS) experiments.

In Chapter 4, we investigated the surface chemistry of formic acid (HCOOH) on Pd−Au bimetallic model surfaces. In this research, various Pd−Au surfaces were generated by depositing various coverages of Pd atoms on the Au(111) surface followed by annealing in UHV. The annealed Pd/Au(111) surfaces were characterized by H_2-TPD. The decomposition of HCOOH into H_2 (dehydrogenation) and H_2O (dehydration) on Pd−Au surfaces was assessed by reactive molecular beam scattering (RMBS) and HCOOH-TPD experiments. The results in this work has been published in *Journal of the American Chemical Society* authored by Yu, W.-Y.; Mullen, G. M.; Flaherty, D. W.; Mullins, C. B.[50]

Chapter 5 presents our investigation for oxygen activation and reaction with CO on Pd−Au bimetallic model surfaces. Similar to the approaches in Chapter 2, a series of Pd−Au surfaces were prepared by annealing the as-deposited Pd/Au(111) surface to various temperatures in UHV and characterized by AES and CO-RAIRS. King-Wells measurements and TPD were conducted to study the interaction of oxygen with these surfaces and the obtained results were correlated to their surface properties. The reactivity of oxygen on the surface at various temperatures was assessed by CO-RMBS by monitoring CO_2 production. This study was recently published by *Journal of Physical Chemistry C* authored by Yu, W.-Y.; Zhang, L.; Mullen, G. M.; Henkelman, G.; Mullins, C. B.[51]

In Chapter 6, we studied the effect of annealing in oxygen on the surface structure of Pd−Au model catalysts. We compared the physicochemical properties of Pd/Au(111) annealed under UHV conditions versus in oxygen ambient. The composition of the near-surface region of UHV-annealed and oxygen-annealed surfaces were characterized by AES. The surface sites were probed by CO and O_2 using CO-RAIRS, O_2 King-Wells measurements, and O_2-TPD. Finally the catalytic activity of UHV-annealed and oxygen-annealed surfaces was compared by CO oxidation via CO-RMBS.

Chapter 7 summarizes the findings in each work mentioned above and includes the recommendations for future work.

Chapter 2: Hydrogen Adsorption and Absorption with Pd−Au Bimetallic Surfaces*

2.1 INTRODUCTION

The interaction of hydrogen with metal surfaces has been an important phenomenon in the field of heterogeneous catalysis, as a great number of metal-catalyzed reactions involve hydrogen as a reactant, intermediate, or product.[52] Recent research on hydrogen-metal surface interactions has been further motivated by the development of renewable energy technologies such as hydrogen storage, electrocatalytic oxidation of H_2, and water splitting for H_2 evolution.[53]

On the close-packed single crystal surfaces of most transition metals H_2 molecules readily dissociate to generate H atoms that bind strongly to the surface, whereas on coinage metals (Cu, Ag, and Au), the barrier for H_2 dissociation is relatively high and the binding of atomic H is much weaker.[54] Some bimetallic surfaces have demonstrated the ability to dissociate H_2 and yet also weakly bind H adatoms, properties that could be beneficial for several catalytic reactions involving hydrogen.[4, 55]

* Yu, W.-Y.; Mullen, G. M.; Mullins, C. B., Hydrogen Adsorption and Absorption with Pd−Au Bimetallic Surfaces. *J. Phys. Chem. C* **2013**, 117, 19535–19543.
W.-Y. Yu, G. M. Mullen and C. B. Mullins conceived and designed experiments, analyzed and discussed results, and commented on the manuscript. W.-Y. Yu performed experiments, analyzed data and wrote the paper.

Among the most extensively studied bimetallic systems, Pd−Au alloys have displayed promising catalytic performance in various chemical processes[5, 10] including low-temperature CO oxidation,[13-14, 39-40] cyclization of acetylene to benzene,[43-45, 56] acetoxylation of ethylene to vinyl acetate[16-17] and selective oxidation of alcohols.[18, 57-58] Recently, Pd−Au bimetallic catalysts have also been reported to be effective for the synthesis of hydrogen peroxide,[34, 59] selective hydrogenation of unsaturated hydrocarbons,[22-24] hydrodechlorination (HDC) of chlorinated compounds,[26-27] hydrodesulfurization (HDS) of sulfur-containing molecules,[29-30] and decomposition of liquid hydrocarbons for H_2 production.[31, 60-61] Hydrogen is involved in all of these reactions as either reactant or product. The number of potential applications of Pd−Au alloys in catalytic reactions involving hydrogen merits the fundamental study of the interactions of hydrogen with Pd−Au bimetallic surfaces. A thorough understanding of these interactions will help guide future developments in the design of Pd−Au catalysts.

The interaction of hydrogen with low-index single-crystal surfaces of Pd has been extensively investigated.[62-67] It is well-known that hydrogen not only adsorbs on the surface but also absorbs into the subsurface of Pd. Formation of both surface and subsurface H on Pd is exothermic with respect to gaseous H_2, which is unusual since the formation of subsurface H on most transition metals is endothermic.[54] In a previous study[66] regarding temperature-programmed desorption (TPD) of hydrogen, it was shown that the surface temperature during hydrogen exposure has a great impact on the sorption behavior of hydrogen on the Pd(111) surface. Three different hydrogen species, i.e.,

near-surface H, surface-chemisorbed H, and bulk-dissolved H (in order of desorption temperature from low to high), were observed. With hydrogen exposure at 80 K, a single desorption peak with peak temperature at 310 K was observed, which is associated with the recombinative desorption of surface-chemisorbed H. Near-surface H was observed when the hydrogen exposure was carried out at slightly higher temperatures (90-140 K), and this hydrogen desorbed at ~150 K. For hydrogen exposure at temperatures greater than 140 K, the total amount of absorbed H significantly increased due to dissolution of H atoms in the Pd bulk (desorption temperature greater than 400 K). Similar effects have been also observed on the Pd(100) surface.[67]

Interactions of hydrogen over Au have not been researched as thoroughly[68-69] as over Pd, primarily because Au has a much higher activation barrier for H_2 dissociation than Pd.[70] Our research group[69] has used an electron-beam heated thermal H atom generator to populate atomic H on the Au(111) surface at 77 K. The desorption feature for hydrogen recombination was found to occur at ~110 K, indicative of a low activation energy for this process, which suggests that hydrogen interacts weakly with the Au(111) surface. We have also demonstrated that these weakly bound H atoms on the Au(111) surface exhibit unique catalytic activities for many reactions[11] such as ether production via aldehydes or aldehyde/alcohol coupling[71] and NO_2 reduction to NO at cryogenic temperatures.[72]

Recently, the interactions of hydrogen with Pd−Au bimetallic model surfaces have been explored both experimentally[53, 73-77] and theoretically.[74-75, 78-83] For example, Tysoe et al.[74] applied Monte Carlo methods to simulate the surface structures of Au/Pd(111) alloys. By comparing the simulated results with the experimental H and Au coverages, they concluded H atoms adsorb on 3-fold hollow sites and then on bridge sites as surface Au coverage increases. Sykes and coworkers[75-76] employed scanning tunneling microscopy (STM) to observe H adatoms on Pd/Au(111) surfaces. STM imaging revealed that significant hydrogen uptake (or dissociative adsorption) only occurred when Pd islands were present on the Au(111) surface. Very recently, Ogura et al.[77] combined thermal desorption spectroscopy (TDS) with nuclear reaction analysis (NRA) to study the interactions of hydrogen with a $Pd_{70}Au_{30}$(110) single crystal. They showed that hydrogen is absorbed into the bulk of this Pd−Au alloy with considerable accumulation in the near-surface region.

In this chapter, the interactions of hydrogen with Pd−Au bimetallic surfaces were systematically studied using temperature-programmed desorption (TPD). A variety of Pd−Au model surfaces were prepared by depositing Pd atoms onto an Au(111) single crystal in ultrahigh vacuum (UHV) followed by annealing to various temperatures in order to study the correlation between surface structure and hydrogen sorption behavior. The prepared surfaces were characterized by Auger electron spectroscopy (AES) and reflection-absorption infrared spectroscopy using CO as a probe molecule (CO-RAIRS). Our results confirm that the presence of contiguous Pd sites is crucial for dissociative

adsorption of hydrogen on the Pd−Au bimetallic surface at 77 K. Upon heating, most of the surface chemisorbed H atoms recombinatively desorbed from Pd−Au interface sites (peak temperature of ~200 K), with some desorption occurring from Pd-island sites (~310 K). With hydrogen exposure at slightly higher temperatures (100-150 K), a small portion of hydrogen is absorbed into the near-surface region as subsurface H atoms that desorb at a lower temperature relative to surface-chemisorbed H. Isotopic studies revealed that saturating the surface with H adatoms prevents the subsequent dissociative adsorption of D_2. H/D scrambling, as evidenced by the desorption of HD, was observed in the case of exposing gaseous D to partially H-precovered Pd/Au(111). These isotope experiments suggest that H-D exchange over the Pd/Au(111) surface observes the Langmuir-Hinshelwood mechanism. Moreover, the H/D adatoms are mobile between the Pd−Au interface sites and Pd-island sites at low temperatures. We hope these observations will provide insight into hydrogen interactions with the Pd−Au bimetallic surface, which may assist in fundamental understanding of associated reaction mechanisms and the future design and improvement of bimetallic catalysts.

2.2 Experimental Methods

All experiments were conducted in an ultrahigh-vacuum (UHV) molecular beam surface scattering apparatus with a base pressure less than 1×10^{-10} Torr.[84-86] Briefly, the apparatus contains an Auger electron spectrometer (AES, Physical Electronics 10-500), a quadrupole mass spectrometer (QMS, Extrel C-50), a Fourier transform infrared spectrometer (FTIR, Bruker Tensor 27) combined with a mercury cadmium telluride

(MCT) detector (Infrared Associates), and nozzles and apertures for generating two separate molecular beams which are used in combination with quadrupole mass spectroscopy (QMS) to conduct temperature-programmed desorption (TPD) and reactive molecular beam scattering (RMBS) experiments.

The Au(111) single crystal sample is a circular disk (Princeton Scientific, 12 mm in diameter × 2 mm thick) and is held in place by a Mo wire fitted around a groove cut into the side of the sample. This wire is also used to resistively heat the sample and to provide thermal contact between the sample and a liquid nitrogen bath for cooling. The temperature of the sample was measured with a K-type (alumel−chromel) thermocouple placed in a small hole in the side of the disk. The Au(111) surface was cleaned by Ar ion bombardment (2 kV), carried out at room temperature, and followed by an anneal to 800 K. The cleanliness of the surface was verified by AES with a beam energy of 3 keV and emission current of 1.5 mA.

Pd−Au bimetallic model surfaces were prepared by depositing either 1 monolayer (ML) or 2 ML of Pd atoms from a homemade thermal evaporator onto the Au(111) surface at 77 K and then annealing the surface to a specified temperature for 10 min. The deposition rate of Pd was calibrated with a quartz crystal microbalance (QCM) controller (Maxtek Inc.) assuming the thickness of 1 ML Pd equals 0.274 nm. The surface compositions as a function of annealing temperature were characterized by AES.

Reflection absorption infrared spectroscopy using CO as a probe molecule was used to characterize the Pd−Au surfaces. The CO-RAIRS experiments in this study were conducted as follows: (1) a specified coverage of Pd was deposited onto the Au(111) surface at 77 K; (2) the Pd/Au(111) surface was annealed to 500 K and held for 10 min; (3) after the sample had cooled to 77 K, an IR background scan was taken; (4) CO was dosed onto the Pd/Au(111) surface at 77 K via exposure from a molecular beam until the surface was saturated with CO, as determined by the method of King and Wells;[87] and (5) an IR spectrum of CO on the Pd−Au surface was taken at 77 K. All spectra were averaged from 512 scans with a resolution of 4 cm^{-1}. The Pd−Au surface was then annealed to a higher temperature (e.g., 550, 600, or 650 K) and held for 10 min to change the surface structure and simultaneously to desorb the adsorbed CO. With the repetition of steps 3-5, a series of IR spectra of CO on various annealed Pd−Au surfaces were obtained.

In H_2-TPD experiments, hydrogen was dosed at 77 K or higher temperatures with an exposure of 1 langmuir (1 langmuir = 1×10^{-6} Torr·s) by backfilling the chamber with molecular H2 through a leak valve. At this exposure the hydrogen coverage was considered to be saturated since no difference was observed between the H_2-TPD spectra taken with 1 and 10 langmuirs exposures. The sample was then heated to 500 K at a rate of 1 K/s while $m/z^+ = 2$ (H_2) was monitored. In the TPD experiments involving codosed H and D, the Pd−Au surface was precovered by hydrogen at 77 K, and then

deuterium was dosed at 77 K or elevated temperatures. The sample was then heated to 500 K at a rate of 1 K/s while $m/z^+ = 2$, 3 (HD) and 4 (D_2) were monitored.

2.3 RESULTS AND DISCUSSION

2.3.1 AES Characterization of Pd/Au(111)

In this work, Pd−Au bimetallic surfaces were prepared by depositing Pd atoms onto a single crystal surface of Au(111). This system is beneficial because it offers the flexibility to compare the activity of the pure Au surface to Au surfaces with various coverages of Pd under the same set of conditions. Furthermore, by controlling the amount of Pd deposited onto the surface and the deposition/annealing temperature with which the surface is prepared, the Pd adatoms can be directed to reside on the Au(111) surface or to diffuse into the subsurface, yielding a subsurface alloy.[4] AES was utilized to determine the surface composition of Pd/Au(111) surfaces as a function of annealing temperatures.

Figure 2.1 depicts the Pd(333 eV)/Au(74 eV) AES peak-to-peak ratios of 1 and 2 ML of Pd deposited on the Au(111) surface at 77 K and those after annealing each surface to various temperatures (200-650 K). Annealing each surface in UHV caused a decrease in the Pd/Au AES ratio, which was much more significant when the annealing temperature was higher than 400 K for 1 ML Pd/Au(111) and 500 K for 2 ML Pd/Au(111). These results indicate that the relative surface ratio of Pd to Au declines as the annealing temperature increases due to diffusion of the Pd admetal into the subsurface

of the Au(111) single crystal.[44, 88] Similar annealing-induced interdiffusion of Pd was also observed by Goodman et al. in a study of a 5 ML Pd/5 ML Au/Mo(110) system.[89]

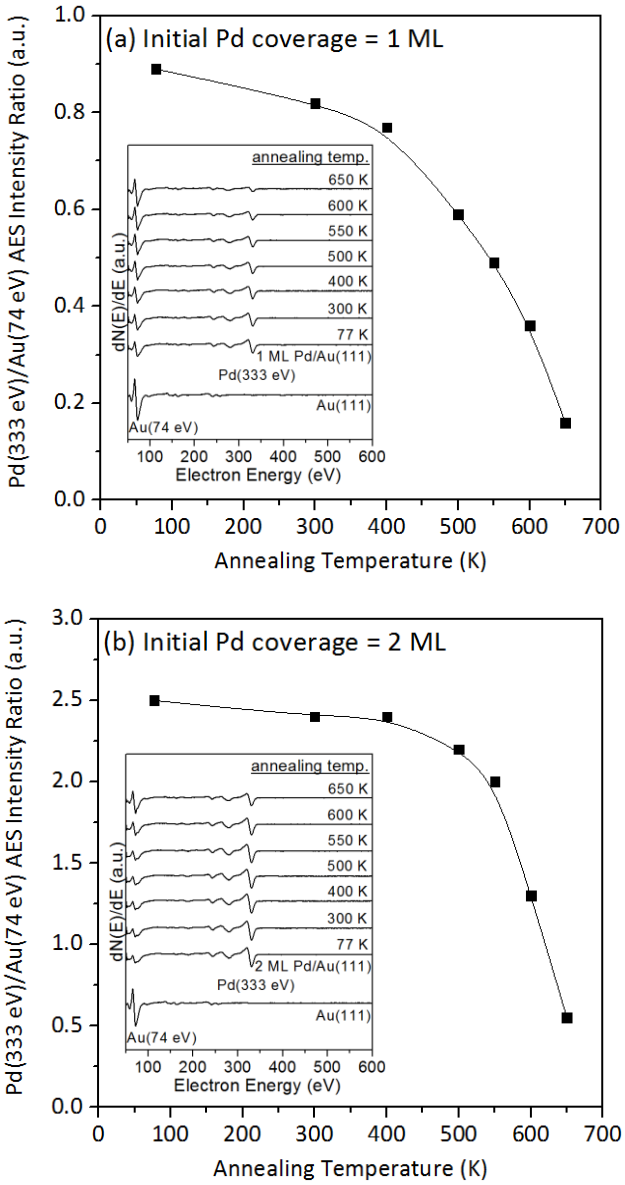

Figure 2.1. Pd(333 eV)/Au(74 eV) AES peak-to-peak ratios of Pd/Au(111) bimetallic surfaces as a function of annealing temperature. (a) 1 ML and (b) 2 ML of Pd overlayers were initially deposited onto Au(111) at surface temperature of 77 K. The corresponding AES spectra are shown in the insets.

2.3.2 CO-RAIRS Characterization of Pd/Au(111)

CO has long been used in reflection absorption infrared spectroscopy as a probe molecule for surface characterization.[90] The type of adsorption site occupied by CO (e.g., atop sites, 2-fold or 3-fold bridged sites) can be inferred by the intramolecular CO stretch frequency (ν_{CO}) as a result of varying degrees of π backdonation from the surface electrons. It has also been shown that CO-RAIRS is an effective technique to investigate the alloy effects of bimetallic model surfaces.[91] In this study, we used CO-RAIRS to characterize the annealed 1 ML Pd/Au(111) and 2 ML Pd/Au(111) surfaces as shown in Figures 2.2 and 2.3, respectively. All IR spectra were acquired with a saturation coverage of CO adsorbed at 77 K. The CO-RAIRS spectrum of the Au(111) surface is included for comparison.

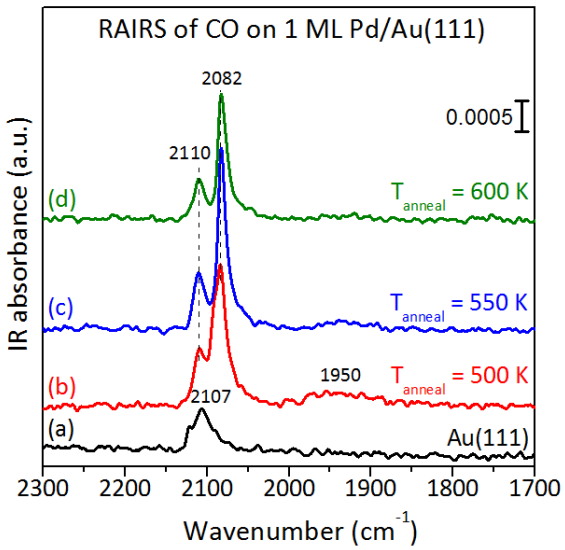

Figure 2.2. RAIRS spectra of CO on annealed Pd/Au(111) bimetallic surfaces taken at a surface temperature (T_S) of 77 K. The initial Pd coverage was 1 ML. The surfaces were saturated with CO at T_S = 77 K.

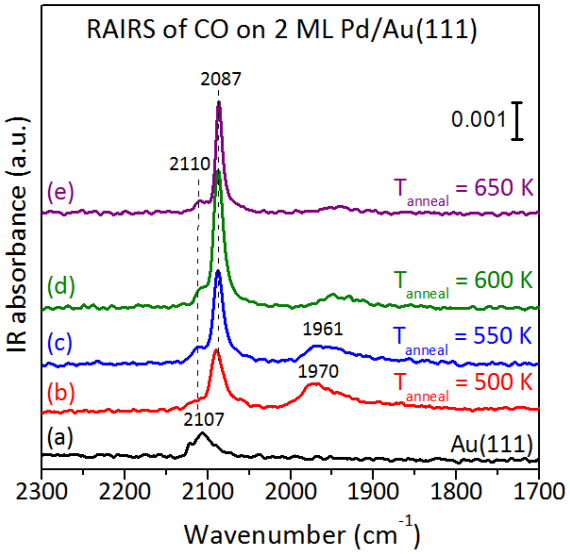

Figure 2.3. RAIRS spectra of CO on annealed Pd/Au(111) bimetallic surfaces taken at a surface temperature (T_S) of 77 K. The initial Pd coverage was 2 ML. The surfaces were saturated with CO at T_S = 77 K.

Only one vibrational band centered at ~2107 cm^{-1} was observed for CO adsorbed on the Au(111) surface at 77 K (Figure 2.2, curve a). The vibrational frequency of this feature is in good agreement with the reported value (2108 cm^{-1}) for saturated CO adsorbed on Au(110)-(1 × 2) at 110 K[92] and on 10 ML Au/Mo(110) at 80 K,[93] which is associated with CO bound to atop Au sites.

On the Pd−Au surface that was annealed to 500 K, three CO vibrational features were observed (Figure 2.2, curve b). The vibrational spectroscopy of CO adsorption on Pd−Au bimetallic surfaces has been studied by high-resolution electron-energy-loss spectroscopy (HREELS)[94] and later RAIRS.[39, 89, 93] According to CO-RAIRS

measurements regarding Pd−Au bimetallic surfaces reported in the literature,[39, 89, 93] the broad feature centered at ~1950 cm^{-1} is due to bridged CO on contiguous Pd sites (ν_{CO}: 1900-2000 cm^{-1}), the sharp peak at ~2082 cm^{-1} can be assigned to atop CO on isolated Pd sites (ν_{CO}: 2060-2085 cm^{-1}), and the peak at ~2110 cm^{-1} is attributed to atop CO on Au sites. However, it is also noted[95] that on the Pd(111) surface the vibrational band of atop CO on Pd sites shifts from ~2085 to ~2109 cm^{-1} as CO coverage increases from submonolayer to saturation coverage. Accordingly, the ~2110 cm^{-1} IR features observed on Pd−Au surfaces in this study could result from either atop CO on Au or Pd sites (or a combination of both).

For the surface annealed at 550 K, the IR band at ~2110 cm^{-1} did not show a significant change in intensity (Figure 2.2, curve c), relative to the Pd−Au surface annealed at 500 K, whereas the IR feature for atop CO on isolated Pd sites (ν_{CO}: 2082 cm^{-1}) intensified and was accompanied by the attenuation of the signal for bridged CO on contiguous Pd sites (ν_{CO}: 1900-2000 cm^{-1}). All IR bands decreased in intensity when the surface was prepared with 600 K annealing (Figure 2.2, curve d), particularly for that of bridged CO on contiguous Pd sites. These IR spectra reveal that upon annealing the morphology of the surface Pd changes from a mixture of isolated atoms and contiguous atoms to exclusively isolated atoms as a result of the Pd diffusion into the Au(111) subsurface.

Contiguous Pd sites on the Pd−Au surface are important for H_2 chemisorption,[96] a principle which will be presented in the discussion of H_2-TPD experiments in a later section of this work, and can be retained by either annealing the surface to a lower temperature (e.g., <500 K) or depositing a higher initial Pd coverage such as 2 ML. In this study, the Pd−Au surfaces were frequently annealed to 500 K to desorb any surface contaminants such as CO. Accordingly, the latter method (with a higher initial Pd coverage) was adopted to prepare Pd−Au surfaces that contain more contiguous Pd sites to facilitate the dissociative adsorption of H_2.

Figure 2.3 depicts the CO-RAIRS spectra obtained from Pd−Au surfaces generated by depositing 2 ML of Pd on the Au(111) surface followed by annealing to temperatures ranging from 500 to 650 K. It is evident that on these particular Pd−Au surfaces the IR signals of bridged CO on Pd contiguous sites (ν_{CO}: 1900-2000 cm^{-1}) are more intense than those observed on the samples prepared from 1 ML Pd on Au(111) (Figure 1); in addition, the vibration bands for atop CO on Pd were sharper with a slight blue-shift to ~2087 cm^{-1}, and the 2110 cm^{-1} features were relatively smaller. As expected from the results shown in Figure 1, the IR signals of bridged CO on contiguous Pd sites (ν_{CO}: 1900-2000 cm^{-1}) attenuated and those of atop CO on Pd sites (ν_{CO} = ~2087 cm^{-1}) intensified when the surface was annealed to temperatures from 500 to 600 K (Figure 2.3, curves b-d). When the surface was annealed to 650 K (Figure 2.3, curve e), all IR signals decreased in intensity and that of bridged CO on Pd sites became very small, indicative of much fewer contiguous Pd sites on this surface.

2.3.3 TPD of H_2 from Pd/Au(111)

TPD was used to study the interaction of hydrogen with the Pd/Au(111) surfaces. Figure 2.4 shows H_2-TPD spectra from annealed Pd/Au(111) surfaces with an initial Pd coverage of 1 ML.

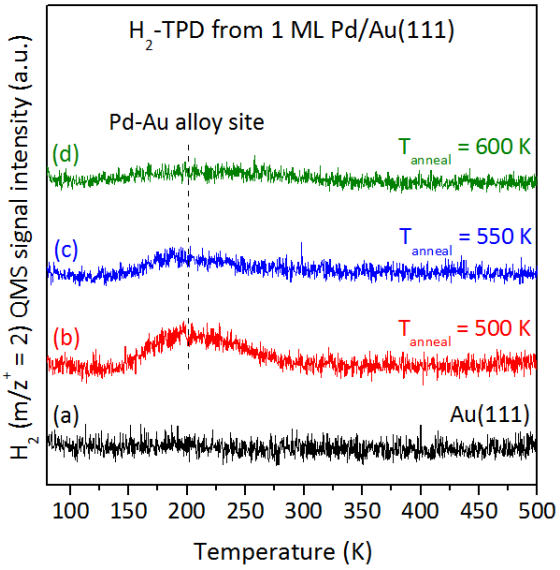

Figure 2.4. H_2-TPD from annealed Pd/Au(111) bimetallic surfaces. The initial Pd coverage was 1 ML. The surfaces were saturated with hydrogen by backfilling 1 langmuir of H_2 at a surface temperature of 77 K. The heating rate was 1 K/s.

For the 1 ML Pd−Au surface annealed to 500 K (Figure 2.4, curve b), a broad H_2 desorption peak centered at ~200 K was observed. Since this desorption temperature lies between those for Au(111) (~110 K)[69] and Pd(111) (~310-320 K)[53, 66] surfaces, we speculate that this desorption site consists of Au and Pd atoms (desorption occurs at the interface between Au and Pd atoms), which mimics the behavior of a Pd−Au alloy. The

desorption peak (200 K) is fairly close to that of Pd/Cu(111) (210 K),[97] which was assigned as the temperature for H_2 desorption from isolated Pd atoms on a Cu(111) surface. As expected, no measurable H_2 desorption was observed from the clean (Pd-free) Au(111) surface under the same set of conditions (Figure 3.4, curve a). Accordingly, our results reveal that the presence of Pd adatoms on Au(111) facilitate H_2 activation for hydrogen uptake via dissociative adsorption, which is consistent with a density functional theory (DFT) report.[81]

The H_2 desorption peak became less pronounced when the Pd−Au surface was annealed to higher temperatures (i.e., 550 and 600 K) prior to H_2 exposure at 77 K, which would be expected since fewer Pd atoms reside on the surface after annealing to higher temperatures. It is noted that there was very little H_2 desorption from the Pd−Au surface that was annealed at 600 K (Figure 2.4, curve d) despite the presence of isolated surface Pd adatoms as evidenced by IR signals of atop CO on Pd sites (Figure 1, curve d). Comparison of H_2-TPD results (Figure 2.4) with the corresponding CO-RAIRS spectra (Figure 2.2) for the entire series of annealed Pd−Au surfaces suggests that the presence of contiguous Pd sites is crucial for H_2 uptake and that surfaces with only isolated Pd sites do not readily uptake H_2. A similar observation was also reported previously in an electrochemical system in which Pd atoms were electrodeposited onto Au(111) surfaces.[96] By comparing the integrated area of current peaks due to H adsorption from H^+ in the voltammetric data with the surface coverages of various Pd ensembles

(monomers, dimers, and trimers) observed from STM images, Maroun et al.[96] concluded that hydrogen adsorption requires at least Pd dimers or larger ensembles.

As mentioned earlier, an initial Pd coverage of 2 ML was also used to prepare annealed Pd−Au surfaces with more contiguous Pd sites for comparison with the surface prepared with an initial coverage of 1 ML Pd. The H_2-TPD spectra associated with the Pd−Au surface prepared with 2 ML Pd are displayed in Figure 2.5.

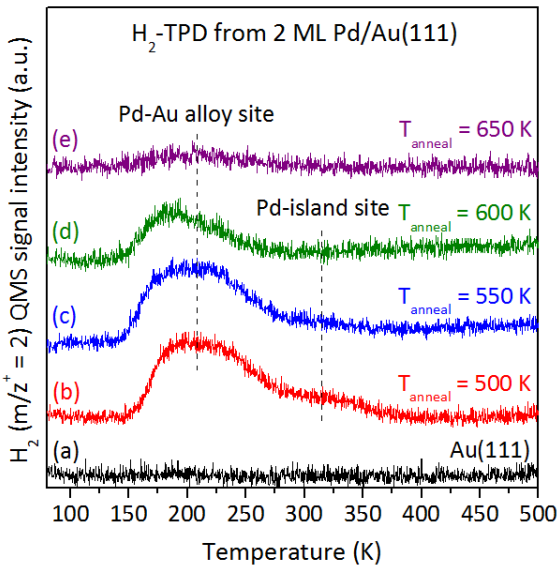

Figure 2.5. H_2-TPD from annealed Pd/Au(111) bimetallic surfaces. The initial Pd coverage was 2 ML. The surfaces were saturated with hydrogen by backfilling 1 langmuir of H_2 at a surface temperature of 77 K. The heating rate was 1 K/s.

For the Pd−Au bimetallic surface that was annealed at 500 K (Figure 2.5, curve b), the H_2 desorption spectrum displayed a broad peak centered at ~210 K and a small

shoulder at ~315 K, suggesting the presence of two distinct sites for H_2 desorption. The desorption peak at a temperature of ~210 K is close to that observed for the 1 ML Pd/Au(111) surface that was annealed at 500 K (Figure 2.4, curve b), suggesting a similarity between the desorption sites on these two surfaces, which we assign to be associated with the Pd−Au interface, whereas the higher temperature (~315 K) feature is close to the desorption temperature of H_2 from Pd(111),[35, 43] implying the presence of Pd(111)-like islands on the surface.

When the Pd−Au surface was prepared with a higher annealing temperature of 550 K (Figure 2.5, curve c), the amount of H_2 desorption from both features decreased, indicative of the loss of sites for dissociative adsorption of H_2. After annealing to 600 K, the TPD feature from the Pd-island sites disappeared and only the H_2-TPD feature from Pd−Au interface sites remained (Figure 2.5, curve d). The amount of H_2 desorption from the 650 K annealed Pd−Au surface was negligible (Figure 2.5, curve e) despite the presence of isolated Pd atoms on this surface, as evidenced by CO-RAIRS (Figure 2.3, curve e). These TPD results together with the corresponding IR spectra (Figure 2.3) again demonstrate the prominent role of contiguous Pd sites (characterized by ν_{CO}: 1900-2000 cm^{-1}) on the Pd−Au surface for H_2 uptake (or dissociative adsorption of H_2). Similarly, Gao et al.[39] have also reported that contiguous Pd sites play a critical role in assisting O_2 dissociation, thus accounting for a high CO oxidation activity over AuPd(110) model surfaces.

2.3.4 Effect of Surface Temperature during H_2 Exposure

It has been shown that the surface temperature during hydrogen exposure has a significant influence on the nature of hydrogen on the Pd(111) surface.[66] In order of desorption temperature from low to high, three different hydrogen species were observed in TPD: near-surface H, surface-chemisorbed H, and bulk-dissolved H.[66] Here, we explored the effect of surface temperature (T_S = 77-150 K) during hydrogen exposure on the hydrogen desorption behavior for the 2 ML Pd/Au(111) surface that had been annealed to 500 K. The resulting H_2-TPD spectra are shown in Figure 2.6.

As discussed earlier, with hydrogen exposure at 77 K the recombinative desorption of H from this Pd−Au bimetallic surface occurs from two distinct sites, Pd−Au interface sites (~210 K) and Pd(111)-like islands (~315 K), which results in a broad desorption feature beginning at ~150 K and terminating at ~350 K. When the Pd−Au surface was exposed to H2 at a higher temperature of 100 K (Figure 2.6, curve b), the low temperature desorption feature extended to a slightly lower temperature region starting at ~145 K. The starting temperature for H_2 desorption reduced to ~140 K (reproducibly) when the hydrogen exposure was performed at higher temperatures of 120 K (Figure 2.6, curve c) and 150 K (Figure 2.6, curve d).

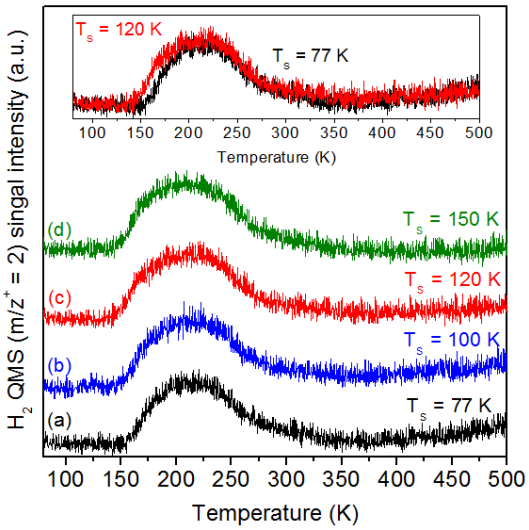

Figure 2.6. Effect of surface temperature (T_S) during hydrogen exposure on H_2-TPD from Pd−Au bimetallic surface. The Pd−Au surface was prepared by depositing 2 ML of Pd onto Au(111) at T_S = 77 K followed by annealing to 500 K in vacuum. One langmuir of H_2 was backfilled at T_S = (a) 77, (b) 100, (c) 120, and (d) 150 K. For TPD measurements, the sample was heated from 77 K with a heating rate of 1 K/s. The inset shows the H_2-TPD from (a) 77 and (c) 120 K hydrogen exposure for comparison.

We attribute the extension of the low temperature desorption feature to the presence of near-surface H, which has a desorption peak temperature at ~150-160 K for Pd(111),[66] Pd(100),[67] and Pd(110) surfaces.[64] Near-surface H (or subsurface H) has been proposed to be an intermediate between the chemisorbed H on Pd surface and dissolved H in the Pd bulk.[64] Because of its instability, the desorption temperature of near-surface H (~150-160 K) is lower than the desorption temperatures of surface-chemisorbed H (~310-320 K) and bulk-dissolved H (greater than 400 K). A higher surface temperature during hydrogen exposure could provide the energy to overcome the

activation barrier for hydrogen diffusion from the surface into the subsurface. The inset in Figure 2.6 clearly shows the difference in H_2-TPD spectra obtained from hydrogen exposure at 120 and 77 K. The TPD area ratio of the H_2 spectrum for exposure at 120 K vs. 77 K is ~1.06, indicating that the near-surface H is ~6% as prevalent as the surface chemisorbed H.

Unlike the bulk Pd single crystal, in this study most Pd atoms in our Pd−Au samples reside in the topmost surface layer or near to the surface as a near-surface alloy. The concentration of Pd is expected to decrease sharply with its distance from the surface. Accordingly, the desorption peak of dissolved H in bulk Pd, which occurs at temperatures higher than 400 K,[66] was not observed in our experiments.

2.3.5 H/D Exchange on Pd/Au(111)

Isotopic studies using deuterium (D) were performed to further explore the behavior of the adsorbed hydrogen (H) on Pd−Au bimetallic surfaces. For the TPD traces shown in Figure 2.7, the Pd−Au surface was precovered with a saturation coverage of H adatoms by backfilling 1 langmuir of H_2 gas at 77 K. Afterward 1 langmuir of D_2 was backfilled at the same temperature. QMS signals for $m/z^+ = 2$ (H_2), 3 (HD), and 4 (D_2) were simultaneously monitored while the sample was heated (red traces). A control experiment carried out without the postexposure of deuterium is also included in Figure 6 (black trace) for comparison.

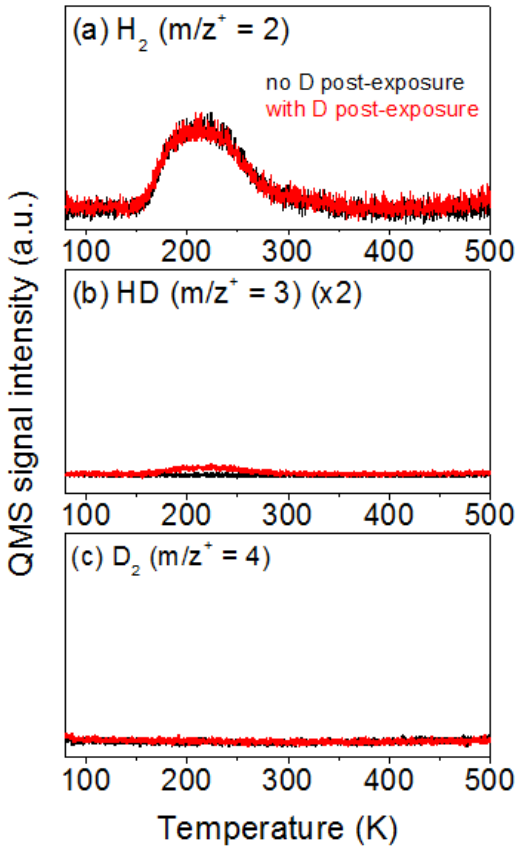

Figure 2.7. Effect of postexposure of D_2 on the saturated H-precovered Pd−Au bimetallic surface. The Pd−Au surface was prepared by depositing 2 ML of Pd onto Au(111) at a surface temperature (T_S) of 77 K followed by annealing to 500 K in vacuum. Saturation coverage of hydrogen was obtained by backfilling 1 langmuir of H_2 at T_S = 77 K. Postexposure of D_2 was carried out by backfilling 1 langmuir of D_2 at the same temperature. For TPD measurements, the sample was heated from 77 K with a heating rate of 1 K/s. The corresponding H_2-TPD without D_2 postexposure was included for comparison. (a)-(c) have the same Y-axis scale.

As shown in Figure 2.7(a), the TPD spectra for m/z^+ = 2 with and without postexposure of D_2 gas are nearly identical, indicating that postexposure of gaseous D_2 has a negligible effect on the desorption behavior of the saturated H atoms precovered on

the Pd−Au surface. With postexposure to deuterium, there was a small peak in the m/z+ = 3 trace (Figure 2.7(b), red trace) due to the thermal desorption of a trace amount of HD molecules. This HD was not from an impurity in gaseous H_2 since there was no HD desorption peak observed in the spectrum without postexposure to deuterium (Figure 2.7(b), black trace). These observations signify that a small portion of the D_2 is able to dissociate on the H-precovered Pd−Au surface. No detectable peak in $m/z^+ = 4$ (D_2) was observed in either case as shown in Figure 2.7(c).

These results reveal that the saturated H adatom precovered Pd−Au surface strongly inhibits the subsequent dissociative adsorption of gaseous deuterium, which is consistent with a previous study[98] in which a Langmuir-Hinshelwood mechanism was observed for H-D exchange on Pd(111). This inhibition is also evidenced by the observation that there was no detected hydrogen uptake when a molecular beam of hydrogen was impinged onto the Pd−Au surface that was presaturated by hydrogen in a King-Wells measurement (Figure 2.8). Accordingly, only a small amount of molecular D_2 dissociated into atomic D and then recombined with atomic H to desorb as HD upon heating. Because of the low concentration of atomic D on the surface, no measurable D_2-TPD peak was observed during TPD.

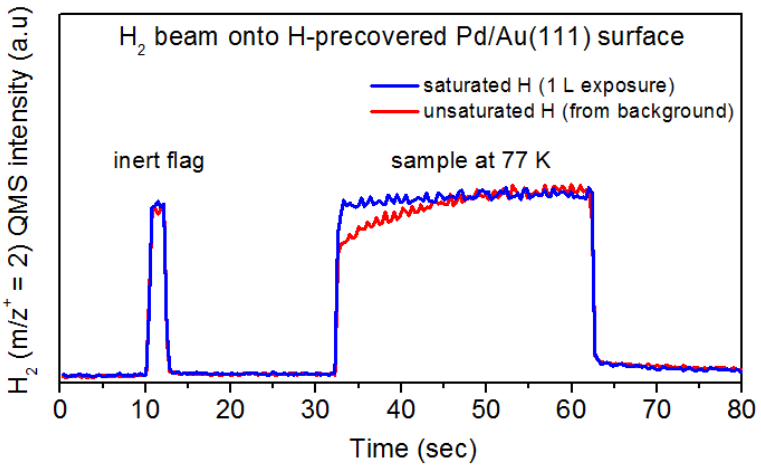

Figure 2.8. King-Wells measurement of H_2 on Pd−Au bimetallic surfaces. The Pd−Au surface was prepared by depositing 2 ML of Pd onto Au(111) at surface temperature of 77 K followed by annealing to 500 K in vacuum. A molecular beam of H_2 was impinged onto an inert flag for 2 s (from 10 to 12 s) and then impinged on the Pd−Au surface that was precovered by unsaturated hydrogen (red trace) or saturated hydrogen (blue trace) at 77 K for 30 sec (from 32 to 62 s).

Similar TPD experiments were conducted for surfaces below the saturation coverage of H adatoms. The Pd−Au surface readily took up hydrogen from the background which is intrinsically present in the UHV chamber. The H populating the surface in the experiments presented in Figure 2.9 was from the background rather than from a dosing procedure. In this case, H_2 desorption started at ~220 K, suggesting most of the hydrogen desorbed from Pd-island sites. The coverage of unsaturated H adatoms at the Pd−Au surface is ~30% of saturation coverage as determined by the H_2-TPD peak areas.

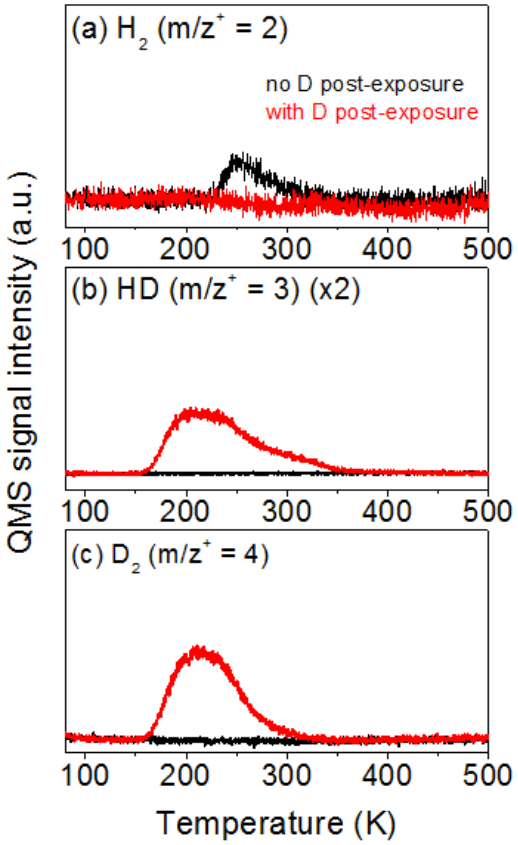

Figure 2.9. Effect of postexposure of D_2 on a partially H-precovered Pd−Au bimetallic surface. The Pd−Au surface was prepared by depositing 2 ML of Pd onto Au(111) at surface temperature (T_S) of 77 K followed by annealing to 500 K in vacuum. This unsaturated coverage of hydrogen was obtained from background H_2 at T_S = 77 K. Postexposure to D_2 was carried out by backfilling 1 langmuir of D_2 at the same temperature. For TPD measurements, the sample was heated from 77 K with a heating rate of 1 K/s. The corresponding H_2-TPD without D_2 postexposure was included for comparison. (a)-(c) have the same Y-axis scale.

When the Pd−Au surface partially precovered by H was postexposed to D_2, no H_2 desorption peak was observed during TPD, while a considerable amount of HD (m/z^+ = 3) and D_2 (m/z^+ = 4) was detected (Figure 2.9, red traces). The formation of HD and D_2

can be explained by the availability of surface sites. When the surface sites are only partially occupied by precovered H atoms, gaseous D_2 is able to find empty sites on which to dissociate into atomic D. The D adatom can then recombine with another D or H adatom and then desorb as D_2 or HD. D_2 molecules desorbed mainly from the Pd−Au interface sites, whereas HD molecules desorbed from both Pd−Au interface sites and Pd-island sites. These results suggest that H and D adatoms are mobile between the Pd−Au interface sites and Pd-island sites at 77 K. The absence of H_2 desorption is likely due to the higher relative concentration of D adatoms on the surface, causing recombination of two H adatoms to be an unlikely event. The different shapes of the HD and D_2 desorption peaks are likely because most of the H adatoms are located on the Pd-island sites prior to D_2 postexposure, which decreases the probability that two D adatoms can recombinatively desorb from the Pd-island sites.

2.3.6 Effect of Surface Temperature on H/D Exchange on Pd/Au(111)

The effect of surface temperature during postexposure of D_2 was studied on the H-precovered Pd−Au surface. The surface was predosed with a saturation coverage of H adatoms by backfilling 1 langmuir of H_2 at 77 K followed by exposure to 1 langmuir of D_2 at various temperatures ranging from 77 to 180 K. QMS signals for $m/z^+ = 2$ (H_2), 3 (HD), and 4 (D_2) were simultaneously monitored when the sample was heated from 77 to 500 K as shown in Figure 2.10.

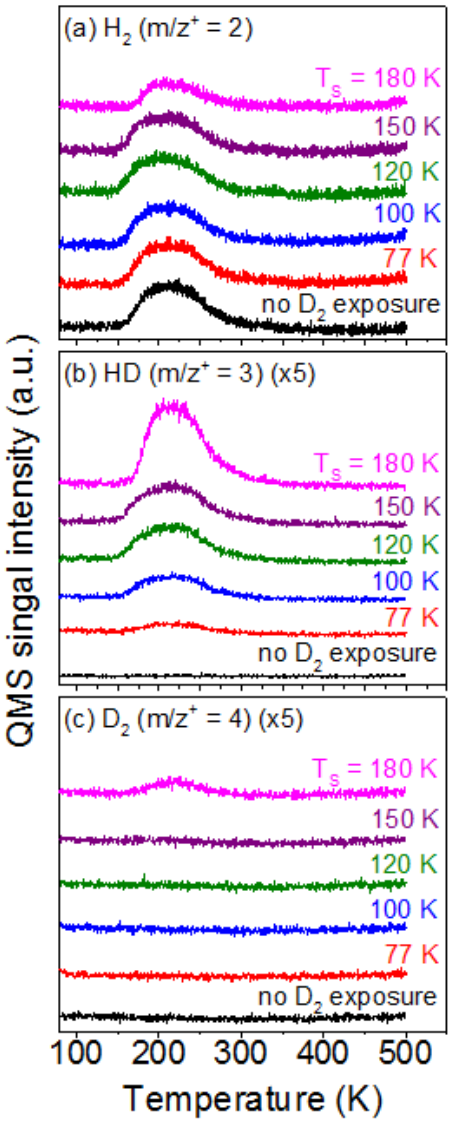

Figure 2.10. Effect of surface temperature (T_S) during D_2 postexposure on H_2-TPD from Pd−Au bimetallic surface. The Pd−Au surface was prepared by depositing 2 ML of Pd onto Au(111) at T_S = 77 K followed by annealing to 500 K in vacuum. The surface was precovered with saturation coverage of hydrogen by backfilling 1 langmuir of H_2 at T_S = 77 K. Postexposure to D_2 was carried out by backfilling 1 langmuir of D_2 at T_S = 77, 100, 120, 150, and 180 K. For TPD measurement, the sample was heated from 77 K with a heating rate of 1 K/s. The corresponding H_2-TPD without D_2 postexposure was included for comparison. (a)-(c) have the same Y-axis scale.

As shown in Figure 2.7, only a trace amount of molecular D_2 dissociated into D adatoms when Pd−Au surface sites were presaturated with atomic H at 77 K. However, when the saturated H-precovered surface was postexposed to D_2 at 100 K, the HD desorption peak became more pronounced, indicative of more dissociative adsorption of D_2. It should be noted that at 100 K hydrogen atoms still remain on the Pd−Au surface since H_2 desorption begins at ∼150 K. This enhancement of HD formation may be due to increased mobility of H adatoms at temperatures slightly above 77 K, which increases the probability of D_2 dissociation and frees up surface sites for further dissociation.

The HD desorption peak gradually grew in intensity as the temperature of postexposure of D_2 was increased. With the postexposure to D_2 at 120 K, H_2 and HD desorption began at a slightly lower temperature. As discussed earlier regarding Figure 2.6, this lower desorption temperature suggests the presence of subsurface H and D atoms due to absorption. A portion of precovered H desorbed when the Pd−Au surface was heated to higher than 150 K, leaving some empty surface sites for D_2 dissociation. Consequently, a significant peak in the HD spectrum and the emergence of a D_2 desorption peak were observed when H-precovered surfaces were exposed to D_2 at 180 K.

2.4 CONCLUSIONS

A variety of Pd−Au bimetallic surfaces were prepared by depositing Pd onto the Au(111) surface followed by controlled annealing under UHV conditions. Based on CO-RAIRS and H_2-TPD results, contiguous Pd sites were found to be crucial for dissociative adsorption of hydrogen on the Pd−Au bimetallic surface. Two types of surface sites for recombinative desorption of H adatoms, Pd−Au alloy sites (majority) and Pd-island sites, were identified in H_2-TPD spectra by their desorption features. The temperature for hydrogen desorption from Pd−Au alloy sites is lower than that from Pd-island sites, indicating H adatoms bind to these sites more weakly, which may be beneficial for catalytic reactions involving hydrogen. The formation of near-surface H atoms (or H absorption) was observed when hydrogen was exposed at higher surface temperatures. The near-surface H was relatively unstable and desorbed at a lower temperature than that of surface-chemisorbed H. Isotope-labeled experiments suggest that H-D exchange follows a Langmuir-Hinshelwood mechanism and the H/D adatoms are mobile between Pd−Au interface sites and Pd-island sites at low temperatures. These observations provide insight into hydrogen interactions with Pd−Au bimetallic surfaces, which may prove useful in the understanding of associated reaction mechanisms and the future design of bimetallic catalysts.

Chapter 3: Interactions of Hydrogen and Carbon Monoxide on Pd−Au Bimetallic Surfaces*

3.1 INTRODUCTION

Hydrogen and carbon monoxide are involved in many metal-catalyzed reactions as reactants (e.g., in Fischer-Tropsch synthesis), products (e.g., in steam or dry reforming of methane), or intermediates/byproducts (e.g., in the direct ethanol fuel cell). Because of their fundamental importance in heterogeneous catalysis, the interactions of H (or D) and CO with monometallic or bimetallic single crystal surfaces have been extensively studied as summarized by White[99] and Guo and King.[100] Apart from a few unconfirmed reports, no reaction product or intermediate (nonreactive coadsorption) has been observed upon interaction of H and CO coadsorbed on transition-metal surfaces under ultra-high-vacuum (UHV) conditions.[100] Nevertheless, many interesting phenomena, such as displacement, site blocking, segregation, mixing, new desorption features, and changes in sticking probability, have been reported.[99-100]

Pd−Au bimetallic catalysts have shown promising performance in a number of chemical processes,[5, 10] such as low-temperature CO oxidation,[13-14, 39-40] cyclization of acetylene to benzene,[43-45, 56] acetoxylation of ethylene to vinyl acetate,[16-17] selective oxidation of alcohols,[18, 57-58] synthesis of hydrogen peroxide,[34, 59] and selective

* Yu, W.-Y.; Mullen, G. M.; Mullins, C. B., Interactions of Hydrogen and Carbon Monoxide on Pd−Au Bimetallic Surfaces. *J. Phys. Chem. C* **2014**, 118, 2129-2137.
W.-Y. Yu, G. M. Mullen and C. B. Mullins conceived and designed experiments, analyzed and discussed results, and commented on the manuscript. W.-Y. Yu performed experiments, analyzed data and wrote the paper.

hydrogenation of unsaturated hydrocarbons.[22-24] Recently, Pd−Au alloys have also been reported to be effective for use in direct ethanol fuel cells[101] and as catalysts for the selective decomposition of formic acid for hydrogen production.[31, 60-61] It is believed that, for these reactions, the catalytic properties are highly influenced by the interactions of hydrogen and CO with Pd−Au surfaces. For example, the high stability displayed by Pd−Au catalysts for hydrogen production via formic acid decomposition has been attributed to the resistance of the surface to CO poisoning due to alloying of Pd with Au.[31, 61] Therefore, it is of significant interest to investigate the coadsorption of CO and H on Pd−Au model surfaces in order to provide mechanistic insights into associated reaction mechanisms, which may be useful for future catalyst design.

The coadsorption of CO and H on low-index single-crystal surfaces of Pd, e.g., Pd(111),[102-108] Pd(100),[109-111] and Pd(110),[64, 112] has been studied by a host of surface science techniques, including temperature-programmed desorption (TPD),[64, 102-106, 109-110, 112] low energy electron diffraction (LEED),[103, 105, 109-112] vibrational spectroscopy,[105-106, 109-111] scanning tunneling microscopy (STM),[107] and low-energy electron microscopy (LEEM),[108] as well as density functional theory (DFT).[106, 108] On the Pd(111) surface, it was found that preadsorbed CO reduced hydrogen uptake by blocking surface sites for subsequent dissociative adsorption of hydrogen,[102-103, 105] and this finding has been supported by the relatively high activation energy estimated by DFT calculations.[106] Preadsorbed H was found to decrease the sticking coefficient of CO,[102] but no new desorption peak was observed for CO during subsequent TPD.[103] The initial adsorption

of CO was argued to induce recombinative desorption of surface H atoms based on the observation that less hydrogen desorbed during subsequent TPD.[102-103] Furthermore, the hydrogen desorption peak shifted to a higher temperature upon exposure to CO. It was proposed that coadsorption of CO induced the dissolution of H into the Pd bulk, and dissolved H desorbed at a higher temperature upon heating.[102-103, 105-106] Similar CO-induced hydrogen dissolution phenomena were also proposed in studies of coadsorbed CO and H on the Pd(100)[109-111] and Pd(110)[64] surfaces. Very recently, Ogura et al.[77] have investigated the interaction of CO and H on the $Pd_{70}Au_{30}$(110) single crystal surface using TPD. They demonstrated that a small amount of adsorbed CO significantly altered the desorption behavior of H by blocking the entrance/exit channel for precovered H (molecular cap effect of CO), which is similar to the behavior displayed on the $Pd_{10}Ag_{90}$(111),[113] $Pd_{70}Cu_{30}$(111),[114] and Pd/Cu(111)[115] bimetallic surfaces.

In this chapter, the interactions of CO and H with the Pd/Au(111) model surface were explored using TPD and molecular beam scattering (MBS) techniques combined with quadrupole mass spectroscopy (QMS). Our results indicate that exposure of a CO molecular beam to the hydrogen-precovered Pd−Au surface induced an additional low-temperature hydrogen desorption feature during subsequent TPD measurements, suggestive of formation of subsurface H atoms. Upon CO beam impingement, a portion of the precovered H adatoms recombinatively desorbed from the Pd−Au surface, which is indicated by the evolution of H_2 during MBS measurements. More H_2 was evolved when the CO beam was impinged on the H-precovered Pd−Au surfaces at higher surface

temperatures. Our MBS results also show that the presence of preadsorbed H atoms decreased the initial sticking probability of CO on the Pd−Au surface. This sticking probability gradually increased as the precovered H adatoms were displaced by CO. These observations provide insight into the interactions of CO and H with the Pd−Au bimetallic surface and may assist in the understanding of catalytic reactions involving CO and hydrogen over Pd−Au alloy catalysts.

3.2 EXPERIMENTAL METHODS

All experiments were conducted in an ultra-high-vacuum (UHV) molecular beam surface scattering apparatus with a base pressure less than 1×10^{-10} Torr.[48, 84-86] Briefly, the apparatus contains an Auger electron spectrometer (AES, Physical Electronics 10-500), a quadrupole mass spectrometer (QMS, Extrel C-50), a Fourier transform infrared spectrometer (FTIR, Bruker Tensor 27) combined with a mercury-cadmium-telluride (MCT) detector (Infrared Associates), as well as nozzles and apertures for generating two separate molecular beams that are used in combination with quadrupole mass spectroscopy (QMS) to conduct temperature-programmed desorption (TPD) and reactive molecular beam scattering (RMBS) experiments.

The Au(111) single crystal sample is a circular disk (Princeton Scientific, 12 mm in diameter × 2 mm thick) and is held in place by a Mo wire fitted around a groove cut into the side of the sample. This wire is also used to resistively heat the sample and to provide thermal contact between the sample and a liquid nitrogen bath for cooling. The

temperature of the sample was measured with a K-type (Alumel-Chromel) thermocouple placed in a small hole in the edge of the disk-shaped sample. The Au(111) surface was cleaned by Ar ion bombardment (2 keV), carried out at room temperature, followed by an anneal to 800 K. The cleanliness of the surface was verified by AES with a beam energy of 3 keV and emission current of 1.5 mA.

Pd−Au bimetallic model surfaces were prepared by depositing 1 monolayer (ML) or 2 ML of Pd atoms from a homemade thermal evaporator onto the Au(111) surface at 77 K and then annealing the surface to 500 K for 10 min. The growth of the Pd overlayer on the Au(111) surface at 77 K is believed to obey a layer-by-layer mechanism based on a previous study[88] in which a Pd film was grown on the Au(111) surface at the higher temperature of 150 K. Upon annealing, the surface Pd atoms diffuse into the bulk of the Au(111) surface, forming a Pd−Au alloy surface. The deposition rate of Pd was calibrated with a quartz crystal microbalance (QCM) controller (Maxtek Inc.) assuming that the thickness of 1 ML of Pd is equal to the diameter of a Pd atom, which is 0.274 nm. In this study, we discuss only the results obtained from the 2 ML Pd surface since the observations from 1 and 2 ML Pd surfaces displayed the same phenomena. The results associated with the 1 ML Pd surface are displayed in Figure 3.1.

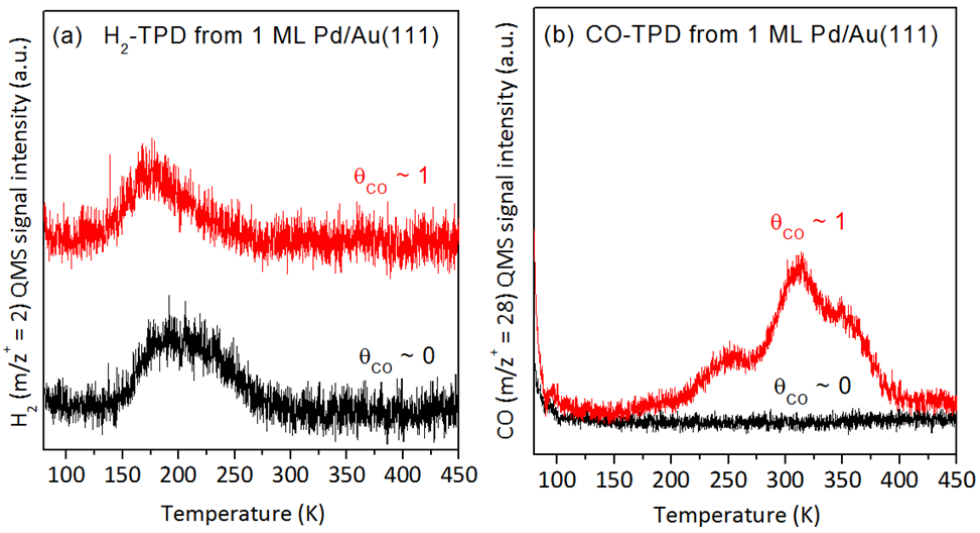

Figure 3.1. (a) H_2-TPD and (b) CO-TPD spectra of H and CO coadsorbed on the Pd−Au bimetallic surface. The Pd−Au surface was prepared by depositing 1 ML of Pd onto the Au(111) surface at 77 K followed by annealing to 500 K in vacuum. A saturation coverage of H was obtained by backfilling 1 L of H_2 at 77 K. A saturation coverage of CO was dosed via a molecular beam at 77 K. The sample was heated from 77 K with a heating rate of 1 K/s. The TPD spectra from the H-saturated Pd−Au surface without CO coadsorption are included for comparison.

Reflection absorption infrared spectroscopy (RAIRS) was used to study the adsorption behavior of CO on the Pd/Au(111) surface with and without H predosing. The Pd−Au surface was first heated to 500 at 1 K/s to desorb any surface contaminants such as CO. After the sample had cooled to 77 K, an IR background scan was taken. Saturation coverage of hydrogen on the surface was achieved by backfilling the chamber with 1 langmuir (L; 1 L = 1×10^{-6} Torr-s) of molecular H_2 through a leak valve with the sample held at 77 K. At this exposure, the hydrogen coverage was considered to be saturated since no difference was observed between the H_2-TPD spectra taken after 1 and

10 L exposures.[48] Various coverages of CO were dosed by a molecular beam of CO with the sample held at 77 K. Finally, an IR spectrum of CO adsorbed on the surface was taken at 77 K. All spectra were averaged from 512 scans with a resolution of 4 cm^{-1}.

In TPD experiments, the Pd−Au surface was first heated to 500 at 1 K/s to desorb any surface contaminants such as CO. After the sample had cooled to 77 K, the surface was considered as the "clean surface" prior to the dosing of hydrogen and CO. The sample was then heated to 500 K at a rate of 1 K/s while $m/z^+ = 2$ (H_2) and 28 (CO) were monitored by QMS. The Pd−Au surface readily took up the hydrogen from the background gas that is intrinsically present in our UHV chamber.[48] The hydrogen coverage observed in TPD spectra without explicitly dosing hydrogen was found to be ~30% of saturation coverage, which was highly reproducible in our system, as determined by integration of H_2-TPD peak areas. In this study, we made use of this exposure method to study the diffusion behavior of lower coverages of H adatoms upon the postdosing of CO.

King and Wells measurements[87, 116-117] were conducted by impinging a pure CO molecular beam onto the H-presaturated Pd−Au surface. Various flux rates of CO were obtained by changing the CO pressure in the nozzle from 0.2 to 0.6 Torr. The surface temperatures during CO beam impingement were varied from 77 to 150 K. QMS

signals of m/z^+ = 2 (H_2) and 28 (CO) were monitored during the King−Wells measurements.

3.3 Results and Discussion

In this study, the Pd−Au bimetallic model surface was prepared by depositing 2 ML of Pd onto the Au(111) surface at 77 K, followed by annealing to 500 K. In a previous study,[48] it was shown that this procedure produces a surface containing a mixture of isolated Pd atoms and contiguous Pd atoms. Of relevance to this work, the presence of contiguous Pd sites is crucial for the dissociative adsorption of H_2 at 77 K. Dissociated H adatoms recombinatively desorb from the Pd−Au alloy sites and Pd island-like sites.[48]

3.3.1 Adsorption of CO on Pd/Au(111)

The adsorption of CO on the Pd−Au model surface has been extensively studied to probe the surface properties and structures.[39, 45, 89, 93-94, 118] Here, the adsorption of CO on the Pd−Au surface was investigated by RAIRS and TPD in order to provide information regarding the CO adsorption behavior on our Pd/Au(111) surface and for comparison with results involving coadsorption with hydrogen to be discussed in a later section. Exposure of CO was achieved by impinging a molecular beam of CO onto the surface at 77 K. Three coverages of CO, ~0.35, ~0.64, and 1 (all relative to saturation coverage), were studied by varying the exposure. The acquired RAIRS and TPD results

are shown in Figure 3.2(a) and (b), respectively. The RAIRS and TPD spectra of saturated CO on the Pd−Au surface are included for comparison.

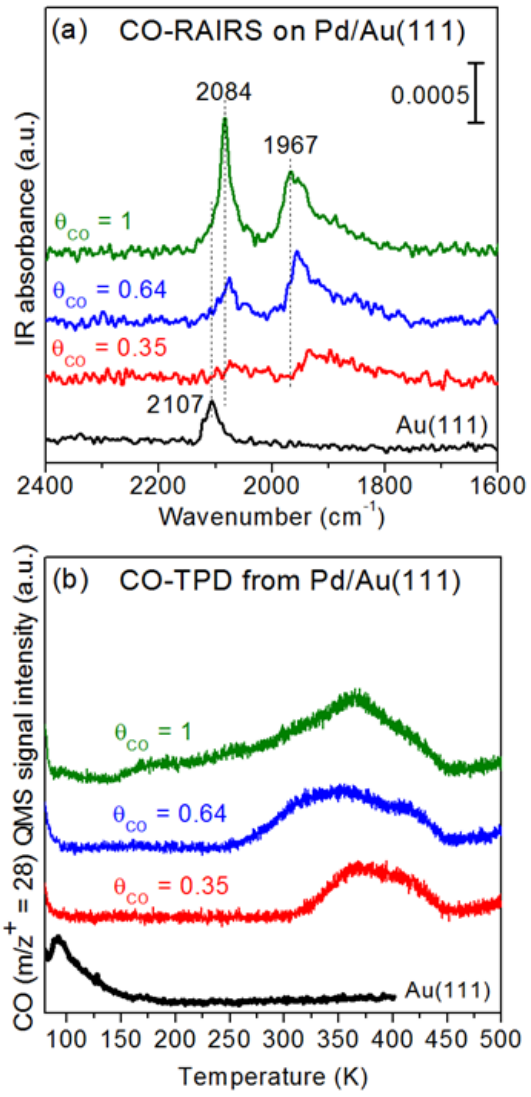

Figure 3.2. (a) RAIRS and (b) TPD spectra of various coverages of CO on the annealed 2 ML Pd/Au(111) bimetallic surface. Various converages of CO were dosed by impinging a CO molecular beam onto the Pd−Au surface at 77 K. IR spectra were taken at 77 K. For TPD measurements, the sample was heated from 77 K with a heating rate of 1 K/s. The results from saturated CO on Au(111) are included for comparison.

CO-RAIRS has long been used to characterize metal surfaces.[90] The type of adsorption site occupied by CO (e.g., atop sites, 2-fold or 3-fold bridge sites) can be inferred by the intramolecular CO stretch frequency (ν_{CO}) as a result of varying degrees of π-antibonding back-donation from the surface electrons. As shown in Figure 4.2(a), two weak vibrational bands at ~2070 and ~1950-1800 cm^{-1} were observed in the IR spectrum when the CO coverage was ~0.35. These two IR features both intensified and shifted to higher frequencices (~2077 and ~1956 cm^{-1}) as the CO coverage on the Pd−Au surface was increased to ~0.64. When the surface CO coverage reached saturation, the IR spectrum was dominated by two IR bands at ~2084 and ~1967 cm^{-1}, which can be assigned to atop CO on isolated Pd sites and bridged CO on contiguous Pd sites, respectively.[39, 89, 93] The dependence of CO coverage on surface structure on the Pd(111) surface has been studied by RAIRS.[95] At low coverage, CO adsorbs primarily on 3-fold hollow sites with a broad IR feature at ~1850 cm^{-1}. When the CO coverage is increased, CO resides on either bridge sites or 3-fold hollow sites (ν_{CO} ~ 1920 cm^{-1}). Further increases in CO coverage lead to a CO vibrational band at ~1965 cm^{-1}, suggestive of CO occupancy on bridge sites. Finally, CO adsorbs on both atop (ν_{CO} ~ 2110 cm^{-1}) and 3-fold hollow sites (ν_{CO} ~ 1895 cm^{-1}) at saturation coverage. In contrast to CO-RAIRS on Pd(111),[95] the IR features of CO on the Pd/Au(111) surface in this study exhibit a relatively asymmetrical peak shape and simultaneous growth in peak intensity as the CO coverage was increased. Similar observations have been reported by

Goodman et al.[93] in a study of the 5 ML Pd/5 ML Au/Mo(110) system, and they attrubuted these phonemena to the limited mobility of CO on the Pd−Au surface.

Figure 3.2(b) shows the corresponding CO-TPD spectra for the Pd−Au surface. For the low CO coverage of ~0.35, CO desorption from the Pd−Au surface began at ~310 K and ended at ~450 K. The initiation temperature for CO desorption shifted to lower temperatures, namely, ~250 and ~140 K, when the CO coverages were increased to 0.64 and saturation, respectively. These CO-TPD spectra resemble those observed on the Pd(111) surface,[119] which is consistent with a previous study by Sellidj and Koel.[94] By using ultraviolet photoemission spectroscopy (UPS), TPD and high-resolution electron energy loss spectroscopy (HREELS), Sellidj and Koel[94] concluded that the CO chemisorption properties on Pd/Au(111) were very similar to those on Pd(111) despite the large differences between the valence-band electronic structure of these two surfaces. It is noted that the temperature of the CO desorption peak changed as the CO coverage was increased. The CO desorption peak was initially centered at ~380 K, then reduced to ~355 K, and finally shifted upward to ~365 K at ~0.35, ~0.64, and saturation CO coverage, respectively. If CO was highly mobile on the Pd−Au surface, upon heating, CO would desorb from the strongest-binding site, the site with the highest desorption temperature. In this case, the temperature of the CO desorption peak would decrease monotonically as the CO coverage was increased. Accordingly, the observed evolution of peak temperature for CO desorption supports the limited mobility of CO on the Pd−Au surface, as suggested earlier by the RAIRS results.

3.3.2 TPD of Hydrogen and CO Coadsorbed on Pd/Au(111)

Figure 3.3 depicts the TPD spectra for saturated hydrogen and CO in various proportions coadsorbed on the Pd−Au bimetallic surface. The surface was presaturated with H adatoms by backfilling 1 L of H_2 at 77 K and then exposed to various coverages of CO by molecular beam impingement.

Addressing first the H_2-TPD spectra (Figure 3.3(a)), in the absence of postdosing of CO, the H desorption spectrum displayed a broad peak centered at ∼215 K with a small shoulder at ∼300 K, which we have attributed, in a previous study,[48] to H_2 desorption from Pd−Au alloy sites and Pd island-like sites, respectively. When CO was coadsorbed on the H-precovered Pd−Au surface at a coverage of ∼0.35, the hydrogen desorption feature shifted to a slightly lower temperature, beginning at ∼140 K (the onset temperature for hydrogen desorption from the CO-free surface was ∼150 K). Furthermore, the higher-temperature feature at ∼300 K was largely attunated upon CO codosing. The attunation of the higher-temperature shoulder suggests that the H adatoms on the Pd island-like sites were displaced by postadsorption of CO. The onset temperature for H desorption was further reduced to ∼135 K as the CO coverage was increased to ∼0.64 and saturation. The peak areas under the TPD traces, which is indicative of the amount of adsorbed H, decreased slightly upon postdosing of CO. These obervations suggest that the H adatoms precovered on the Pd−Au surface recombine and desorb during CO impingement, a phenomenon that will be discussed further with regard to scattering experiments in a later section of this work.

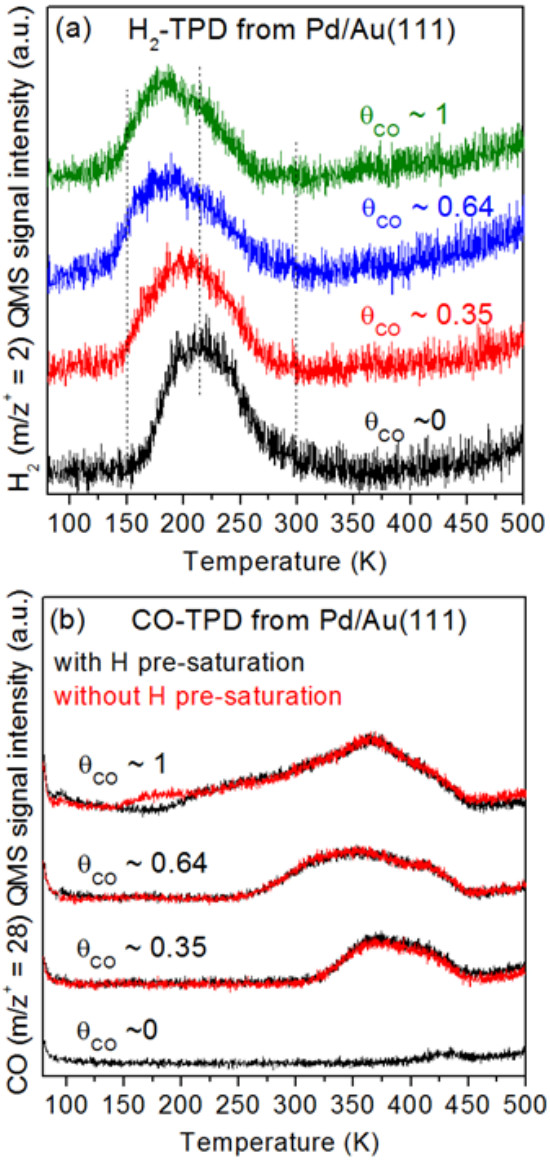

Figure 3.3. (a) H_2-TPD and (b) CO-TPD spectra of coadsorbed H and CO on the annealed 2 ML Pd/Au(111) bimetallic surface. Saturation coverage of hydrogen was obtained by backfilling 1 L of H_2 at 77 K. Various coverages of CO were dosed by impinging a CO molecular beam onto the Pd−Au surface at 77 K. The sample was heated from 77 K with a heating rate of 1 K/s. The CO-TPD spectra from the Pd−Au surface without hydrogen predosing are included for comparison.

The shift in the onset temperature for hydrogen desorption to a lower temperature in TPD spectra could be due to repulsive interactions caused by the coadsorbed CO on the surface leading to the formation of near-surface H. We have observed a similar extension of the low-temperature desorption feature when hydrogen was exposed to the Pd−Au surface at slightly higher temperatures (i.e., 100-150 K).[48] We attribute this effect to the presence of near-surface H, which has a desorption temperature of ∼150−160 K for Pd(111),[66] Pd(100),[67] and Pd(110) surfaces.[64] It has been proposed[64] that near-surface H (or subsurface H) is an intermediate between chemisorbed H on the Pd surface and dissolved H in the Pd bulk. Because of its instability, the desorption temperature of near-surface H (∼150−160 K) is lower than the desorption temperature of surface-chemisorbed H (∼310-320 K) and bulk-dissolved H (greater than 400 K).[66] CO-induced hydrogen dissolution has been proposed on the single crystal surfaces of Pd(111),[102-103, 105-106] Pd(100),[109-111] and Pd(110).[64] For example, Rupprechter and co-workers reported[105] that the desorption temperature of H_2 from the Pd(111) surface was increased from 295 to 375 K when the surface was postdosed with CO. They proposed that the CO replaced hydrogen from the surface and likely forced the hydrogen below the surface. Unlike the bulk Pd single crystal, in this study, most Pd atoms in our Pd−Au samples reside in the topmost surface layer or near the surface since only 1 or 2 ML of Pd was deposited on the surface, followed by an anneal. The concentration of Pd is expected to decrease sharply with its distance from the surface. Accordingly, upon CO

adsorption, the surface hydrogen adatoms likely can only diffuse to the Pd atoms in the near-surface region and desorb at a lower temperature.

The CO-TPD spectra from the same course of experiments are depicted in Figure 3.3(b) (in black traces). The CO-TPD spectra that were obtained under the same set of conditions, but without presaturation of H adatoms (Figure 1b), are also included (in red traces) for comparison. For coverages of CO of ~0.35 and ~0.64, the CO-TPD spectra from the Pd−Au surfaces with and without presaturation with H adatoms are nearly identical. The CO-TPD spectra were slightly different for a saturation coverage of CO; less CO desorption was observed from the H-presaturated Pd−Au surface in the temperature range between 150 and 200 K. When the hydrogen desorption spectra in Figure 2a are also taken into account, the slight decrease in CO uptake is most likely due to the occupancy of H adatoms on the Pd−Au alloy sites. These observations reveal that precovering with H adatoms has little influence on the CO desorption behavior on the Pd−Au surface, which is also supported by the nearly identical CO-RAIRS spectra for the surfaces with and without presaturation with hydrogen (Figure 3.4).

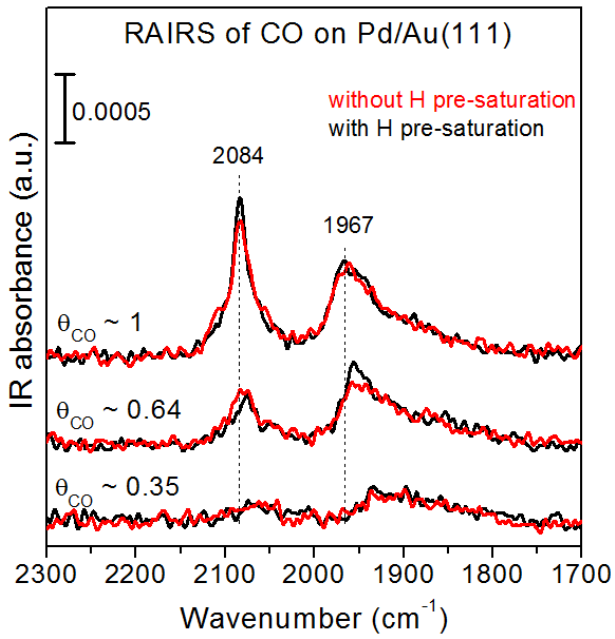

Figure 3.4. Effect of hydrogen pre-saturation on the CO-RAIRS spectra of the Pd−Au bimetallic surface. The Pd−Au surface was prepared by depositing 2 ML of Pd onto Au(111) at a surface temperature of 77 K followed by annealing to 500 K in vacuum. A saturation coverage of H was obtained by backfilling 1 L of H_2 at 77 K. Various coverages of CO were dosed by impinging a CO molecular beam onto the Pd−Au surface at 77 K. IR spectra were taken at 77 K.

Similar TPD experiments for surfaces with ~30% of saturation hydrogen coverage were performed to further investigate the diffusion behavior of H adatoms on the annealed Pd−Au bimetallic surface upon CO postdosing. H_2-TPD spectra from the surface with and without CO postexposure are depicted in Figure 3.5 (curves a and b), and the analogous results from the H-presaturated Pd−Au surface are included (curves c and d) for comparison. With the lowest coverage of coadsorbed CO, the desorption of unsaturated H adatoms began at ~215 K with a peak at ~246 K (Figure 3.5, curve a),

suggesting that the desorption occurred from the Pd island-like sites on the Pd−Au surface.[48] As shown in curve b of Figure 3.5, the onset temperature of H_2 desorption was reduced to ~180 K when the partially H-precovered Pd−Au surface was postexposed to a saturation coverage of CO. The peak temperature for H_2 desorption with the coadsorbed CO on the Pd−Au surface was ~213 K, which is in reasonable agreement with the desorption temperature of hydrogen from the Pd−Au alloy sites, as suggested in a previous study.[48] These observations indicate that, upon CO coadsorption, the H adatoms on the unsaturated surface diffuse away from the Pd island-like sites to the Pd−Au alloy sites. This surface diffusion is most likely due to the competitive adsorption of CO on the surface sites. When the saturated H adatom precovered Pd−Au surface is exposed to saturation coverage of CO, a portion of the surface H adatoms move to the near-surface region, due to a deficiency of empty Pd−Au alloy sites on the surface for accommodation. It should be noted that the type of adsorption sites for H and CO on the Pd−Au surface may not be the same.[48, 96] In our previous study,[48] we showed that the Pd−Au surface consists of isolated Pd sites and contiguous Pd sites, both of which are capable of adsorbing CO, while only the contiguous Pd sites have shown significant H_2 uptake at 77 K, as surfaces with only isolated Pd sites do not readily uptake hydrogen. Similar observations have been also reported in an electrochemical Pd−Au system,[96] in which Pd monomers were identified as the smallest ensemble for CO adsorption and oxidation, whereas H adsorption required sites consisting of two or more contiguous Pd atoms.

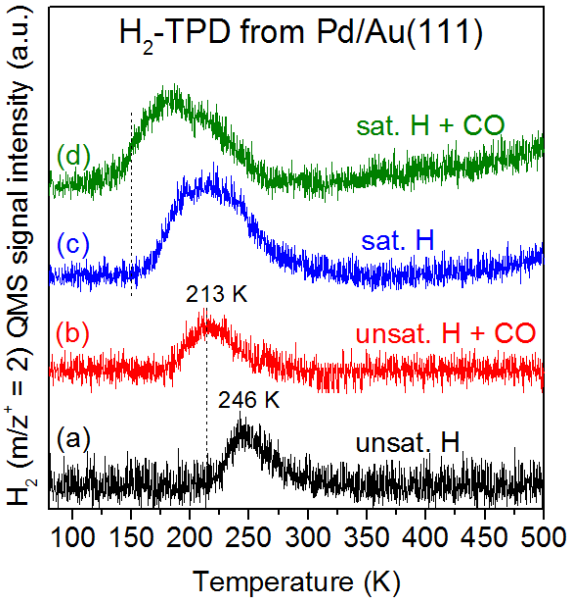

Figure 3.5. Effect of hydrogen coverage on H_2-TPD from the annealed 2 ML Pd/Au(111) bimetallic surface with and without CO coadsorption. Subsaturation coverage of hydrogen was obtained from background H_2 at 77 K. A saturation coverage of CO was dosed by a molecular beam of CO at a sample temperature of 77 K. The sample was heated from 77 K with a heating rate of 1 K/s. The H_2-TPD spectra from the H-presaturated Pd−Au surface with and without CO coadsorption are included for comparison.

3.3.3 Scattering Experiments of CO on H-Precovered Pd/Au(111)

Figure3.6 (a) shows the H_2 QMS signal during the King−Wells measurements of a CO beam impinging on the H-presaturated Pd−Au surface as a function of surface temperature ranging from 77 to 150 K. The neat CO molecular beam (nozzle pressure of 0.8 Torr) was first impinged onto the inert flag that was held in front of the sample for

5 s (from 10 to 15 s) to establish a baseline signal. The beam was then impinged onto the Pd−Au surface at the specified temperature for 60 s (from 35 to 95 s).

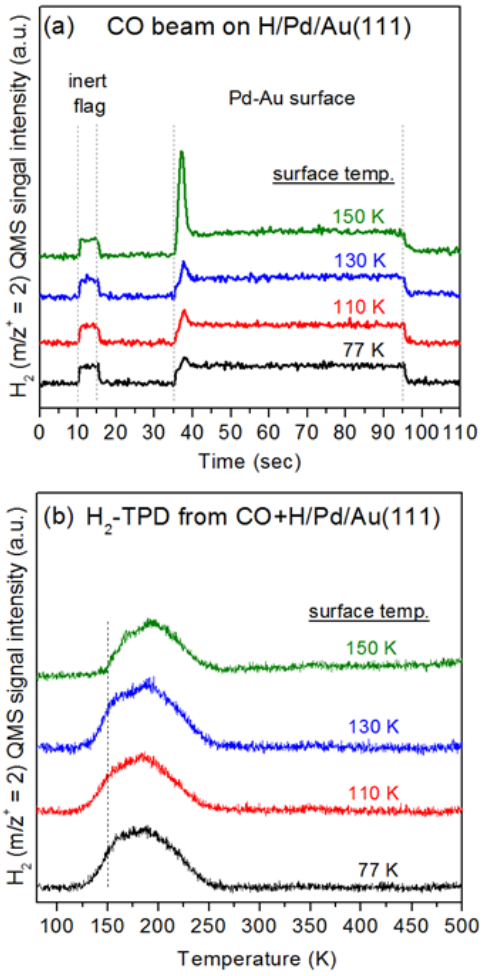

Figure 3.6. (a) King-Wells measurements of a CO beam impinging on the H-precovered annealed 2 ML Pd/Au(111) bimetallic surface at various surface temperatures (T_S). Saturation coverage of hydrogen was predosed by backfilling 1 L of H_2 at T_S = 77 K. A molecular beam of CO (nozzle pressure = 0.8 Torr) was impinged onto the inert flag for 5 s (from 10 to 15 s) and then impinged on the Pd−Au surface at T_S = 77-150 K for 60 s (from 35 to 95 s). (b) H_2-TPD spectra subsequent to the experiments in (a). For the TPD measurements in (b), the sample was cooled to 77 K and then heated at a rate of 1 K/s.

When the CO beam struck the inert flag, a constant QMS signal of H_2 was observed. The emergence of this H_2 QMS signal is likely due to the displacement of hydrogen from the walls of the chamber by competitive adsorption of CO. After removing the inert flag, the CO beam was directed at the H-saturated Pd−Au surface at 77 K, and a peak in the H_2 QMS signal was observed, indicative of the evolution of H_2 from the surface. It has been reported that nascently adsorbed CO on the Pd(111) surface can induce the recombinative desorption of precovered H adatoms,[102-103] since a lower amount of H desorption was detected from the CO-coadsorbed surface relative to a CO-free surface in TPD measurements. The molecular beam experiments in this study provide direct evidence that surface H adatoms recombinatively desorb from the Pd−Au surface during CO postexposure. When CO impingement was carried out at higher surface temperatures, the H_2 evolution peak became sharper and larger, which is consistent with the decreasing trend in H_2 desorption areas observed in the subsequent TPD measurements (Figure 3.6(b)).

Saturated H adatoms on the surface become less stable and begin to desorb at ~150 K from the (CO-free) Pd−Au substrate (Figure 3.3(a)). Accordingly, a higher surface temperature is speculated to destabilize the surface H adatoms, thus increasing the probability for recombinative desorption of hydrogen (or H_2 evolution) induced by the CO coadsorption. Figure 3.6(b) also shows that, upon CO coadsorption, the onset temperature for hydrogen desorption shifted to a lower temperature and a shoulder was

observed at ~160-170 K, which is suggestive of the formation of relatively unstable near-surface H as discussed earlier.

Not surprisingly, the CO-induced recombinative desorption of H adatoms from the Pd−Au surface is also dependent on the flux rate of CO onto the surface. Figure 3.7(a) and (b) displays the QMS signals for H_2 and CO, respectively, during the King−Wells measurements of the H-presaturated Pd−Au surface upon impingement of a CO beam with various fluxes at 150 K. Variations in flux rates of CO were achieved by changing the pressure of CO in the nozzle from 0.2 to 0.6 Torr, and the signal strength shown from 10 to 15 s in Figure 3.7(b) scales with the beam flux.

As shown in Figure 3.7(a), with the lowest CO flux rate used here (i.e., CO nozzle pressure = 0.2 Torr), the evolution of hydrogen from the Pd−Au surface during CO impingement lasted for ~32 s. The hydrogen evolution period became shorter when the flux rate of CO was increased due to quicker saturation of CO on the surface.

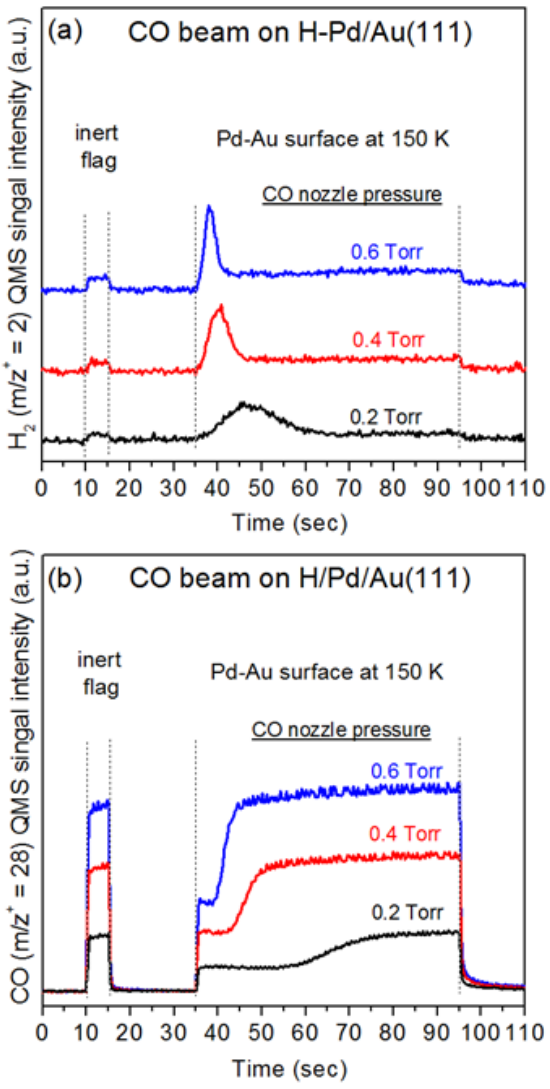

Figure 3.7. QMS signals of (a) H_2 and (b) CO during King−Wells measurements of a CO beam impinging on the H-precovered annealed 2 ML Pd/Au(111) bimetallic surface with various nozzle pressures of CO. A saturation coverage of hydrogen was achieved by backfilling 1 L of H_2 at 77 K. A molecular beam of CO was impinged onto the inert flag for 5 s (from 10 to 15 s) and then impinged on the Pd−Au surface at 150 K for 60 s (from 35 to 95 s).

Figure 3.7(b) shows the detected QMS signals for CO during the same course of King−Wells measurements. When the CO beam was impinged on the inert flag, a flat CO QMS signal was detected due to scattering of the beam with negligible adsorption on the sample. As mentioned earlier, the areas of the measured CO QMS signals from the inert flag can be used to estimate the relative flux rates of the CO beams generated from the various nozzle pressures. The flux rates of CO beams at 0.6 and 0.4 Torr are estimated to be ~3.4 and 2.3 times greater (respectively) than that achieved with the 0.2 Torr nozzle pressure. When the CO beam was impinged onto the H-precovered Pd−Au surface, the intensity of the CO QMS signal was lower than that observed for impingement on the inert flag due to the adsorption of CO on the surface. The measured initial sticking probabilities of CO for the entire CO nozzle pressures studied here were between ~0.47 and ~0.5. As the adsorbed CO molecules saturated the Pd−Au surface, the sticking probability approached zero, and the intensities of the CO QMS signals from the inert flag and from the sample surface became nearly identical.

A subtle change in the adsorption probability of CO versus time (i.e., coverage) for CO impingement on the Pd−Au surfaces with and without H presaturation is shown in Figure 3.8. Here, a CO molecular beam generated with a CO nozzle pressure of 0.6 Torr was impinged upon each surface, held at a surface temperature of 150 K.

As expected, virtually no difference in the H_2 and CO QMS signals was observed when the CO beam impinged on the inert flag (from 10 to 15 s) for the two experiments

(Figure 3.8(a)). However, the initial intensities of the CO QMS signals were different when the CO beam struck the two differently prepared surfaces, indicating that there was a difference in initial sticking probabilities for CO on each surface, which were estimated to be ~0.5 and ~0.65 for the surfaces with (red trace) and without H presaturation (green trace), respectively. These results reveal that presaturated H on the Pd−Au surface caused a decrease in the initial sticking probability of CO. Similar observations have also been reported for the Pd(111) surface.[102] For the Pd−Au surface without H presaturation, the sticking probability of CO monotonically decreased as the CO coverage increased, whereas, on the H-presaturated Pd−Au surface, the sticking probability of CO first increased and then decreased upon CO impingement.

Figure 3.8(b) depicts the CO and H_2 signals for CO impingement on the H-presaturated Pd−Au surface, enlarged to highlight features. It is noted that the change in CO sticking probability from increasing to decreasing (observed for the red trace at the dotted line) coincided with the evolution of hydrogen from the surface (blue trace). Accordingly, the increase in CO sticking probability in the early stages of CO impingement on the H-presaturated Pd−Au surface could be explained by site opening due to displacement of H adatoms by postexposed CO. The sticking probability for CO increased until the site displacement was completed and then decreased in a manner similar to that on the Pd−Au surface without H presaturation.

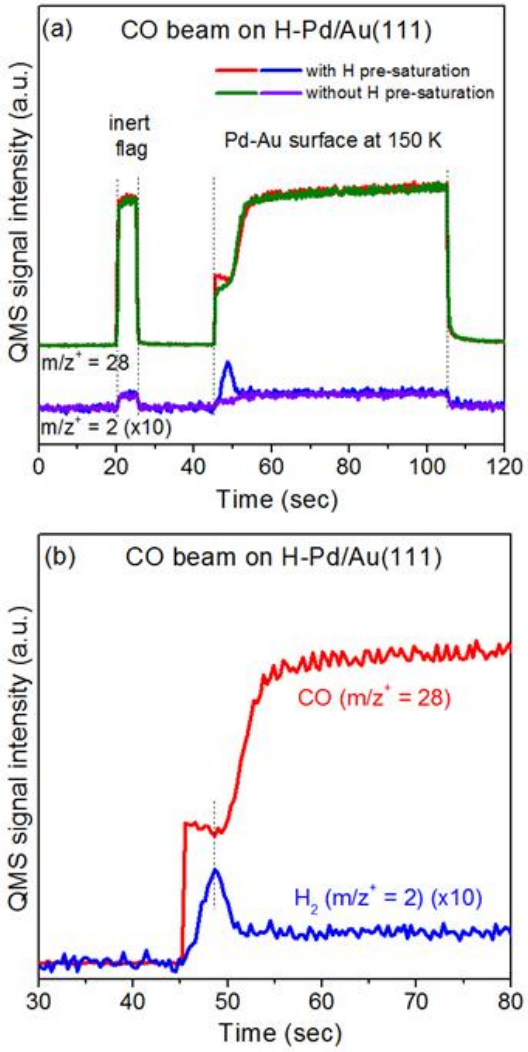

Figure 3.8. (a) King−Wells measurements of CO beam impingement on the 2 ML Pd/Au(111) surface. A saturation coverage of hydrogen was achieved by backfilling 1 L of H_2 at a surface temperature of 77 K. A molecular beam of CO (nozzle pressure = 0.6 Torr) was impinged onto the inert flag for 5 s (from 20 to 25 s, as shown by vertical dashed lines) and then impinged on the H-presaturated Pd−Au surface at 150 K for 60 s (from 45 to 105 s, as shown by vertical dashed lines) while monitoring CO (red trace) and H_2 (blue trace) via QMS. For comparison, a control experiment was performed under the same conditions, but without hydrogen predosing (green trace: CO; purple trace: H_2). (b) Enlargements of CO (red trace) and H_2 (blue trace) QMS signals for King−Wells measurement of CO impingment on the H-presaturated Pd−Au surface in (a).

3.4 CONCLUSIONS

The interactions of hydrogen and CO with the Pd−Au bimetallic surface were studied by molecular beam scattering of CO on the H-precovered Pd/Au(111) model surface, followed by temperature-programmed desorption. TPD results show that, upon CO exposure, the hydrogen desorption peak shifted to a lower temperature and a high-temperature shoulder was largely attenuated. These observations suggest that CO competitively adsorbed on Pd island-like sites, causing surface H adatoms to diffuse away from these sites to Pd−Au alloy sites and/or into the subsurface. The evolution of H_2 was observed in CO molecular beam scattering experiments with hydrogen precovered surfaces, providing direct evidence of recombinative desorption of the H adatoms induced by CO coadsorption (even at 77 K). An increased amount of recombinative desorption of hydrogen was observed when CO was impinged at a higher surface temperature due to decreased stability of the H adatoms at higher temperatures. The presence of precovered H adatoms on the Pd−Au surface decreased the initial sticking probability of CO but displayed little influence on the subsequent desorption behavior of CO. These observations could provide insight into the interactions of hydrogen and CO with Pd−Au bimetallic surfaces, which may aid future catalyst design.

Chapter 4: Selective Hydrogen Production from Formic Acid Decomposition on Pd−Au Bimetallic Surfaces*

4.1 INTRODUCTION

Hydrogen is a promising energy carrier for electricity generation in a fuel cell; however, hydrogen storage and distribution remains a challenging issue. Recently, formic acid (HCOOH) has been proposed as a potential liquid storage medium capable of releasing H_2 under mild conditions via catalytic decomposition.[120-124] For practical applications, suitable catalysts are essential to facilitate HCOOH decomposition via dehydrogenation ($HCOOH \rightarrow H_2 + CO_2$) as opposed to dehydration ($HCOOH \rightarrow H_2O + CO$). Recently, considerable advances have been made in the selective dehydrogenation of HCOOH at ambient and near-ambient temperatures using homogeneous catalysts.[125-128] Nevertheless, the separation issues associated with homogeneous catalysts and requisite use of organic solvents and additives hamper their practical applications.[129-130] Use of heterogeneous catalysts may circumvent these issues, but improved catalytic performance under ambient conditions is still required.[129-130]

Pd is one of the most active catalysts for HCOOH decomposition.[130] Recently, heterogeneous catalysts containing Pd have been extensively studied for H_2 production

* Yu, W.-Y.; Mullen, G. M.; Flaherty, D. W.; Mullins, C. B., Selective Hydrogen Production from Formic Acid Decomposition on Pd−Au Bimetallic Surfaces. *J. Am. Chem. Soc.* **2014**, 136, 11070–11078.
W.-Y. Yu, G. M. Mullen, D. W. Flaherty and C. B. Mullins conceived and designed experiments, analyzed and discussed results, and commented on the manuscript. W.-Y. Yu performed experiments, analyzed data and wrote the paper.

via HCOOH decomposition;[31-32, 60-61, 130-138] among them, Pd−Au bimetallic catalysts have received substantial attention due to their promising performance in selective HCOOH dehydrogenation.[31-32, 60-61, 131, 138] Yet, the key factors controlling the catalytic performance (e.g., activity and selectivity) of Pd−Au bimetallic catalysts on HCOOH decomposition remain topics of debate.[31-32, 60-61, 130, 135, 138] For instance, Pd−Au alloy catalysts were reported to possess improved HCOOH dehydrogenation activity and stability relative to monometallic Pd catalysts.[31-32, 61] Such improvement has been attributed to a higher resistance to CO poisoning due to alloying of Pd with Au.[31, 61] However, a recent study indicated that alloying of Pd with Au leads to lower HCOOH decomposition activity, which was suggested to result from a ligand effect as indicated by a slight shift of the Pd $3d_{5/2}$ binding energy in X-ray photoelectron spectroscopy (XPS).[135] Apart from alloy catalysts, supported Pd−Au catalysts with core−shell structures were also tested for selective HCOOH decomposition;[60, 130, 138] a higher hydrogen yield was observed[60, 138] and attributed to the possible charge transfer between Au and Pd (i.e., a ligand effect).[138] However, it has been shown that the charge transfer between Au and Pd is insignificant owing to similar work functions between the Au and the Pd,[130] and a lower rate of HCOOH decomposition was observed for the colloidal Au−Pd core−shell nanoparticles relative to colloidal Pd nanoparticles.[130] The inconsistencies between these studies may be due to the vast diversity of preparation methods, catalyst supports, and reaction conditions employed in these studies. Indeed, classical heterogeneous catalysts are generally complex and operate at high temperatures and pressures,

increasing the level of difficulty to unravel the factors governing the catalytic properties (e.g., reactivity and selectivity). In model catalyst studies, reactions are investigated on well-defined single-crystal surfaces under ultrahigh vacuum (UHV) conditions, which enable thorough surface characterization, precise control of reactant coverages, and minimal environmental interference, thereby allowing the study between surface structures and catalytic properties of catalytic materials at the molecular level.[5-8, 10]

In this chapter, the surface chemistry of HCOOH on Pd−Au bimetallic model surfaces was investigated using temperature-programmed desorption (TPD) and reactive molecular beam scattering (RMBS) methods in an attempt to improve the fundamental understanding of the selective decomposition of HCOOH on Pd−Au catalysts. A variety of Pd−Au bimetallic surfaces, prepared by varying the Pd coverage deposited on the Au(111) surface followed by annealing, were characterized by H_2-TPD and tested via HCOOH-RMBS and HCOOH-TPD under UHV conditions. Two types of surface sites, i.e., Pd−Au interface sites and Pd(111)-like sites (sites that lack neighboring Au atoms), were characterized qualitatively and quasi-quantitatively for the Pd−Au surface by H_2-TPD. Reactivity tests based on HCOOH-RMBS demonstrate the critical role of Pd−Au interface sites for selective hydrogen production via catalytic HCOOH dehydrogenation. Although increasing the fraction of Pd(111)-like sites on the surface increased the rate of HCOOH decomposition, the selectivity toward hydrogen production decreased because the Pd(111)-like sites primarily catalyze dehydration of HCOOH. HCOOH-TPD results reveal that reaction-limited desorption of CO_2 occurred at a relatively low temperature,

indicating that the reaction intermediate(s) from HCOOH decomposition could be readily decomposed on the Pd−Au surface. These observations suggest that the exceptional performance of Pd−Au catalysts for selective HCOOH decomposition could be rationalized by the "ensemble" effect. The experimental results shown in this study provide direct evidence that the selectivity for HCOOH reaction pathways can be tailored by the intermixing of Pd and Au atoms on catalytically active surfaces, which is consistent with predictions from a recent theoretical study.[139]

4.2 Experimental Methods

All experiments in this study were conducted in a molecular beam surface scattering apparatus with a base pressure of less than 1×10^{-10} Torr.[48-49, 84-86] Briefly, the apparatus contains an Auger electron spectrometer (Physical Electronics 10−500), a quadrupole mass spectrometer (Extrel C-50), a Fourier transform infrared spectrometer (Bruker Tensor 27) combined with a mercury−cadmium−telluride (MCT) detector (Infrared Associates), as well as nozzles and apertures for generating two separate molecular beams.

The Au(111) single-crystal sample is a circular disk (Princeton Scientific, 12 mm in diameter × 2 mm thick) and held in place by a Mo wire fitted around a groove cut into the side of the sample. This wire is also used to resistively heat the sample and provide thermal contact between the sample and a liquid nitrogen bath for cooling. The temperature of the sample was measured with a K-type (Alumel−Chromel) thermocouple

placed into a small hole in the edge of the disk-shaped sample. The Au(111) surface was periodically cleaned by Ar ion bombardment (2 keV), carried out at room temperature, followed by an anneal to 800 K. The cleanliness of the surface was verified by Auger electron spectroscopy (AES) with a beam energy of 3 keV and emission current of 1.5 mA.

Pd−Au model surfaces were prepared by depositing Pd atoms from a homemade thermal evaporator onto the Au(111) surface at 77 K and then annealing the surface to 500 K for 10 min under UHV conditions. The deposition rate of Pd was calibrated with a quartz crystal microbalance (QCM) controller (Maxtek Inc.) by assuming that the thickness of 1 monolayer (ML) of Pd is equal to the diameter of a Pd atom, which is 0.274 nm. Growth of the Pd overlayer on the Au(111) surface at 77 K is believed to obey a layer-by-layer mechanism based on a previous study[88] in which a Pd film was grown on the Au(111) surface at the higher temperature of 150 K. Upon annealing, some of the surface Pd atoms diffuse into the subsurface of the Au(111) sample, forming a Pd−Au alloy surface.[31-32, 17, 44, 88] AES spectra for the as-deposited and annealed Pd/Au(111) surfaces are shown in Figure 4.1. Table 4.1 summarizes the Pd(333 eV)/Au(74 eV) AES intensity ratios of as-deposited and annealed Pd/Au(111) surfaces.

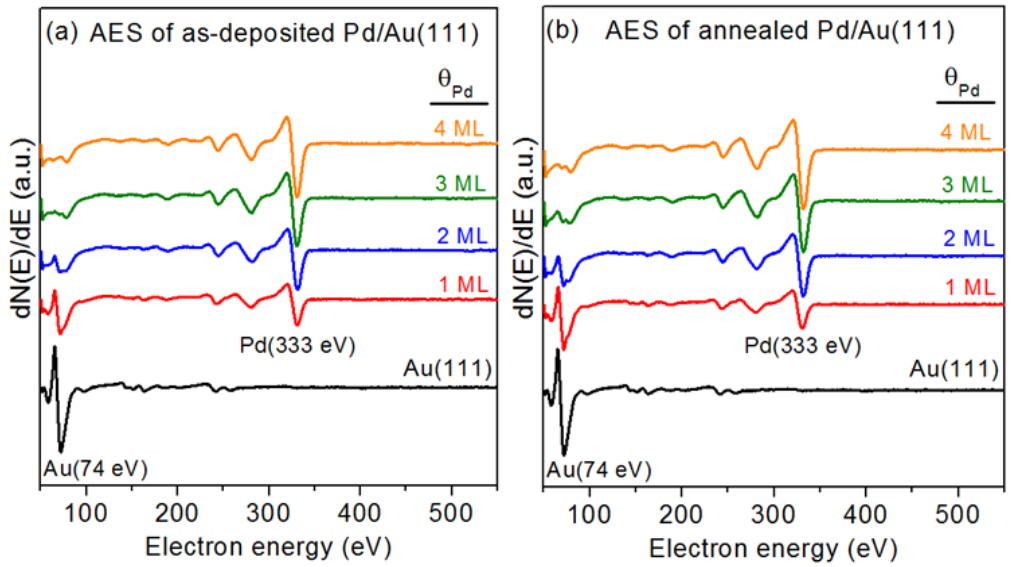

Figure 4.1. AES spectra for the Pd/Au(111) surfaces (a) before and (b) after annealing to 500 K for 10 min in UHV. Various coverages of Pd overlayers were initially deposited onto the Au(111) surface at a surface temperature of 77 K.

Table 4.1. Pd(333 eV)/Au(74 eV) AES intensity ratios of as-deposited and annealed Pd/Au(111) surfaces.

Initial Pd coverage (ML)	Pd(333 eV)/Au(74 eV) AES intensity ratios (a.u.)	
	As-deposited Pd/Au(111) surface	Annealed Pd/Au(111) surface
1	0.9	0.6
2	3.7	2.1
3	-	6.6
4	-	-

Temperature-programmed desorption (TPD) is a useful tool for providing information concerning the interactions between the surface (adsorbent) and the adsorbed species (adsorbate).[140-142] In the TPD measurement, a temperature ramp is applied to the surface and the rate of desorbing molecules is measured by monitoring the increase in

evolving gas-phase species as a function of surface temperature using a mass spectrometer. Analyses of a series of TPD spectra can provide information such as the activation energy for desorption, the strength of the adsorbate−adsorbent interaction, and the relative surface coverage of adsorbate.[140-142] The interactions (i.e., adsorption, absorption, diffusion, and desorption) of hydrogen with Pd/Au(111) surfaces have been studied previously using H_2-TPD.[48] In this study, H_2-TPD was conducted to characterize the annealed Pd/Au(111) surfaces for qualitative and quasi-quantitative analyses of surface sites. Hydrogen was dosed by impinging a molecular beam of H_2 onto the Pd−Au surface at a surface temperature of 77 K to yield a saturation coverage. Afterward, the H-presaturated surface was heated to 500 K at a rate of 1 K/s, while the signal for $m/z^+ = 2$ (H_2) was monitored by a quadrupole mass spectrometer (QMS).

Application of molecular beam methods to well-defined model catalysts enables the detailed investigation of the chemical kinetics of surface reactions.[9, 143] By correlating the chemical kinetics with the surface structure, mechanistic insights into the kinetic phenomena on catalyst surfaces can be obtained.[9, 143] In this study, we used reactive molecular beam scattering (RMBS) to acquire kinetic information (i.e., HCOOH decomposition rate and turnover frequency for hydrogen production) on our Pd−Au surface. HCOOH-RMBS experiments were conducted by impinging a molecular beam of HCOOH onto the sample surface that was held at a temperature of 500 K. The flux of the HCOOH beam was estimated to be $\sim 5 \times 10^{14}$ molecules cm^{-2} s^{-1} using HCOOH-TPD spectra from the clean Au(111) surface (Figure 4.2) and assuming 1 ML of HCOOH

equals ~1.39 × 10^{15} molecules cm^{-2} [the surface atom density of Au(111)]. Prior to exposure to the sample surface, the HCOOH beam was first impinged onto an inert stainless steel flag that was held in front of the sample to establish baseline signals. Products and unreacted HCOOH molecules were detected by monitoring the following QMS signals for each species: HCOOH (m/z^+ = 46, 44, 29, and 28), CO_2 (m/z^+ = 44 and 28), H_2 (m/z^+ = 2), CO (m/z^+ = 28), and H_2O (m/z^+ = 18). The amount of each species is proportional to the integral of its QMS intensity. The integrals of QMS intensities for CO_2 (m/z^+ = 44) and CO (m/z^+ = 28) were corrected by considering the contribution from the corresponding mass fragments of HCOOH and those from HCOOH and CO_2, respectively.

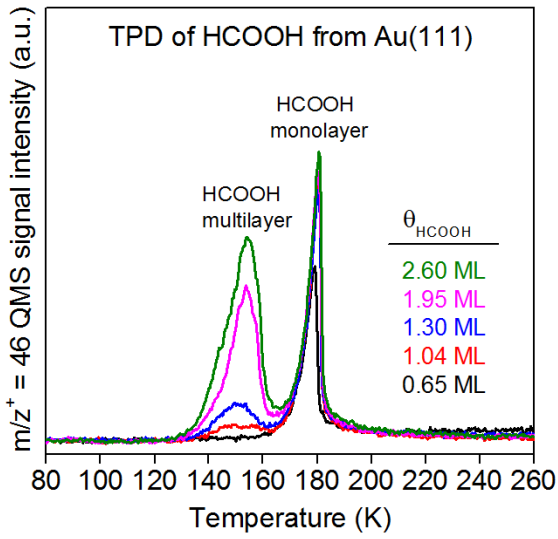

Figure 4.2. TPD spectra of HCOOH from the Au(111) surface. Various coverages of HCOOH were dosed onto the Au(111) surface by impinging a molecular beam of HCOOH onto the surface at a surface temperature of 77 K. The heating rate was 1 K/sec.

HCOOH-TPD was carried out by adsorbing HCOOH onto the sample surface at 77 K via a molecular beam followed by annealing to 500 K at a rate of 1 K/s. The QMS signals during HCOOH-TPD were detected in a manner similar to that described for HCOOH-RMBS experiments. The coverage of the HCOOH overlayer was determined by TPD of HCOOH from the clean (Pd-free) Au(111) surface.

4.3 Results and Discussion

4.3.1 H_2-TPD from Pd−Au Surfaces

In order to establish a structure−activity relationship for HCOOH decomposition on the Pd−Au surface, a characterization technique that can provide both qualitative and quantitative information on surface properties is essential. Probe molecules such as CO and H_2 are commonly used to characterize the structure and composition of catalytic surfaces.

Adsorption of CO on the Pd−Au model surface has been extensively studied using CO-RAIRS (reflection−absorption infrared spectroscopy)[17, 39, 49, 89, 93, 144] and CO-TPD.[45, 49, 89, 94, 144] Using CO-RAIRS, qualitative information such as the type of adsorption sites occupied by CO (e.g., atop sites, 2-fold or 3-fold bridge sites) on the Pd−Au surface can be inferred by the intramolecular CO stretch frequency[17, 39, 49, 89, 93, 144] due to varying degrees of π-antibonding back-donation from the surface electrons; however, it has been shown that quantitative analysis using CO-RAIRS becomes difficult when contiguous Pd sites are present on the Pd−Au surface, probably due to the

vibrational coupling effect that attenuates the IR intensity at high surface CO coverages.[93] Quantitative analysis based on CO-TPD is complicated for the annealed Pd/Au(111) surfaces as the CO desorption peak is fairly broad[49] (likely as a result of the superposition of multiple CO desorption peaks), making the surface site assignment and peak deconvolution difficult.

The interaction of hydrogen with the Pd−Au model surface has been investigated using H_2-TPD.[48, 53, 74, 77] In a previous study using H2-TPD we showed that the presence of contiguous Pd atoms (characterized by CO-RARIS) on the annealed Pd/Au(111) surfaces is crucial for dissociative adsorption of hydrogen molecules at 77 K.[48] Upon heating, hydrogen adatoms recombinatively desorb from the Pd−Au surface. According to the desorption temperature of hydrogen, two distinct surface sites, i.e., Pd−Au interface and Pd(111)-like sites (lacking adjacent Au atoms), were qualitatively assigned.[48] Furthermore, a quasi-quantitative analysis is feasible by performing peak deconvolution for the H_2-TPD spectra. Accordingly, here we utilized H_2-TPD to characterize the Pd−Au surfaces that were generated by annealing the as-deposited Pd/Au(111) surfaces in UHV.

Figure 4.3 depicts the H_2-TPD spectra for desorption of saturation coverages of hydrogen from the annealed Pd−Au surfaces with initial Pd coverages ranging from 0 to 4 ML. The annealed 1 ML Pd/Au(111) surface exhibited a broad H_2-TPD peak centered at ~208 K. Since this hydrogen desorption temperature lies between those for Au(111)

(~108 K)[69] and Pd(111) surfaces (~310−320 K),[53, 66] we speculate that this desorption site consists of Au and Pd atoms and hydrogen desorption likely occurs at the interface between Au and Pd atoms.[48] This H_2-TPD feature is relatively broad because the desorption temperature of hydrogen depends on the relative number of Pd and Au atoms associated with the Pd−Au interface sites during the desorption process. In general, a higher hydrogen desorption temperature would be expected when H atoms bind to more Pd atoms in the Pd−Au interface sites since the bond strength of Pd−H is stronger than that of Au−H.

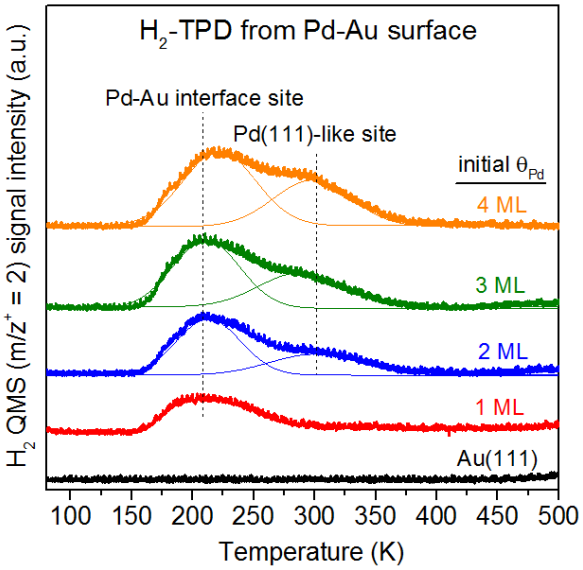

Figure 4.3. H_2-TPD spectra from Pd−Au surfaces with initial Pd coverages ranging from 0 to 4 ML. Pd−Au surfaces were prepared by depositing Pd atoms onto the Au(111) surface at a surface temperature (T_S) of 77 K followed by annealing to 500 K in UHV. A molecular beam of H_2 was impinged onto each surface at T_S = 77 K to yield a saturation coverage of H adatoms. Heating rate was 1 K/s.

For the annealed 2 ML Pd/Au(111) surface, the peak of hydrogen desorption from the Pd−Au interface sites (at ~210 K) intensified and an additional shoulder at a higher temperature (~300 K) was observed. The desorption temperature of this high-temperature shoulder is fairly close to the desorption temperature of hydrogen from the Pd(111) surface,[53, 66] which suggests formation of Pd(111)-like sites on the annealed 2 ML Pd/Au(111) surface. Both hydrogen desorption features (i.e., from the Pd−Au interface and Pd(111)-like sites) grew in intensity on the Pd−Au surfaces prepared with higher initial Pd coverages of 3 and 4 ML.

The integral of the peak area under each H_2-TPD trace is proportional to the amount of hydrogen that desorbed from each Pd−Au surface.[140-142] It is noted that no measurable H_2 desorption was observed from the clean (Pd-free) Au(111) surface under the same set of conditions. In other words, the surface sites for hydrogen uptake are associated with surface Pd atoms. Sykes and co-workers[75-76] employed scanning-tunneling microscopy (STM) to observe H adatoms on Pd/Au(111) surfaces. STM imaging revealed that hydrogen molecules dissociatively adsorb on surface Pd atoms, and no spillover onto the Au terrace sites was observed.[75-76] Therefore, the integral peak area under each H_2-TPD trace should also reflect the relative number of surface Pd atoms for dissociative adsorption of hydrogen. By integrating the peak for H_2-TPD spectra, the relative number of surface Pd atoms on each Pd−Au surface was calculated (relative to that of the annealed 4 ML Pd/Au(111) surface). As listed in Table 4.2, the relative

number of surface Pd atoms is 0.32, 0.63, 0.84, and 1 for the Pd−Au surface with the initial Pd coverage of 1, 2, 3, and 4 ML, respectively.

Table 4.2. Relative number of surface Pd atoms, relative dispersion, fraction of Pd−Au interface sites, HCOOH conversion, HCOOH decomposition rate, turnover frequency for H_2 production, and relative H_2/CO QMS ratio on the annealed Pd/Au(111) surfaces.

Initial θ_{Pd} (ML)	Relative no. of surface Pd atoms (-)$^{\alpha, \beta}$	Relative dispersion (-)$^{\alpha, \beta}$	Fraction of Pd−Au interface sites (-)$^{\beta}$	HCOOH conversion (%)$^{\gamma}$	HCOOH decomposition rate (HCOOH cm^{-2} sec^{-1})$^{\gamma}$	TOF for H_2 production (H_2 Pd_S^{-1} sec^{-1})$^{\beta, \gamma}$	Relative H_2/CO QMS ratio (-)$^{\alpha, \gamma}$
1	0.32	1.29	1	0.7	3.5×10^{12}	0.006	2.08
2	0.63	1.26	0.66	2.8	1.4×10^{13}	0.012	1.19
3	0.84	1.12	0.62	6.7	3.3×10^{13}	0.011	1.05
4	1	1	0.60	8.8	4.4×10^{13}	0.009	1

$^{\alpha}$ relative to that of the annealed 4 ML Pd/Au(111) surface; $^{\beta}$ determined from H_2-TPD spectra (Figure 4.3); $^{\gamma}$ determined from HCOOH-RMBS spectra (Figure 4.5).

Dispersion, defined as the fraction of atoms of a material exposed to the surface, is an important indicator in heterogeneous catalysis since catalytic reactions occur on surfaces. For supported Pd catalysts, dispersion is generally expressed as the ratio of the amount of hydrogen uptake (determined from hydrogen chemisorption) to the total amount of Pd. In this study, the relative dispersion was computed by dividing the relative number of surface Pd atoms (determined from H_2-TPD) on each Pd−Au surface by its initial Pd coverage (relative to that of the annealed 4 ML Pd/Au(111) surface). The relative dispersion was found to gradually decrease as the initial Pd coverage was increased (Table 4.2), suggesting that a higher portion of Pd atoms was not surface accessible when the Pd−Au surface was prepared with a higher initial Pd coverage.

In order to quantify the relative number of Pd−Au interface and Pd(111)-like sites on each Pd−Au surface, the H_2-TPD spectra in Figure 4.3 were fitted by peak deconvolution, and the corresponding peak integrals are displayed in Figure 4.4. As the initial Pd coverage was increased, the amount of hydrogen desorption from the Pd−Au interface and Pd(111)-like sites both increased (Figure 4.4), indicating that the number of both types of surface sites increased since the amount of hydrogen desorption is proportional to the number of surface sites. The fraction of Pd−Au interface sites on each Pd−Au surface was calculated by the integral of hydrogen desorption from Pd−Au interface sites divided by that of the total hydrogen desorption from both Pd−Au interface and Pd(111)-like sites. The fraction of Pd−Au interface sites is unity for the annealed 1 ML Pd/Au(111) surface and reduces to ~0.6 for surfaces with higher initial Pd coverages, i.e., 2−4 ML (see Table 4.2).

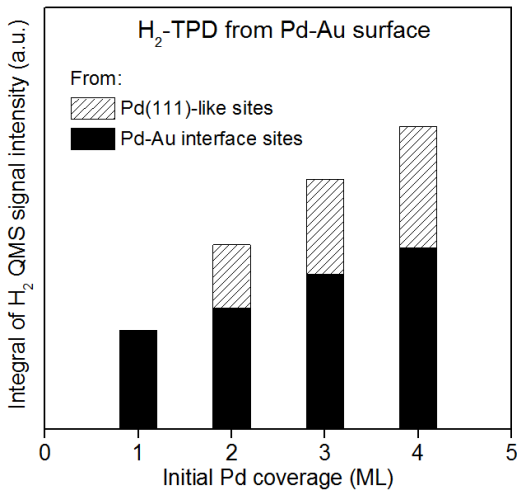

Figure 4.4. Integrals of H_2 QMS signal intensity for H_2-TPD spectra shown in Figure 4.3 after peak deconvolution.

4.3.2 HCOOH-RMBS on Pd−Au Surfaces

The reactivity of HCOOH on Pd−Au surfaces was evaluated by HCOOHRMBS. A room-temperature beam of HCOOH vapor was generated with a translational energy of ~0.1 eV. The trapping probability of HCOOH under these conditions will be very close to unity regardless of the surface temperature. At elevated surface temperatures trapped molecules will undergo a kinetic competition between surface reaction and desorption.[145-148]

Figure 4.5 shows the HCOOH-RMBS results for annealed Pd/Au(111) surfaces with various initial Pd coverages. The HCOOH beam was first impinged onto the inert stainless steel flag that was held in front of the sample for 5 s (from 30 to 35 s) to establish baseline signals and then impinged onto the Pd−Au surface that was held at a surface temperature at 500 K for 5 s (from 65 to 70 s) to complete a King and Wells measurement.[116-117]

When the HCOOH molecular beam struck the inert flag, QMS signals for m/z^+ = 46, 44, and 28 were observed, in which the m/z^+ = 46 signal is the parent mass of HCOOH and the m/z^+ = 44 and 28 signals are mass fragments of HCOOH from QMS ionizer dissociation (similar m/z^+ ratios for masses 46, 44, and 28 were observed when shooting the HCOOH beam directly into QMS). The m/z^+ = 18 signal is due to a water impurity in the HCOOH[85] as we observed this mass signal when shooting the HCOOH beam directly into QMS as well. As expected, no QMS signal for H_2 (m/z^+ = 2) was

observed when scattering the beam from the inert flag. After removing the inert flag, the HCOOH beam was directed onto the annealed 1 ML Pd/Au(111) surface, where a QMS signal for H_2 production ($m/z^+ = 2$) was observed (Figure 4.5a). The emergence of the H_2 QMS signal clearly shows that the dehydrogenation reaction occurred on the 1 ML Pd/Au(111) surface.

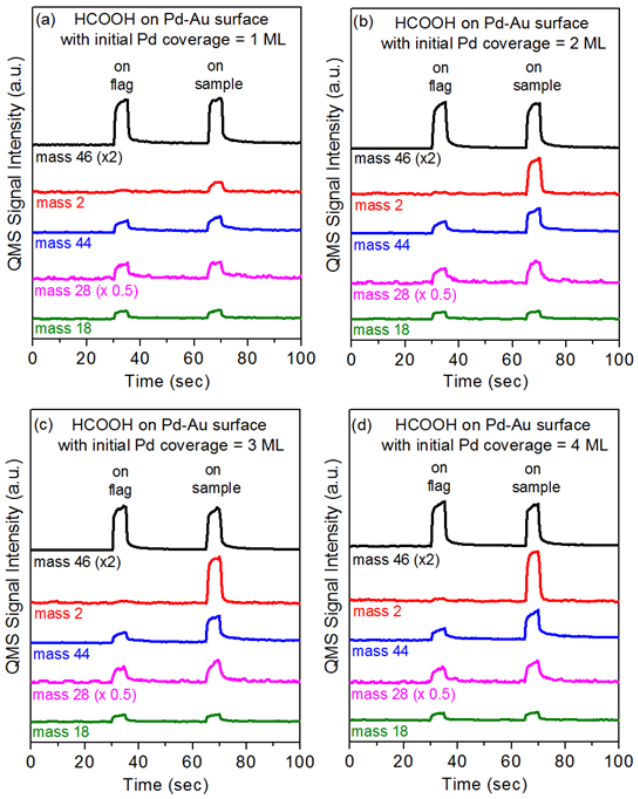

Figure 4.5. HCOOH-RMBS results for Pd−Au surfaces with various initial Pd coverages. Pd−Au surfaces were prepared by depositing Pd atoms onto the Au(111) surface at a surface temperature of 77 K followed by annealing to 500 K in UHV. The surface was held at 500 K during HCOOH-RMBS measurements. HCOOH beam was impinged onto the inert flag for 5 s (from 30 to 35 s) and then onto the sample surface for 5 s (from 65 to 70 s). HCOOH flux was $\sim 5 \times 10^{14}$ molecules $cm^{-2}\,s^{-1}$. Panels a−d have the same ordinate scale.

Apart from H_2 production, CO_2 (the byproduct of HCOOH dehydrogenation) and CO (the byproduct product from HCOOH dehydration) also formed as indicated by comparison of m/z^+ = 44 and 28 signals for impingement of the HCOOH beam on the inert flag and on the Pd−Au surface. These results show that the presence of Pd adatoms on the Pd−Au surface can facilitate HCOOH decomposition since no reactivity was observed on the Au(111) surface under the same testing conditions (Figure 4.6). It is noted that formation of H_2O due to HCOOH dehydration was difficult to observe in this system, which likely results from efficient pumping of H_2O by the cryogenic probe cooled by liquid nitrogen.

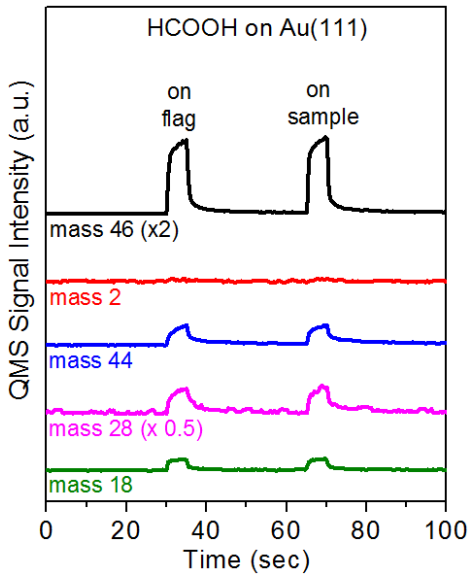

Figure 4.6. RMBS results for HCOOH on the Au(111) surface. The surface was held at 500 K during the HCOOH-RMBS measurement. The HCOOH beam was impinged onto the inert flag for 5 sec (from 30 to 35 sec) and then onto the sample surface for 5 sec (from 65 to 70 sec). The flux rate of the HCOOH molecular beam was ~5×10^{14} molecules cm^{-2} sec^{-1}.

Figure 4.5b−d shows the HCOOH-RMBS results for Pd−Au surfaces with higher initial coverages of Pd (i.e., 2−4 ML). For convenience of comparison, the integrals of QMS intensities for each species produced (i.e., H_2, CO_2, and CO) during HCOOH-RMBS (Figure 4.5) are summarized in Figure 4.7.

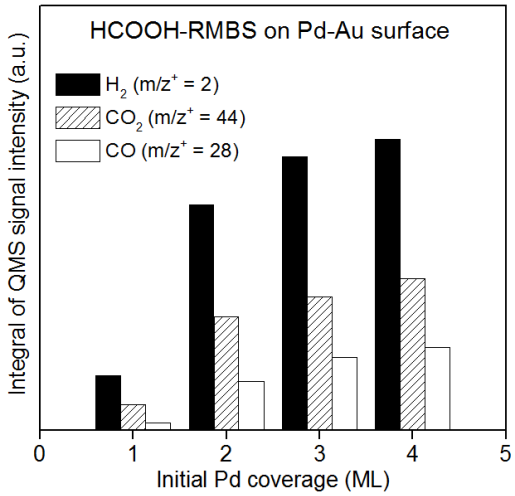

Figure 4.7. Integrals of QMS signal intensities for H_2, CO, and CO_2 produced on annealed Pd/Au(111) surfaces with various initial Pd coverages during HCOOH-RMBS (Figure 4.5).

The amount of H_2, CO_2, and CO generated on the Pd−Au surface increased as the initial Pd coverage was increased, suggestive of an activity enhancement for overall HCOOH decomposition. By comparing the $m/z^+ = 46$ signals obtained from the HCOOH beam impinging on the inert flag and on the sample surface, conversion of HCOOH on each surface can be estimated. As listed in Table 4.2, the estimated single-

collision conversion of HCOOH on the Pd−Au surface increased from 0.7% to 8.8% as the initial Pd coverage was increased from 1 to 4 ML.

Figure 4.8a depicts the rate of HCOOH decomposition as a function of the relative number of surface Pd atoms on Pd−Au surfaces. The rate of HCOOH decomposition is the product of the conversion of HCOOH and the flux of the HCOOH molecular beam (~5×10^{14} molecules cm^{-2} s^{-1}) in HCOOHRMBS experiments.

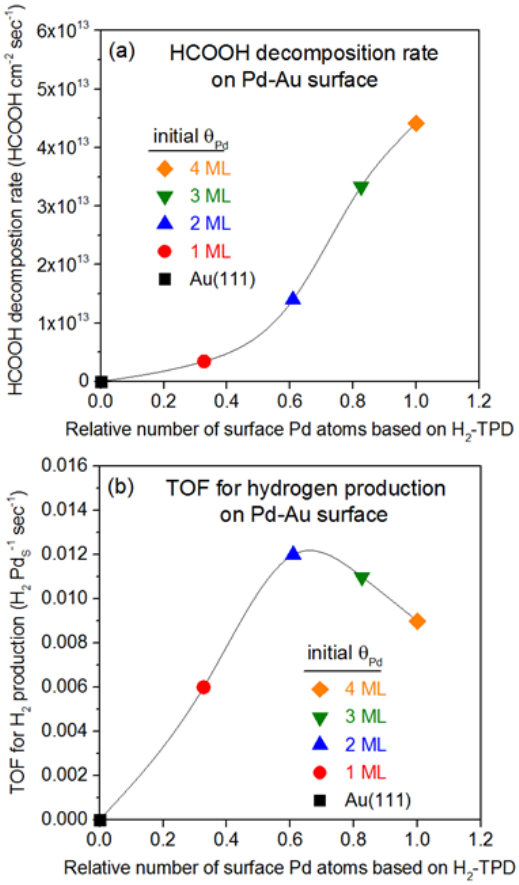

Figure 4.8. (a) Rate of HCOOH decomposition and (b) turnover frequency for H_2 production on Pd−Au surfaces during HCOOH-RMBS experiments shown in Figure 4.5.

As illustrated in Figure 4.8a, the rate of HCOOH decomposition increased as the relative number of surface Pd atoms increased. A sharp increase in the rate of HCOOH decomposition was observed when the relative number of surface Pd atoms was larger than 0.32 (i.e., the annealed 1 ML Pd/Au(111) surface). Taking the relative number of Pd−Au interface and Pd(111)-like sites into account, this sharp increase in the HCOOH decomposition rate observed here is believed to be related to formation of Pd(111)-like sites on the Pd−Au surface. In other words, Pd(111)-like sites are more catalytically active for HCOOH decomposition than Pd−Au interface sites.

The specific activity of Pd−Au surfaces for H_2 production is expressed in terms of turnover frequency (TOF_{H2}) or the number of H_2 molecules produced per surface Pd site (Pd_S) per unit time. In this study, the TOF_{H2} on Pd−Au surfaces was computed from the integral of QMS signal intensities for H_2 production from HCOOH-RMBS experiments and H_2 desorption from TPD measurements (details associated with these calculations can be found in the Appendix). Figure 4.8b displays the calculated TOF_{H2} of each Pd−Au surface as a function of the relative number of surface Pd atoms on the Pd−Au surface. With the increase of the relative number of surface Pd atoms, the TOF_{H2} first increased to 0.012 H_2 Pd_S^{-1} s^{-1} and then slightly decreased to 0.009 H_2 Pd_S^{-1} s^{-1}. Because the rate of HCOOH decomposition increased monotonically (Figure 4.8a), the decrease in TOF_{H2} observed here suggests that the activity of HCOOH dehydration was

enhanced, causing the selectivity for hydrogen production to be reduced as the relative number of surface Pd atoms increased.

The selectivity for H_2 production via HCOOH decomposition depends directly on the fraction of Pd atoms that exist at the Pd−Au interface or Pd(111)-like sites on the Pd−Au surface. The selectivity for hydrogen production (or dehydrogenation selectivity) can be expressed by the relative H_2/CO or CO_2/CO QMS area ratios (relative to that of the annealed 4 ML Pd/Au(111) surface) in HCOOH-RMBS experiments. Figure 4.9 shows the relative H_2/CO QMS area ratios and the fraction of Pd−Au sites on Pd−Au surfaces as a function of the relative number of surface Pd atoms (the trends of relative H_2/CO and CO_2/CO QMS area ratios were almost identical, Figure 4.10).

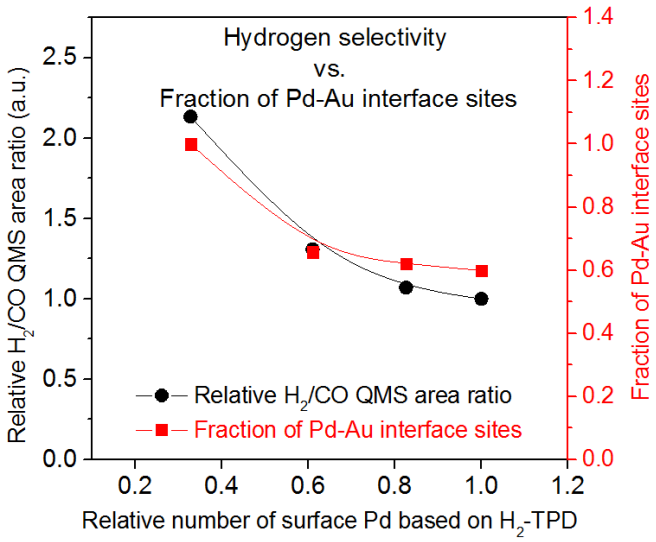

Figure 4.9. Relative H_2/CO QMS area ratios measured from HCOOH-RMBS experiments (Figure 4.5), and fraction of Pd−Au interface sites on Pd−Au surfaces determined by H_2-TPD measurements (Figure 4.3).

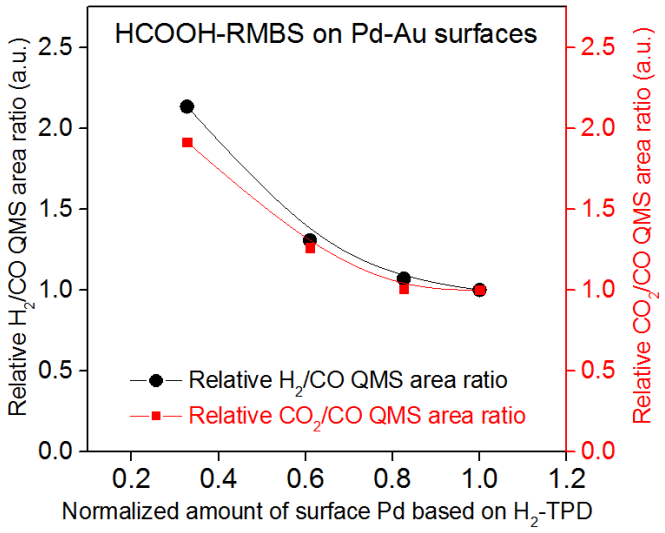

Figure 4.10. Relative CO_2/CO QMS area ratios measured from HCOOH-RMBS experiments (Figure 4.5), and fraction of Pd−Au interface sites on Pd−Au surfaces determined by H_2-TPD measurements (Figure 4.3).

Figure 4.9 shows that the relative QMS ratio of H_2/CO, the selectivity toward hydrogen production, decreased with increasing relative number of surface Pd atoms. This decrease in hydrogen selectivity correlates with a decrease in the fraction of Pd atoms that exist as Pd−Au interface sites, suggesting that HCOOH dehydrogenation occurs at Pd−Au interface sites on the surface. The observations based on H_2-TPD and HCOOH-RMBS correlate the structure of Pd−Au surfaces with their catalytic properties on HCOOH decomposition: (1) the presence of Pd−Au interface sites on Pd−Au surfaces is crucial for selective HCOOH dehydrogenation; (2) formation of Pd(111)-like sites on Pd−Au surfaces enhances the overall HCOOH decomposition at the expense of the dehydrogenation selectivity. It is noted that high selectivity for HCOOH

dehydrogenation was reported in some studies employing supported monometallic Pd catalysts.[133, 135, 137] Since the catalytic performance of supported monometallic metal catalysts often results from an accumulative contribution from both metal nanoparticles and the support used, the observed high selectivity[133, 135, 137] may be due to participation of the support in the surface reaction or metal−support interactions.

Our experimental observations are conceptually consistent with a recent theoretical study.[139] Using density function theory (DFT) methods, Yuan and Liu[139] calculated the potential energy profile for possible reaction pathways for HCOOH decomposition on four different surfaces: the Pd(111) surface, the Pd monolayer supported on the Au(111) surface (abbreviated Pd ML), and two Pd-decorated Au(111) surfaces (abbreviated Pd_6Au_3 and Pd_3Au_6). Energy barriers for HCOOH activation to form formate (HCOO) (via O−H bond cleavage) or carboxyl (COOH) intermediates (via C−H bond cleavage) are lower on the Pd(111) and Pd ML surfaces in comparison to those on the Pd_6Au_3 and Pd_3Au_6 surfaces.[139] These results support our observations that the rate of the HCOOH decomposition is enhanced by formation of Pd(111)-like sites on the Pd−Au surface. They also found that the energy barriers for further decomposition of HCOO or COOH intermediate to CO_2 and H are comparable for all surfaces investigated; however, higher energy barriers are required for dissociation of COOH into CO and OH on the Pd_6Au_3 and Pd_3Au_6 surfaces (∼1 eV) than on the Pd(111) and Pd ML surfaces (∼0.5−0.6 eV).[139] In other words, the dehydration pathway is inhibited relative to the dehydrogenation pathway on the Pd_6Au_3 and Pd_3Au_6 surfaces, which is consistent

with the importance of Pd−Au interface sites for HCOOH dehydrogenation selectivity (Figure 4.9).

The catalytic properties of bimetallic catalysts are often discussed in terms of the ligand (or electronic) effect and ensemble (or geometric) effect.[5, 149-150] The ligand effect describes electronic modifications caused by formation of heterometallic bonding, which leads to a charge transfer between the metals.[5] As mentioned earlier, the ligand effect has been suggested to explain the catalytic performance of Pd−Au catalysts observed for HCOOH decomposition.[135, 138] Nevertheless, it is noted that the work functions for Au and Pd are similar,[17, 130] and their electronegativities are identical.[17] Furthermore, XPS spectra indicate that very little (<0.2 eV) or no shifts occur in the binding energies of Pd(3d) and Au(4f) or Pd Auger electrons on Pd−Au surfaces,[88] which implies a very limited charge transfer between Pd and Au in Pd−Au alloys. The ensemble effect depicts that the atoms that exist in a particular arrangement are required for facilitating a particular catalytic process.[5] The ensemble effect for HCOOH decomposition on Pd−Au surfaces has been investigated theoretically by DFT calculations.[139] In this study, we have experimentally shown that the fraction of Pd atoms that exist in Pd−Au interface or Pd(111)-like sites has a significant influence on the reactivity and selectivity of HCOOH decomposition on the Pd−Au surface. Pd atoms in Pd(111)-like sites, which lack neighboring Au atoms, were found to exhibit a higher catalytic activity for HCOOH decomposition (Figure 4.8a) via the undesired dehydration pathway, resulting in a lower selectivity for hydrogen production. Pd atoms that exist at

the Pd−Au interface display a lower activity for overall HCOOH decomposition but enhanced dehydrogenation selectivity (Figure 4.9). These observations suggest that the ensemble effect plays an important role in determining the catalytic properties of Pd−Au catalysts for selective HCOOH decomposition.

4.3.3 HCOOH-TPD from Pd−Au Surfaces

The interactions of HCOOH with transition metal surfaces have been extensively studied using HCOOH-TPD as reviewed by Madix,[151] Barteau,[152] and Columbia and Thiel.[153] CO_2 desorption from metal surfaces during HCOOH decomposition is typically a reaction-limited process, i.e., CO_2 desorbs immediately upon formation.[153] Thus, the catalytic activities of metal surfaces for HCOOH decomposition are frequently characterized by the desorption temperature of CO_2, where lower temperatures for CO_2 desorption are indicative of higher activities for HCOOH decomposition.[151-152] The interactions of HCOOH with low-index single-crystal surfaces of Pd have been investigated.[154-159] It was reported that the temperature for CO_2 desorption from HCOOH decomposition is ∼240−260 K on the Pd(111) surface,[154-155] ∼237 K on the Pd(110) surface,[156] and ∼180 K on the Pd(100) surface.[157] These results suggest that the reactivity of Pd surfaces for HCOOH decomposition is sensitive to the arrangement of surface Pd atoms and the (100) facet is the most active among these structures.

Figure 4.11 shows the TPD spectra for various species following adsorption of 2.6 ML of HCOOH on the clean Au(111) surface and annealed 2 ML Pd/Au(111) surface.

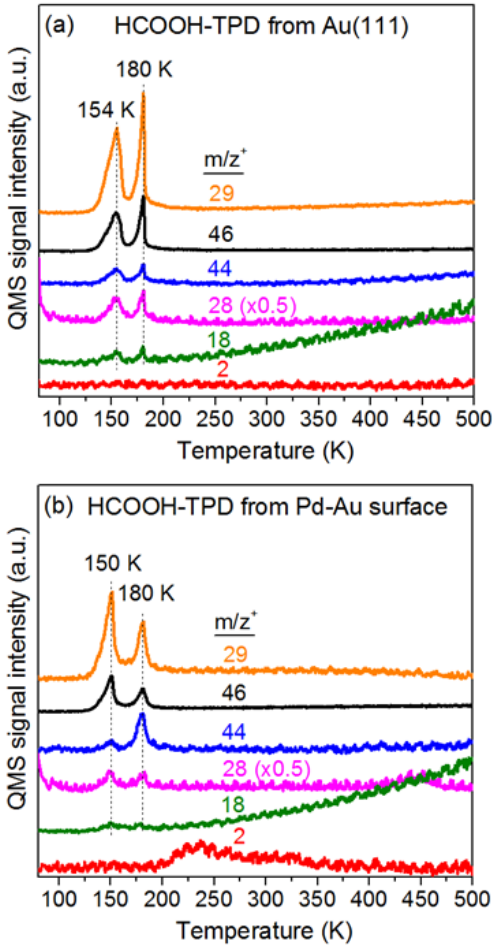

Figure 4.11. TPD spectra of HCOOH from the (a) Au(111) and (b) Pd−Au surfaces. The Pd−Au surface was prepared by depositing 2 ML of Pd onto the Au(111) surface at a surface temperature (T_S) of 77 K followed by annealing to 500 K in ultrahigh vacuum. Each surface was dosed with ~2.6 ML of HCOOH at T_S = 77 K. Heating rate was 1 K/s. Panels a and b have the same ordinate scale.

As shown in Figure 4.11a, the desorption spectrum for the parent mass of HCOOH ($m/z^+ = 46$) from the Au(111) surface displayed peaks at 154 and 180 K, which are due to desorption of multilayer and monolayer HCOOH, respectively (Figure 4.2).

We suggest that the observed $m/z^+ = 44$ and 28 signals originate from the mass fragments of HCOOH rather than from formation of CO_2 and CO because of the following: (1) the desorption temperatures of $m/z^+ = 44$ and 28 signals line up with those of the $m/z^+ = 46$ and 29 (the most intense mass fragment of HCOOH), and (2) the ratios of integral intensities of these QMS signals are similar to those obtained from the HCOOH beam impingement onto the inert flag. No measurable H_2 ($m/z^+ = 2$) desorption was observed during TPD from the HCOOH-precovered Au(111) surface. As mentioned earlier, the observed signal for $m/z^+ = 18$ was due to the water impurity in HCOOH. Results in Figure 4.11a confirm that the Au(111) surface is inactive for HCOOH decomposition during TPD measurements, which is also consistent with observations from the HCOOH-RMBS experiment on the clean Au(111) surface (Figure 4.6) and with reports that HCOOH interacts weakly with the clean Au(111) surface using XPS and RAIRS.[160]

TPD spectra of HCOOH from the Pd−Au surface were measured under the same set of conditions (Figure 4.11b). Significant attenuation of the desorption feature for the HCOOH monolayer at ~180 K indicates that HCOOH decomposed on this surface. The small peak in the $m/z^+ = 28$ signal at ~450 K is due to desorption of CO adsorbed on the surface from the background gas[48] or from decomposition of HCOOH. It is noted that the $m/z^+ = 44$ spectrum is dissimilar from the $m/z^+ = 46$, 29, and 28 spectra. The pronounced signal for $m/z^+ = 44$ at ~180 K shows that CO_2 molecules evolved from the Pd−Au surface during heating. CO_2 evolution observed here is a reaction-limited process rather than a desorption-limited process as CO_2 molecules desorb at much lower

temperatures from Au(111)[161] and Pd(111) surfaces.[162] Thus, CO_2 desorption occurred immediately upon its formation, which was due to decomposition of the reaction intermediate(s) such as formate (HCOO) and carboxyl (COOH).[139] Unfortunately, we were unable to identify the reactive intermediate(s) on the Pd−Au surface via RAIRS (Figure 4.12) due to the small surface concentration of these intermediates which gave a low signal-to-noise ratio. The temperature of CO_2 evolution via HCOOH decomposition from the Pd−Au surface (~180 K) is coincident with that from the Pd(100) surface,[157] which suggests that the Pd−Au surface is comparably active to the Pd(100) surface for HCOOH decomposition during heating.

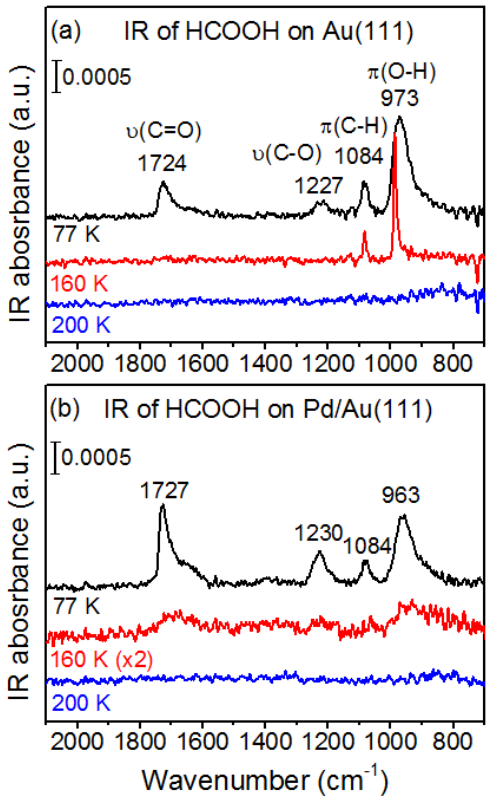

Figure 4.12. RAIRS spectra of HCOOH on Au(111) and Pd/Au(111). The Pd/Au(111) surface was prepared by depositing 2 ML of Pd onto the Au(111) surface at a surface temperature (T_S) of 77 K followed by annealing to 500 K in UHV for 10 min. ~2.6 ML of HCOOH was dosed onto each surface by impinging a beam of HCOOH at T_S = 77 K. The surface was then heated to the indicated temperature and rapidly cooled to 77 K before collecting each spectrum. All spectra were taken at T_S = 77 K and averaged from 512 scans with a resolution of 4 cm^{-1}.

4.4 CONCLUSIONS

We conducted a model catalyst study to investigate the reactivity of HCOOH on a variety of Pd−Au bimetallic surfaces using temperature-programmed desorption and reactive molecular beam scattering. Our results reveal that Pd atoms are the active component for HCOOH decomposition on the Pd−Au alloy surface. The selectivity of the reaction is governed by the type of the nearest neighbor atoms adjacent to the Pd atoms. Pd atoms which lack adjacent Au atoms favor dehydration of HCOOH, whereas Pd atoms that possess Au atoms as nearest neighbors favor dehydrogenation of HCOOH, which is desirable for efficient production of hydrogen. These observations suggest that the reactivity and selectivity of HCOOH decomposition on Pd−Au bimetallic catalysts could be optimized by controlling the arrangement of Pd and Au atoms on the surface through the ensemble effect. We believe these findings will be beneficial for the future design of Pd−Au bimetallic catalysts for associated reactions including selective HCOOH decomposition for hydrogen production and electro-oxidation of HCOOH in the direct formic acid fuel cell.[163] We hope our observations will inspire more advanced surface characterization to further investigate the relationship between the catalytic activities and the surface nature of Pd−Au surfaces.

4.5 APPENDIX

The turnover frequency for HCOOH dehydrogenation, TOF_{H_2}, is defined as the number of H_2 molecules produced during scattering per catalytic site per unit of time, and can be expressed by (eq. 4.1)

$$TOF_{H_2} = \frac{N^S_{H_2}}{N_{site} \times \Delta t} \qquad \text{(eq. 4.1)}$$

where $N^S_{H_2}$: number of H_2 molecules produced during scattering [=] (# of H_2)

N_{site}: number of catalytic sites [=] (# of site)

Δt: reaction period during scattering [=] (sec)

The number of H_2 molecules produced during scattering, $N^S_{H_2}$, is proportional to the integral area of H_2 QMS signals during scattering, and can be expressed as (eq. 4.2)

$$N^S_{H_2} = k^S_{H_2} \times I^S_{H_2} \qquad \text{(eq. 4.2)}$$

where $k^S_{H_2}$: proportional constant [=] (# of H_2) $(count)^{-1}$ $(sec)^{-1}$

$I^S_{H_2}$: integral area of H_2 H_2 QMS signals during scattering [=] (count) (sec)

In catalysis studies, it is always challenging to determine the number of active sites on the catalyst surface, raising the difficulty associated with computing the TOF. Here we adopted an approach similar to the method reported by Goodman and coworkers.[17] Since the clean (Pd-free) Au(111) surface showed no HCOOH dehydrogenation activity, the catalytic sites on Pd/Au(111) surfaces are assumed to consist of surface Pd atoms. Accordingly, the TOF_{H_2} can be computed based on the number of surface Pd atoms. However, instead of using the initial Pd coverage (which is subject to change due to annealing in the preparation procedure),[17] the number of surface Pd atoms in this study were determined by the integral area of H_2-TPD.

Assuming the dissociative adsorption of one H_2 molecule requires two surface catalytic sites (or surface Pd atoms), the number of catalytic sites, N_{site}, is equal to twice the number of H_2 molecules desorbed in H_2-TPD, and can be expressed as (eq. 4.3)

$$N_{site} = 2 \times N_{H_2}^{T} \qquad \text{(eq. 4.3)}$$

where $N_{H_2}^{T}$: number of H_2 molecules desorbed in H_2-TPD [=] (# of H_2)

Similar to the calculation of $N_{H_2}^{S}$, the number of H_2 molecules desorbed in H_2-TPD, $N_{H_2}^{T}$, is proportional to the integral area of H_2 in H_2-TPD, and can be expressed as (eq. 4.4)

$$N_{H_2}^{T} = k_{H_2}^{T} \times I_{H_2}^{T} \qquad \text{(eq. 4.4)}$$

where $k_{H_2}^{T}$: proportional constant [=] (# of H_2) $(count)^{-1}$ $(sec)^{-1}$

$I_{H_2}^{T}$: integral area of H_2 in H_2-TPD [=] (count) (sec)

We substitute (eq. 4) into (eq. 3) to obtain (eq. 4.5)

$$N_{site} = 2 \times k_{H_2}^{T} \times I_{H_2}^{T} \qquad \text{(eq. 4.5)}$$

Then substitute (eq. 5) and (eq. 2) into (eq. 1) to obtain (eq. 4.6)

$$TOF_{H_2} = \frac{k_{H_2}^{S}}{k_{H_2}^{T}} \times \frac{I_{H_2}^{S}}{I_{H_2}^{T}} \times \frac{1}{2\,\Delta t} \qquad \text{(eq. 4.6)}$$

If the chamber conditions are held constant (e.g., same chamber volume and pumping speed…), proportional constants will remain the same for scattering and TPD experiments

$$k_{H_2}^{S} = k_{H_2}^{T} \qquad \text{(eq. 4.7)}$$

Finally, (eq. 5.6) can be further simplified to give (eq. 5.8)

$$TOF_{H_2} = \frac{I_{H_2}^{S}/\Delta t}{I_{H_2}^{T} \times 2} \qquad \text{(eq. 4.8)}$$

In this study, we used (eq. 4.8) to compute TOF_{H_2} based on the integral area ratio of H_2 QMS signal in the scattering experiment to that in the TPD measurement.

The validity of (eq. 4.8) was also confirmed by comparing the TOF_{H_2} value to the TOF_{HCOOH} value that was alternatively obtained using the estimated HCOOH conversion. Two methods should give values for TOF_{H_2} and TOF_{HCOOH} within an order of magnitude. Here we take the annealed 1 ML Pd/Au(111) surface as an example. The estimated HCOOH conversion is ~0.7% on the annealed 1 ML Pd/Au(111) surface (with the HCOOH flux rate of ~5×10^{14} molecules cm^{-2} sec^{-1} or 0.36 ML/sec). Since annealing a 0.9 ML Pd/Au(111) surface at 500 K causes the Au LEISS signal reaching the value of 78% of its bulk value due to interdiffusion of Pd adatoms,[88] we assume the surface Pd coverage on the annealed 1 ML Pd/Au(111) surface is ~0.22 ML. Therefore, the TOF_{HCOOH} is estimated to be ~0.011 HCOOH $site^{-1}$ sec^{-1} [(0.36 ML/sec) × (0.7%) / (0.22 ML)]. This TOF_{HCOOH} value is in a reasonable range with the computed TOF_{H_2} (~0.006 H_2 $site^{-1}$ sec^{-1}), thus verifying the validity of (eq. 4.8).

Chapter 5: Oxygen Activation and Reaction on Pd−Au Bimetallic Surfaces*

5.1 INTRODUCTION

The study of bimetallic catalysts is important in the field of heterogeneous catalysis as bimetallics often exhibit physicochemical properties that are distinctly different from those of the parent metals. These properties provide the potential to design catalysts with enhanced activity, selectivity, and stability.[4-5] As one of the most extensively studied bimetallic systems, Pd−Au catalysts have displayed promising performance in a number of oxidative chemical reactions including CO oxidation,[13-14] acetoxylation of ethylene to vinyl acetate,[16-17] selective oxidation of alcohol to aldehyde[18, 57-58] and the direct synthesis of hydrogen peroxide from hydrogen and oxygen.[34, 59] A molecular-level understanding of how oxygen molecules interact with Pd−Au surfaces (e.g., adsorption, dissociation, and desorption) would be informative for the optimization of Pd−Au catalysts employed for these reactions and other reactions involving oxygen. In model catalyst studies, reactions are normally investigated on well-defined single-crystal surfaces under ultrahigh vacuum (UHV) conditions, which enable the correlation of catalytic properties to surface structures at the molecular level.[4-8, 10-11]

---

* Yu, W.-Y.; Zhang, L.; Mullen, G. M.; Henkelman, G.; Mullins, C. B., Oxygen Activation and Reaction on Pd–Au Bimetallic Surfaces. *J. Phys. Chem. C* **2015**, 119, 11754-11762.
W.-Y. Yu, G. M. Mullen and C. B. Mullins conceived and designed experiments. W.-Y. Yu, L. Zhang, G. M. Mullen, G. Henkelman and C. B. Mullin analyzed and discussed results, and commented on the manuscript. L. Zhang performed theoretical calculations. W.-Y. Yu performed experiments, analyzed data and wrote the paper.

Interactions of oxygen with the Pd(111) single-crystal surface have been studied extensively.[164-170] It was reported that oxygen molecularly chemisorbs on the Pd(111) surface at the temperature of 80 K.[166] High-resolution electron energy loss spectroscopy (HREELS)[166, 168] showed that chemisorbed oxygen molecules exist in three molecular states that exhibit different vibrational frequencies of O−O stretching due to varying degrees of electron transfer from the surface into the oxygen molecule. At low coverages (dosed by small exposure of molecular oxygen), adsorbed oxygen molecules dissociate into oxygen adatoms at ~180−200 K,[166-168] which recombine and desorb from the Pd(111) surface at temperatures higher than 600 K in temperature-programmed desorption (TPD) measurements.[165, 167] The direct desorption of oxygen admolecules (without dissociation into oxygen adatoms) was observed when molecular oxygen was dosed on the Pd(111) surface at high coverages.[165, 167] Three molecular desorption features with peak temperatures of ~125, 150 and 200 K were observed,[167] which are consistent with the three molecular states characterized in HREELS spectra.[166, 168] In contrast to the ease of activation on Pd single-crystal surfaces, it is well-accepted that oxygen molecules do not readily activate (or dissociate) on clean Au single-crystal surfaces.[10, 171]

Recently the interaction of oxygen with Pd−Au bimetallic model surfaces has been studied both experimentally[39, 42, 47] and theoretically.[150, 172-182] For example, Tysoe and co-workers[47] have investigated the interaction of oxygen with Au/Pd(100) surfaces with various surface compositions using O_2-TPD. Following oxygen exposure at 80 K,

direct desorption of oxygen admolecules was observed at 114 and 179 K, and recombinative desorption of oxygen adatoms was detected at ~750 K during heating.[47] The coverage of oxygen adatoms was reported to decrease as the gold coverage was increased.[47] The reaction with CO to form CO_2 is commonly used to probe the reactivity of surface oxygen on Pd−Au model surfaces.[39, 42, 47, 172, 175-176, 178, 180-182] By combining reaction kinetics measurements and polarization-modulation infrared reflection spectroscopy (PM-IRAS) characterizations, Gao et al.[39] reported that neither Au nor isolated Pd sites on the AuPd(100) surface are capable of dissociating oxygen molecules. Contiguous Pd sites are required for O_2 dissociation, which in turn accounts for a high CO oxidation activity over the AuPd(110) surface.[39]

In this study, we combine experimental and theoretical methods to investigate the activation of oxygen and its reaction with CO on Pd/Au(111) bimetallic surfaces. The adsorption of oxygen molecules was studied by King−Wells measurements, in which an O_2 beam was impinged onto a variety of Pd/Au(111) surfaces at 77 K. These surfaces were physically characterized employing Auger electron spectroscopy (AES) and reflection-absorption infrared spectroscopy (RAIRS) using CO as a probe molecule. The interactions of oxygen admolecules with Pd/Au(111) surfaces (i.e., desorption and dissociation) were then investigated using O_2-TPD. The energy for O_2 desorption and energy barrier for O_2 dissociation on Pd/Au(111) surfaces with Pd ensembles of various sizes were calculated via DFT methods. CO-RMBS was used to probe the reactivity of oxygen species on Pd/Au(111) surfaces by monitoring CO_2 production. Finally,

possible reaction mechanisms (i.e., associative and dissociative pathways) for CO oxidation on Pd/Au(111) surfaces were discussed in terms of the Pd ensemble size using DFT calculations.

5.2 Experimental and Computational Methods

5.2.1 UHV Experiments

All experiments in this study were performed in an UHV chamber that has been described in detail previously.[48, 84, 86] Briefly, the chamber is equipped with an Auger electron spectrometer (Physical Electronics 10-500), a quadrupole mass spectrometer (Extrel C-50), and a Fourier transform infrared spectrometer (Bruker Tensor 27) combined with a mercury−cadmium−telluride (MCT) detector (Infrared Associates), as well as nozzles and apertures for generating two separate molecular beams.

The Au(111) single-crystal sample is a circular disk (Princeton Scientific, 12 mm in diameter × 2 mm thick) held in place by a Mo wire fitted around a groove cut into the side of the sample. This wire is also used to resistively heat the sample and provide thermal contact between the sample and a liquid nitrogen bath for cooling. The temperature of the sample was measured with a K-type (Alumel−Chromel) thermocouple placed into a small hole in the edge of the disk-shaped sample. The Au(111) surface was periodically cleaned by Ar ion bombardment (2 keV), carried out at room temperature, followed by an anneal to 800 K. The cleanliness of the surface was verified by AES with a beam energy of 3 keV and emission current of 1.5 mA.

Pd−Au bimetallic model surfaces were prepared by depositing ~2.9 monolayer (ML) of Pd atoms from a homemade thermal evaporator onto the Au(111) surface at 77 K followed by annealing to a specified temperature for 10 min.[48-50] The growth of the Pd overlayer on the Au(111) surface at 77 K is believed to obey a layer-by-layer mechanism, and upon annealing surface Pd atoms can diffuse into the bulk of the Au(111) surface, forming a Pd−Au alloy at the surface.[88] The deposition rate of Pd in this study was calibrated with a quartz crystal microbalance (QCM) controller (Maxtek Inc.) assuming the thickness of 1 ML Pd equals 0.274 nm.

The adsorption of oxygen molecules on Pd−Au surfaces that were annealed to various temperatures (500-675 K) was investigated by King and Wells measurements.[87, 116-117, 183] A neat O_2 molecular beam with a translational energy of ~0.1 eV was first impinged on the stainless steel inert flag to establish a baseline. The beam was then impinged on the annealed Pd/Au(111) surface at a surface temperature of 77 K. The O_2 QMS signal ($m/z^+ = 32$) was monitored during the King−Wells measurements.

Reflection absorption infrared spectroscopy using CO as a probe molecule (CO-RAIRS) was used to characterize the annealed Pd−Au surfaces. The Pd−Au surface was first heated to 500 K at 1 K/s to desorb any surface contaminants such as CO. After the sample had cooled to 77 K, an IR background scan was taken. Saturation coverage of CO was dosed by a molecular beam of CO with the sample held at 77 K. The IR

spectrum of saturated CO adsorbed on the surface was taken at 77 K. All spectra were averaged from 512 scans with a resolution of 4 cm^{-1}.

For O_2-TPD and CO-RMBS experiments, the Pd−Au bimetallic surface was generated by depositing 2.9 ML Pd on the Au(111) surface followed by annealing to 500 K for 10 min. This surface consists of ~77% Pd and ~23% Au based on low-energy ion-scattering spectroscopy (LEISS) characterizations.[88] In O_2-TPD measurements, oxygen was dosed by impinging an O_2 beam on the Pd−Au surface at 77 K. The surface was then heated at a rate of 1 K/s while $m/z^+ = 32$ (O_2) was monitored by QMS. For CO-RMBS experiments, the Pd−Au surface was first saturated with oxygen at 77 K by backfilling the chamber with 1 langmuir (L; 1 L = 1×10^{-6} Torr-s) of O_2 through a leak valve. The oxygen-precovered Pd−Au surface was then heated to a specific temperature (77−250 K) prior to CO beam impingement. QMS signals of $m/z^+ = 32$ (O_2), 44 (CO_2) and 28 (CO) were simultaneously monitored during CO-RMBS experiments.

5.2.2 DFT Calculations

All DFT calculations were performed with the Vienna ab initio simulation package.[184-187] The interaction between the ionic core and the valence electrons was described by the project augmented wave method,[188] and the valence electrons were described with a plane-wave basis up to an energy cutoff of 300 eV.[189-190] The energy cutoff was increased to 400 eV to test for convergence, and the O_2 dissociation barrier on Au was found to vary by less than 0.005 eV. The exchange correlation contribution to

the total energy functional was determined using the Perdew−Burke−Ernzerhof (PBE) generalized gradient approximation functional.[191] The location and energy of the transition states were calculated with the climbing-image nudged elastic band method.[192-193] The gold surface was modeled as a four-layer 4×4 Au(111) slab with the bottom two layers fixed and 10 Å of vacuum. The Pd-decorated Au(111) surfaces in this study are modeled by replacing Au atoms on the top layer of the Au(111) slab with various Pd ensembles, as illustrated in Figure 5.1. The Brillouin zone was sampled using a 3×3×1 Monkhorst−Pack k-point mesh.[194] The convergence criteria for the electronic structure and the atomic geometry were 10^{-5} eV and 0.01 eV/Å, respectively. The binding energies of O_2 and CO on the surface are referenced to the gas-phase O_2 and CO molecules, respectively.

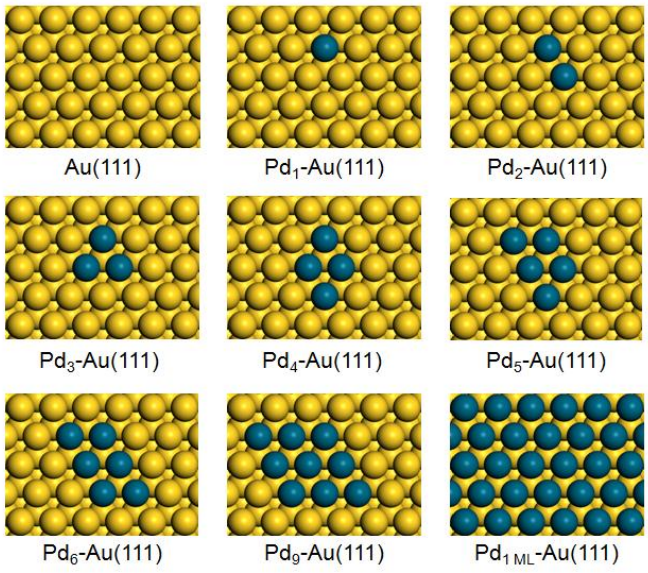

Figure 5.1. Top views of Pd/Au(111) surfaces considered in DFT calculations. The yellow and blue balls represent Au and Pd atoms, respectively.

5.3 Results and Discussion

5.3.1 Adsorption of Oxygen on Pd−Au Surfaces

In this study, the adsorption of oxygen molecules on Pd−Au surfaces was investigated by King−Wells measurements. Figure 5.2 shows the O_2 QMS signal during a series of King−Wells measurements in which an O_2 beam was impinged onto the 2.9 ML Pd/Au(111) surface that was previously annealed to various temperatures (i.e., 500−675 K). The O_2 molecular beam was first impinged onto the inert flag that was held in front of the sample surface for 5 s (from 10 to 15 s) to establish a baseline signal (all O_2 molecules scattering from the inert flag). After removing the inert flag, the beam was impinged onto the Pd−Au surface that was held at 77 K for 30 s (from 15 to 45 s). The measurement was also conducted on the clean (Pd-free) Au(111) surface and is included for comparison.

When the O_2 beam was impinged on the inert flag, a constant O_2 QMS signal was detected due to scattering of the beam with negligible adsorption on the sample. After the removal of the inert flag, a constant O_2 QMS signal was observed from the clean Au(111) surface, signifying no oxygen adsorption (or uptake) occurred on the clean Au(111) surface.

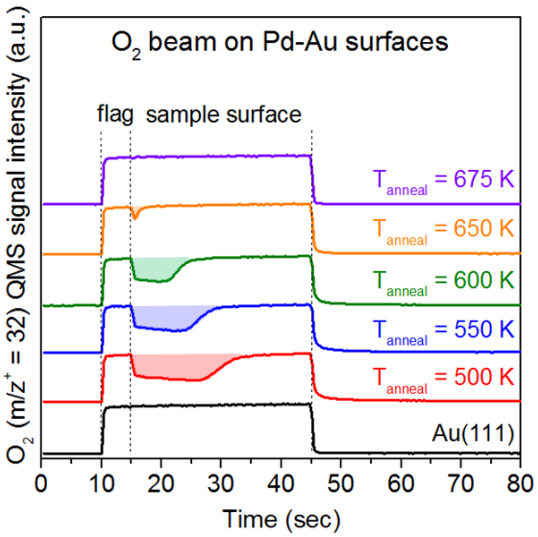

Figure 5.2. King−Wells measurements of an O_2 beam impinging on Au(111) and annealed 2.9 ML Pd/Au(111) surfaces at a surface temperature of 77 K. The O_2 uptake on each surface is proportional to the shaded area indicated in each curve.

For the Pd/Au(111) surface annealed to 500 K, the intensity of the O_2 QMS signal was initially lower than that observed for impingement onto the inert flag due to the adsorption of oxygen on the surface. Since no oxygen uptake was observed on the Au(111) surface, it is proposed that the adsorption sites for oxygen on the annealed Pd/Au(111) surface consist of Pd surface atoms. It has been reported that with exposure to oxygen molecules at 100 K oxygen adsorbs molecularly on the Pd(111) surface and the dissociation of oxygen admolecules occurs at temperatures of ~180−200 K.[167] Accordingly, the oxygen adsorption on the Pd−Au surface observed here is likely molecular adsorption without dissociation. The initial sticking probability of oxygen is

~0.43 for the Pd/Au(111) surface annealed at 500 K. The sticking probability eventually decreases to zero (where the intensity of the O_2 QMS signal from the sample surface became nearly identical with that from the inert flag) as adsorbed oxygen saturated the Pd−Au surface.

When the Pd/Au(111) surface was progressively annealed to higher temperatures (550-675 K), the time to saturate the surface with oxygen molecules gradually reduced, indicative of less oxygen uptake since the flux of the O_2 beam was kept constant for all of these measurements. The uptake of oxygen on each surface during the King−Wells measurements is proportional to the magnitude of integral of the intensity of the O_2 QMS signal from the sample surface using the intensity of the O_2 QMS signal from the inert flag as a baseline. Relative to the Pd/Au(111) surface annealed at 500 K, the oxygen uptake for Pd/Au(111) surfaces annealed to 550, 600 and 650 K reduced to ~75%, 49% and 2%, respectively. The oxygen uptake was negligible on the Pd/Au(111) surface that was annealed at 675 K.

The oxygen uptake on the Pd−Au surface is correlated with the concentration of surface Pd atoms. We characterized the relative surface compositions for annealed Pd/Au(111) surfaces by AES. Figure 5.3 shows the AES spectra of as-prepared and annealed 2.9 ML Pd/Au(111) surfaces.

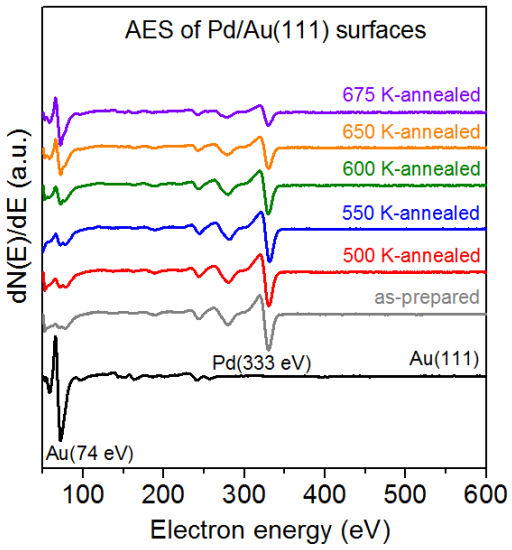

Figure 5.3. AES spectra of as-prepared and annealed 2.9 ML Pd/Au(111) surfaces.

As the annealing temperature was increased, the Pd AES signal intensity was attenuated and the Au AES signal intensity was enhanced, which has been previously observed by Koel and co-workers.[88] This effect is attributed to diffusion of surface Pd atoms into the subsurface of the Au(111) single-crystal sample during the annealing process.[88]

The oxygen uptake during King−Wells measurements as a function of the Pd/Au AES signal intensity ratio of each annealed surface is illustrated in Figure 5.4. The oxygen uptake is linearly proportional to the Pd/Au AES signal intensity ratio for all surfaces except those that were annealed at 650 and 675 K. This deviation suggests that other surface properties (e.g., arrangement of Pd and Au surface atoms) may also

influence the oxygen uptake on the Pd−Au surface, and oxygen uptake may not simply be a function of the concentration of Pd atoms on the Pd/Au(111) surface.

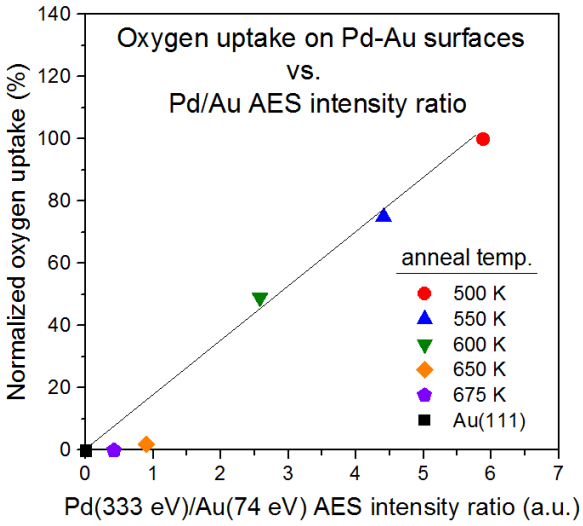

Figure 5.4. Oxygen uptake during King−Wells measurements on annealed 2.9 ML Pd/Au(111) bimetallic surfaces versus Pd(333 eV)/Au(74 eV) AES intensity ratio.

The annealed Pd/Au(111) surfaces were further characterized by RAIRS using CO as a probe molecule (CO-RAIRS). CO-RAIRS has been extensively employed to characterize the surface properties and structures of the Pd−Au model surface.[17, 39, 48, 89, 93, 118] The type of adsorption site occupied by CO (e.g., atop sites, 2-fold or 3-fold bridge sites) can be inferred by the intramolecular CO stretch frequency (ν_{CO}) as a result of varying degrees of π-antibonding backdonation from the surface electrons.[90] Figure 5.5

shows the RAIRS spectra for saturated CO adsorbed on the clean Au(111) and annealed 2.9 ML Pd/Au(111) surfaces at 77 K.

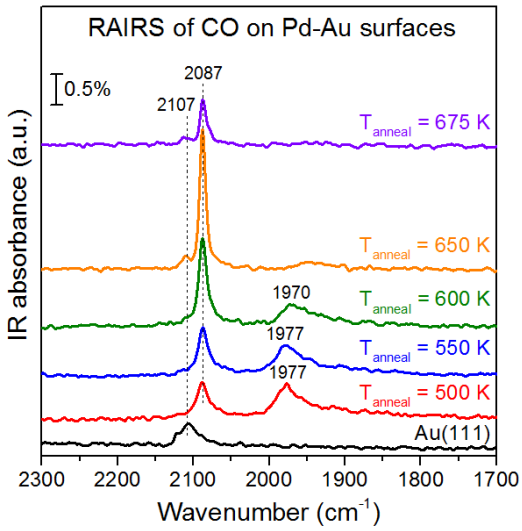

Figure 5.5. RAIRS spectra of saturated CO on Au(111) and annealed 2.9 ML Pd/Au(111) bimetallic surfaces taken at a surface temperature of 77 K.

For the clean Au(111) surface, only one vibrational band at ~2107 cm^{-1} was observed, which is associated with CO bound to atop Au sites.[39, 89, 92-93, 118] The Pd/Au(111) surface annealed at 500 K displayed two IR features at ~2087 and ~1977 cm^{-1}, which have been assigned to atop CO on isolated Pd sites (or Pd monomer) and bridged CO on contiguous Pd sites, respectively.[39, 89, 93, 118] Increasing the annealing temperature resulted in the attenuation of IR signal associated with bridged CO on contiguous Pd sites (ν_{CO} = ~1977 cm^{-1}) and intensification of signal associated with CO atop on isolated Pd sites (ν_{CO} = ~2087 cm^{-1}). The IR band due to bridged CO on contiguous Pd sites

became relatively small for the Pd/Au(111) surfaces annealed at 650 K and disappeared when annealed at 675 K. Considering the CO-RAIRS spectra (Figure 5.5) and oxygen uptake (Figure 5.4), it suggests that the presence of contiguous Pd sites on the Pd−Au surface is crucial for adsorption of oxygen molecules.

These experimental observations are conceptually consistent with our DFT calculations of oxygen adsorption. The binding energy of an oxygen molecule as a function of Pd ensemble size on Pd/Au(111) surfaces is presented in Figure 5.6.

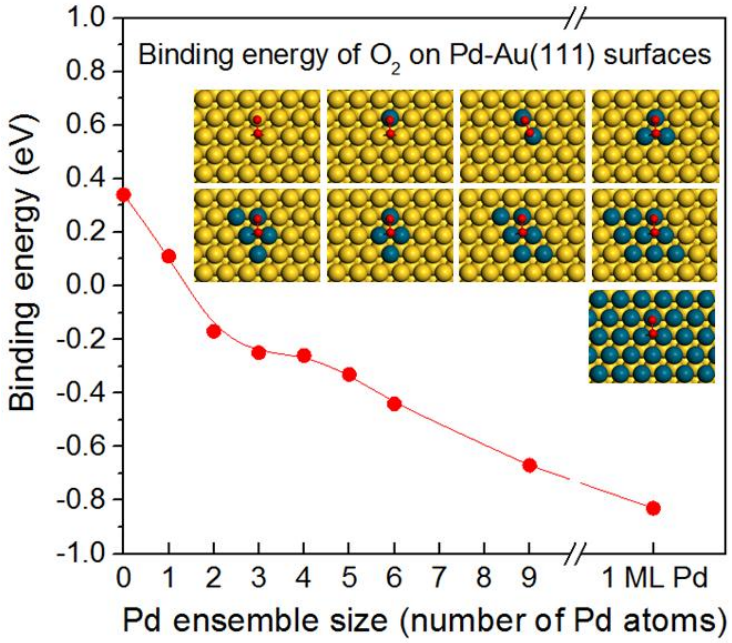

Figure 5.6. Calculated binding energies of the oxygen molecule adsorbed on Pd/Au(111) surfaces. Inset shows the top views of adsorption configuration images, in which yellow, blue and red balls represent Au, Pd and O atoms, respectively.

As shown in the inset of Figure 5.6, molecular oxygen binds on the fcc hollow site aligned in a top-hollow-bridge (t-h-b) geometry on these surfaces, except for the Pd_2-Au(111) surface, where the oxygen molecule bridges on two Pd atoms. The calculated binding energy for the oxygen molecule on the Au(111) surface is 0.34 eV. With the presence of the Pd monomer, the binding energy decreases to 0.11 eV on the Pd_1−Au(111) surface. These positive values of binding energy indicate that the adsorption of oxygen molecule is energetically unfavorable on the clean Au(111) and Pd_1−Au(111) surfaces. The binding energy of the oxygen molecule reduces to the negative value of -0.17 eV on the Au(111) surface with a Pd dimer (i.e., Pd_2−Au(111) surface), which supports our experimental observation of the importance of contiguous Pd sites for adsorption of oxygen molecules on the Pd−Au surface. These results are also consistent with previous DFT reports, in which the effects of Pd ensembles (i.e., monomer, dimer and trimer) on adsorption oxygen molecule were investigated using 1 ML Au/Pd(111)[173] and Au(111) surfaces[178] as substrates. The binding energy of the oxygen molecule on the Pd/Au(111) surface gradually decreases as the Pd ensemble size increases. For the Au(111) surfaces fully covered by 1 ML of Pd overlayer, the calculated binding energy of the oxygen molecule is -0.83 eV, indicating that the oxygen molecule binds more strongly to this surface than to other Pd/Au(111) surfaces.

5.3.2 Desorption of Oxygen from Pd−Au Surfaces

The interaction of oxygen with the Pd−Au surface was investigated via O_2-TPD as shown in Figure 5.7. The Pd−Au surface was generated by depositing 2.9 ML Pd onto the Au(111) surface at 77 K followed by annealing at 500 K. Dosing of O_2 was achieved by impinging a molecular beam of O_2 onto the surface at 77 K prior to heating.

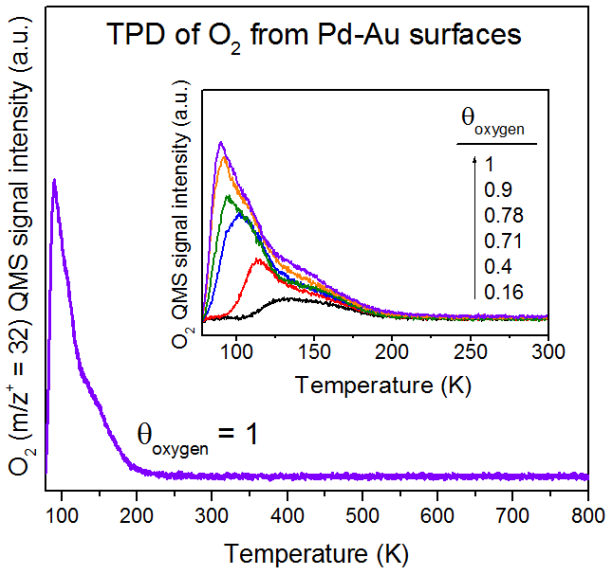

Figure 5.7. TPD of saturated O_2 from the Pd/Au(111) bimetallic surface. Inset shows the TPD of various coverages of O_2 from the same surface. The heating rate was 1 K/s.

O_2-TPD has been extensively studied on the Pd(111) surface.[164-165, 167-168] According to the desorption temperature, two types of oxygen desorption processes have been identified from the Pd(111) surface:[167] associative desorption (or recombinative desorption of oxygen adatoms; peak temperature at ~800 K) and molecular desorption (or

direct desorption of oxygen admolecules; peak temperatures at ~200, 150, and 125 K). In Figure 5.7, the oxygen desorption peak ended at ~220 K, and no other feature was observed during heating to 800 K. These results suggest that oxygen admolecules desorb molecularly from the Pd−Au surface without detectable dissociation into oxygen adatoms. It is noted that the Pd/Au(111) surface that was generated by annealing at 500 K undergoes significant changes when the temperature is heated to above 500 K (as shown in AES (Figure 5.3) and CO-RAIRS (Figure 5.5) characterizations), which increases the difficulty of investigating the phenomena for recombinative desorption of oxygen adatoms during heating. Nevertheless, it is clear that the surface concentration of oxygen adatoms from dissociation of oxygen molecules (if any) is not sufficient to detect via O_2-TPD. The inset in Figure 5.7 shows desorption of oxygen molecules with various coverages from the Pd−Au surface. In these TPD measurements, various coverages of oxygen were dosed onto the same Pd−Au surface at 77 K followed by heating to 500 K. To more clearly visualize desorption peaks, the obtained spectra were plotted within the temperature range between 77 and 300 K (no oxygen desorption was observed when the temperature was higher than 300 K) as shown in the inset of Figure 5.7. In contrast with the sharp features in molecular oxygen desorption observed from the Pd(111) surface,[167] the desorption peaks for oxygen molecules from the Pd−Au surface are relatively broad, which is likely due to the relatively high degree of heterogeneity of the annealed Pd/Au(111) surface in comparison to that of the Pd(111) surface.

The competition between desorption and dissociation of the molecular oxygen on Pd−Au surfaces upon heating was also explored by DFT calculations. Figure 5.8 represents the energy for desorption and energy barrier for dissociation of an oxygen molecule on Pd/Au(111) surfaces as a function of Pd ensemble size. The corresponding potential energy diagram is shown in Figure 5.9. It is noted that the energy for desorption of the oxygen admolecule is essentially the negative value of the binding energy shown in Figure 5.6.

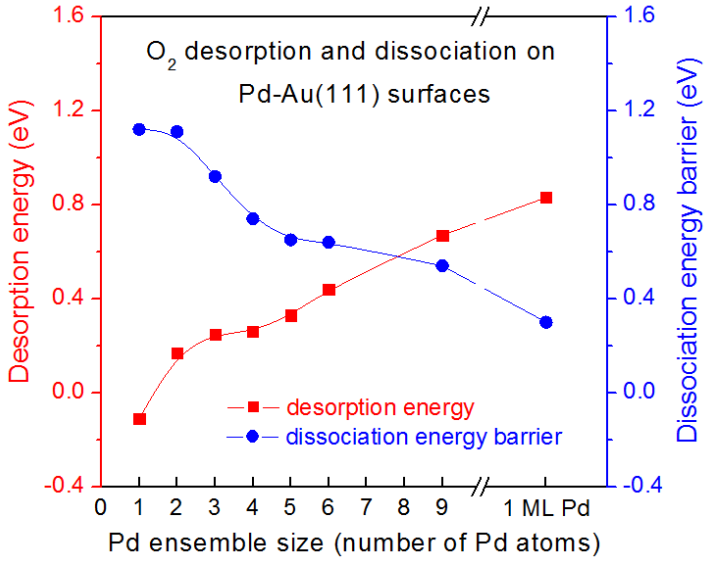

Figure 5.8. Energy for desorption and energy barrier for dissociation of an oxygen molecule adsorbed on Pd/Au(111) surfaces as determined by DFT calculations.

As shown in Figure 5.8, the energy for desorption of an oxygen admolecule (i.e., $O_{2(ad)} \rightarrow O_{2(g)}$) gradually increases from 0.17 to 0.44 eV as the Pd ensemble on the

Au(111) surface changes from a dimer to a hexamer. On the other hand, the energy barrier for dissociation of an oxygen admolecule (i.e., $O_{2(ad)} \rightarrow 2O_{(ad)}$) decreases from 1.11 to 0.64 eV under the same conditions. It is noted that the energy for desorption is smaller than the energy barrier for dissociation on each of these Pd/Au(111) surfaces. Furthermore, it has been reported that the desorption prefactor (ν_{des}) is usually significantly larger than the dissociation prefactor (ν_{diss}) for a molecular adsorbate ($\nu_{diss} = \sim 10^{-3}\ \nu_{des}$).[195] Accordingly, desorption of O_2 is favored over its dissociation on these Pd/Au(111) surfaces.In other words, upon heating the oxygen admolecule would prefer to desorb from the surface at the temperature below its dissociation temperature. These results are in good agreement with our O_2-TPD observations (Figure 5.7), in which molecular desorption of oxygen was observed but the recombinative desorption of atomic oxygen that comes from dissociation was undetectable. As shown in Figure 5.8, the dissociation of an oxygen admolecule becomes energetically favorable over desorption when larger Pd ensembles (e.g., consisting of nine Pd atoms) are present on the Au(111) surface. For the Au(111) surface covered by 1 ML of Pd (i.e., the Pd1ML/Au(111) surface), the calculated energy barrier for dissociation of an oxygen admolecule (0.3 eV) is much lower than the energy for desorption of an oxygen admolecule (0.83 eV). This is consistent with the observation that low coverages of oxygen admolecules can completely dissociate into oxygen adatoms on the Pd(111) surface.[167]

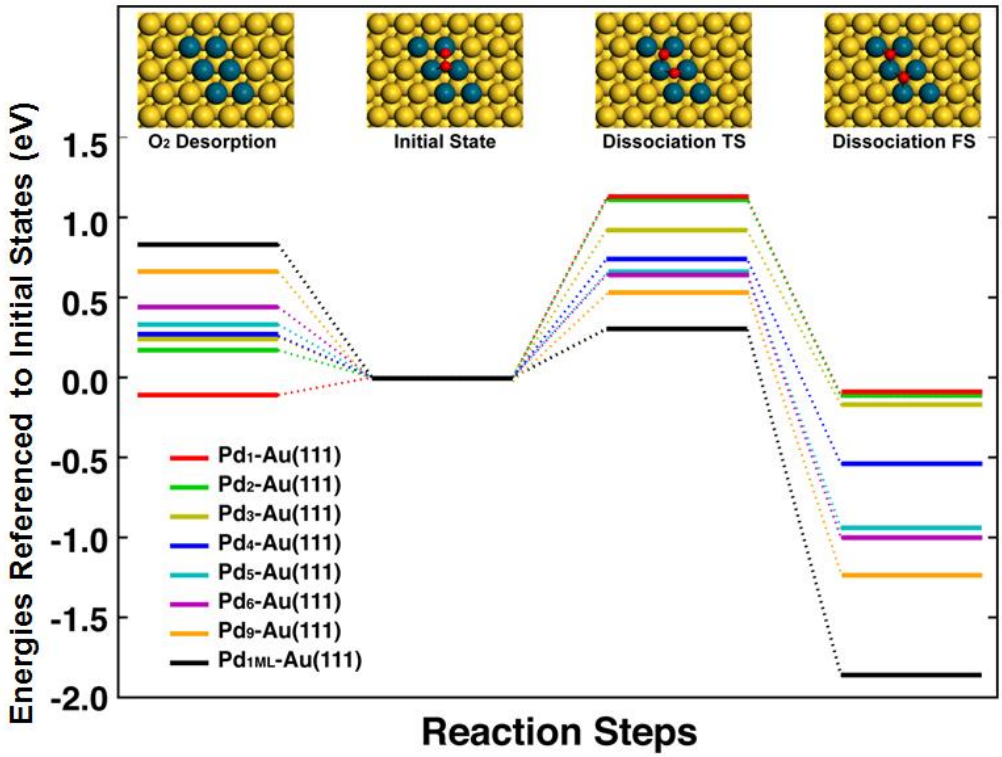

Figure 5.9. Predicted potential energy diagram for O_2 desorption and dissociation on Pd/Au(111) surfaces. Inset shows the corresponding images for initial, transition (TS) and final (FS) state configurations (using Pd_6-Au(111) surface as a example). Yellow, blue and red balls represent Au, Pd and O atoms, respectively.

5.3.3 Reaction of Oxygen and CO on Pd−Au Surfaces

The reaction with CO to form CO_2 has been used to experimentally probe the reactivity of surface oxygen on Pd−Au model surfaces.[39, 42, 47] In this study, the reactivity of molecular oxygen adsorbed on the Pd/Au(111) surface upon heating was assessed by CO-RMBS via monitoring CO_2 production. CO-RMBS experiments were

conducted by impinging a molecular beam of CO onto the inert flag for 5 s (from 15 to 20 s) and then onto the molecular oxygen-precovered Pd−Au surface for 60 s (from 20 to 80 s) as shown in Figure 5.10. For these measurements, the Pd−Au surface (generated by depositing 2.9 ML Pd onto the Au(111) surface at 77 K followed by annealing at 500 K) was presaturated with molecular oxygen at 77 K and then heated to a specific temperature (77−250 K) prior to CO beam impingement. The measured O_2 and CO_2 QMS signals are depicted in Figures 5.10(a) and 5.10(b), respectively.

As expected, neither O_2 nor CO_2 QMS signals were detected when the CO beam was impinged onto the inert flag. When the CO beam struck the oxygen-precovered Pd−Au surface at 77 K, a peak in the O_2 QMS signal emerged (Figure 5.10(a)), indicating that impingement of CO onto the surface caused evolution of O_2. This O_2 evolution is likely due to the competitive adsorption of CO on the surface sites, which displaces the preadsorbed O_2 into the gas phase. Since no measurable O_2 adsorption was detected when an O_2 beam struck the CO-presaturated Pd−Au surface at 77 K (Figure 5.11), we speculate that the adsorption strength of CO on the surface is much stronger than that of O_2. This suggestion is also supported by DFT calculations in which the binding of CO (Figure 5.12) to Pd/Au(111) surfaces is found to be stronger relative to that of O_2 (Figure 5.6). The oxygen evolution decreased in intensity when the Pd−Au surface was preheated to 120 K, which is likely due to desorption of O_2 during heating (Figure 5.7) before CO beam impingement. The intensity of oxygen evolution decreased further as the surface was preheated and held at higher temperatures (180−250 K).

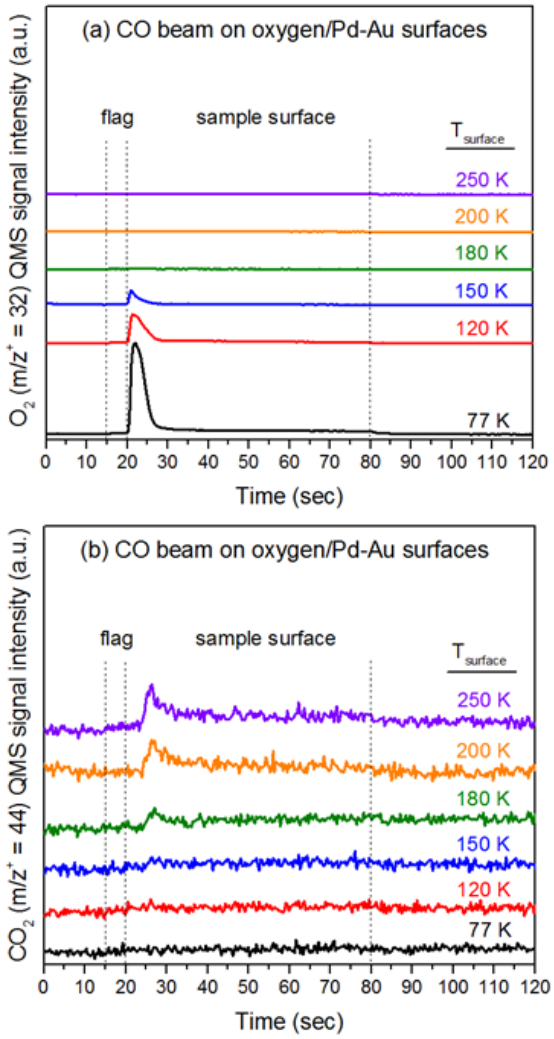

Figure 5.10. (a) O_2 ($m/z^+ = 32$) and (b) CO_2 ($m/z^+ = 44$) QMS signals during CO-RMBS on the oxygen-presaturated Pd/Au(111) bimetallic surface at various surface temperatures.

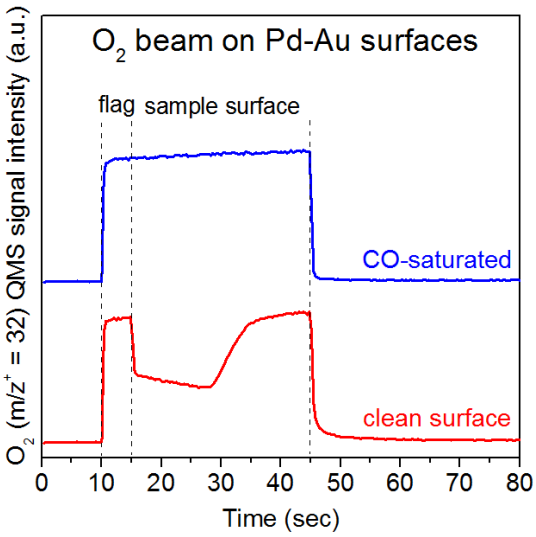

Figure 5.11. O_2 (m/z^+ = 32) QMS signals during King–Wells measurements of an O_2 beam impinging on the clean and CO-presaturated 500 K-annealed 2.9 ML Pd/Au(111) bimetallic surfaces at 77 K.

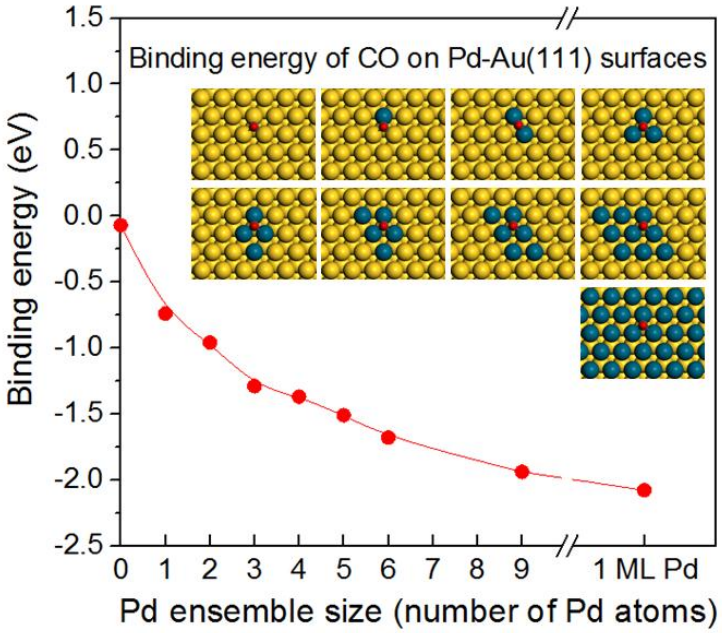

Figure 5.12. Calculated binding energies of the CO adsorbed on Pd/Au(111) surfaces. Inset shows the top views of adsorption configuration images, in which yellow, blue and red balls indicate Au, Pd and O atoms, respectively.

As shown in Figure 5.10(b), no CO_2 signal was detected when the CO beam was impinged onto the oxygen-precovered Pd−Au surface held at temperatures ranging from 77 to 150 K. These results show that the surface oxygen species is inactive to react with CO to form CO_2 within this temperature range (77-150 K). A small peak in CO_2 production was observed when the CO beam struck the oxygen-precovered Pd−Au surface at 180 K, suggestive of the thermal activation of adsorbed oxygen molecules. It is noted that the CO2 peak emerged at ~24 s, which is ~4 s after CO beam impingement which began at 20 s. This is likely due to the site blocking from oxygen and hydrogen impurities (from adsorption of background gas that is intrinsically present in our UHV chamber)[48] on the Pd−Au surface. Figure 5.13 shows the QMS signals of O_2, CO_2, H_2 and CO during a CO-RMBS experiment at 180 K. The emergence of a CO_2 production peak was observed after the evolution of O_2 and H_2 that were induced by CO beam impingement. The phenomena of CO-induced recombinative desorption of H adatoms from the Pd/Au(111) surface have been observed previously.[49]

The CO_2 production peak became more significant when the surface was heated to higher temperatures (200 and 250 K) prior to CO beam impingement. As shown in Figure 5.7, the process for molecular desorption of adsorbed oxygen ended at a temperature of ~220 K. Accordingly, the CO_2 production from the Pd−Au surface observed at 250 K is likely due to the reaction of CO with oxygen adatoms rather than oxygen admolecules. This observation suggests dissociation of oxygen admolecules could occur on the Pd−Au surface during heating (the amount of oxygen that reacted with

CO above 200 K is estimated as ~0.3% of saturation oxygen coverage), which was undetected in the O_2-TPD measurements in Figure 5.7. It is noted that oxygen admolecules dissociate into oxygen adatoms on the Pd(111) surface at ~180−200 K,[166-168] which is coincident with the temperature range in which we observed CO_2 production from the reaction of CO with oxygen species on the Pd−Au surface in CO-RMBS experiments (Figure 5.10(b)).

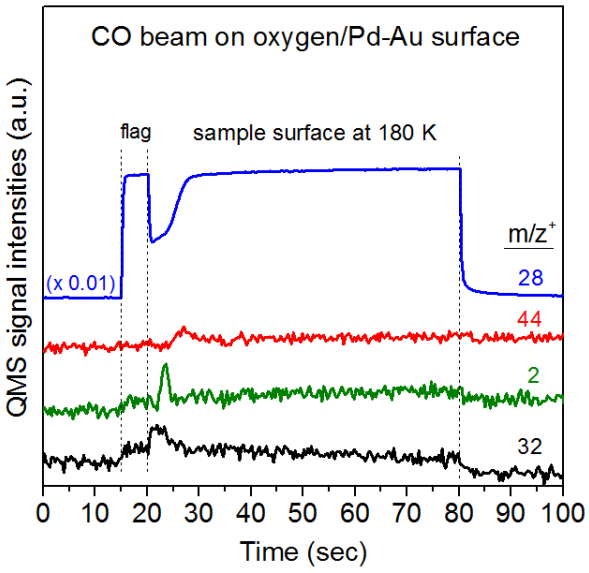

Figure 5.13. O_2 ($m/z^+ = 32$), CO_2 ($m/z^+ = 44$), H_2 ($m/z^+ = 2$) and CO ($m/z^+ = 28$) QMS signals during CO-RMBS on the oxygen-precovered 500 K-annealed 2.9 ML Pd/Au(111) surface at 180 K.

DFT calculations were performed to examine the influence of the Pd ensemble size on the reaction mechanism of CO oxidation on Pd−Au surfaces. In this study, we consider two possible Langmuir−Hinshelwood mechanisms, i.e., dissociative and associative mechanisms, as shown in Scheme 1.[176]

Scheme 5.1. Potential dissociative and associative mechanisms for the reaction of oxygen with CO to form CO_2.[176]

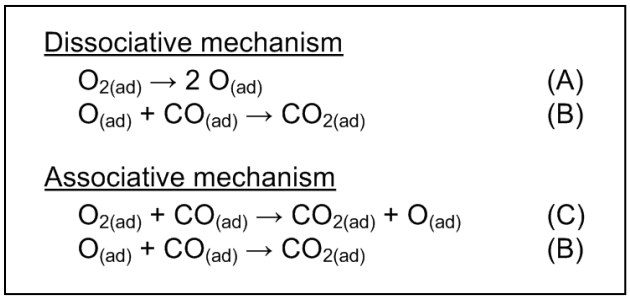

The dissociative and associative mechanisms are different from each other in regards to their initial step. For the dissociative mechanism, the O_2 admolecule dissociates into O adatoms as the first step (step A). In the associative mechanism, the first step is the bimolecular reaction between the O_2 admolecule and adsorbed CO to form adsorbed CO_2 and an O adatom (step C). The dissociative and associative mechanisms result in the same overall reaction as the second step (step B), i.e., the O adatom reacts with adsorbed CO to form adsorbed CO_2.[176]

Figure 5.14 shows the calculated energy barriers for each step in the dissociative and associative CO oxidation on Pd/Au(111) surfaces. The corresponding reaction enthalpies are summarized in Table 5.1. It is noted that the Pd−Au surfaces with a Pd

ensemble size of less than four atoms are excluded due to the lack of a capacity for CO and O_2 coadsorption. The initial, transition and final state configurations on each surface are similar; accordingly, only those on the Pd_6−Au(111) surface are illustrated in Figure 5.15 as an example.

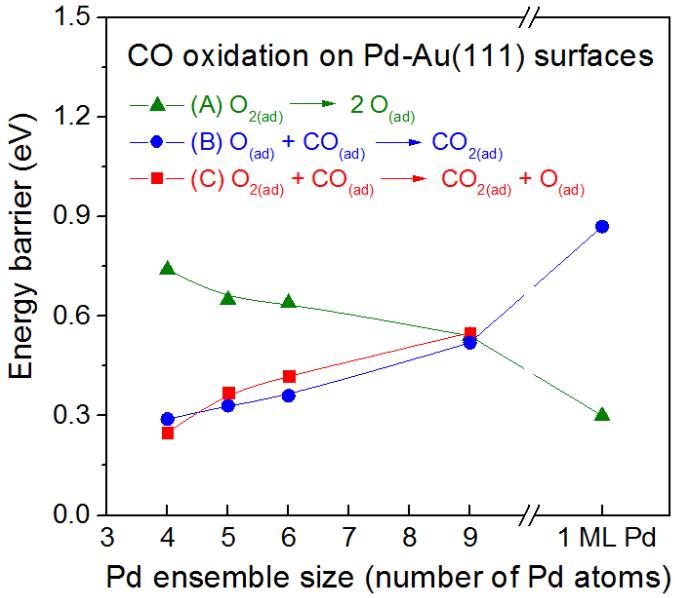

Figure 5.14. Energy barriers for dissociative and associative CO oxidation on Pd/Au(111) surfaces as determined by DFT calculations.

Table 5.1. Calculated enthalpies for associative and dissociative CO oxidation on Pd/Au(111) surfaces.[a]

Reaction steps	Pd-decorated Au(111) surfaces				
	Pd_4-	Pd_5-	Pd_6-	Pd_9-	Pd_{1ML}-
(A) $O_{2(ad)} \rightarrow 2\ O_{(ad)}$	-0.54	-0.94	-1.00	-1.29	-1.86
(B) $O_{(ad)} + CO_{(ad)} \rightarrow CO_{2(ad)}$	-1.83	-1.74	-1.13	-0.87	-0.30
(C) $O_{2(ad)} + CO_{(ad)} \rightarrow CO_{2(ad)} + O_{(ad)}$	-2.65	-2.44	-2.32	-2.06	n/a

[a] all energy values are in eV.

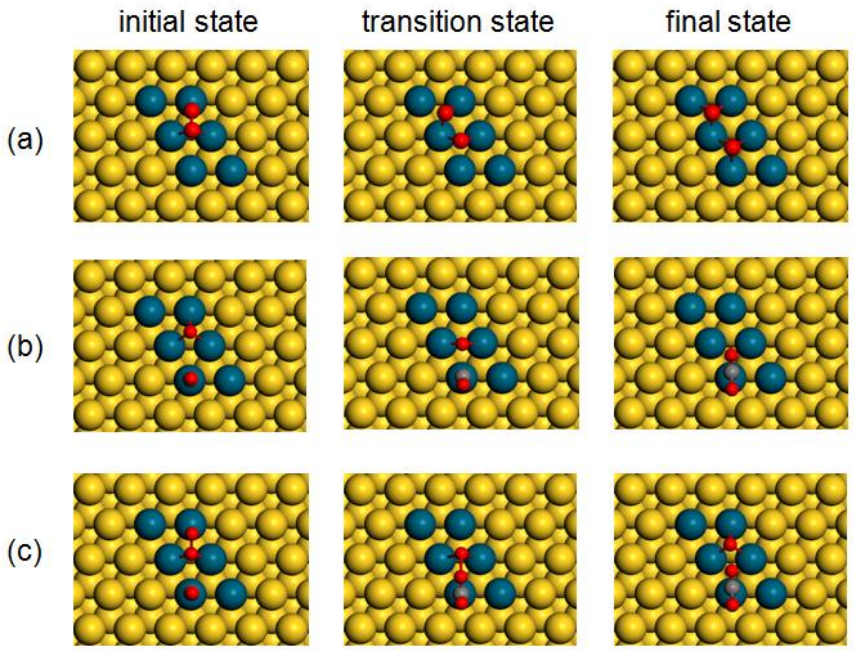

Figure 5.15. Top views of adsorption configuration images for initial, transition and final states for (a) $O_{2(ad)} \rightarrow 2\ O_{(ad)}$, (b) $O_{(ad)} + CO_{(ad)} \rightarrow CO_{2(ad)}$, and (c) $O_{2(ad)} + CO_{(ad)} \rightarrow CO_{2(ad)} + O_{(ad)}$ on the Pd_6-Au(111) surface. Yellow, blue, red and grey balls indicate Au, Pd, O and C atoms, respectively.

On the Pd_4−Au(111) surface, the energy barriers for $O_{2(ad)} \rightarrow 2O_{(ad)}$ (step A), $O_{(ad)} + CO_{(ad)} \rightarrow CO_{2(ad)}$ (step B) and $O_{2(ad)} + CO_{(ad)} \rightarrow CO_{2(ad)} + O_{(ad)}$ (step C) are 0.74, 0.29 and 0.25 eV, respectively. These results suggest that associative CO oxidation is favorable on this surface, whereas dissociative CO oxidation is inhibited by a higher energy barrier for dissociating the O_2 admolecule. It is worth mentioning that the energy for O_2 desorption on the Pd_4−Au(111) surface is 0.26 eV (Figure 5), which is

comparable to the reaction barriers for $O_{(ad)} + CO_{(ad)} \rightarrow CO_{2(ad)}$ (step B) and $O_{2(ad)} + CO_{(ad)} \rightarrow CO_{2(ad)} + O_{(ad)}$ (step C).

As the Pd ensemble size increases, the energy barrier for O_2 dissociation (step A) reduces, while energy barriers for $O_{(ad)} + CO_{(ad)} \rightarrow CO_{2(ad)}$ (step B) and $O_{2(ad)} + CO_{(ad)} \rightarrow CO_{2(ad)} + O_{(ad)}$ (step C) both increase. These energy barriers become comparable on the Pd_9−Au(111) surface, which suggests that CO oxidation could proceed via both associative and dissociative pathways on this surface. As mentioned earlier, the dominant oxygen species on the Pd_{1ML}−Au(111) surface is the O adatom rather than the O_2 admolecule due to a lower energy barrier for O_2 dissociation. Accordingly, dissociative CO oxidation is favorable on the Pd_{1ML}−Au(111) surface, which is consistent with the experimental observations from the Pd(111) surface.[9, 196-199]

On the basis of these DFT calculations, a generalization regarding the effect of Pd ensemble size on oxygen activation and reaction with CO was derived as follows: for the Pd−Au surface containing small Pd ensembles, O_2 desorption and associative CO oxidation are the two major competing processes, whereas the pathway for dissociative CO oxidation is limited by a high energy barrier for O_2 dissociation. On the Pd−Au surface with bigger Pd ensembles, the oxygen admolecule dissociates readily and, in turn, promotes CO_2 formation via the dissociative CO oxidation pathway.

It is well-accepted that CO oxidation occurs on the Pd(111) surface via a dissociative pathway,[9, 196-199] in which chemisorbed CO reacts with dissociatively

adsorbed oxygen to form CO_2. DFT calculations in this study and previous reports[175, 178] suggest that CO oxidation could also occur through an associative mechanism on the Pd−Au surface containing small Pd ensembles. Nevertheless, it is noted that an associative pathway was not experimentally supported in this study (Figure 5.10(b)), in which no CO_2 production was detected when the CO beam was impinged onto the molecular oxygen-precovered Pd−Au surface at and below 150 K. This absence of CO_2 production can be explained by the facile CO-induced displacement of O_2 (Figure 5.10(a)) due to significantly higher binding energies of CO relative to those of O_2 (Figures 5.6 and 5.12), which inhibits CO oxidation from proceeding via associative mechanism.

5.4 CONCLUSIONS

A model catalyst study combining UHV experiments and DFT calculations was performed to investigate the activation and reaction of oxygen molecules on the Pd−Au surface. Results based on O_2 King−Wells, CO-RAIRS, and DFT show that the presence of contiguous Pd sites is essential for adsorption of oxygen molecules on the Pd−Au surface. Upon heating, the adsorbed oxygen molecules molecularly desorbed from the Pd−Au surface (< 220 K) without detectable dissociation (signified by a lack of recombinative desorption of oxygen atoms) in O_2-TPD experiments. DFT calculations show that as the Pd ensemble size increases on the Pd/Au(111) surface the energy for O_2 desorption increases and the energy barrier for O_2 dissociation decreases. Oxygen molecules adsorbed on the Pd/Au(111) surface were readily displaced by CO at lower temperatures (77−150 K) due to competitive adsorption on surface sites. The adsorbed oxygen molecule can be thermally activated at higher temperatures (180−250 K) to react with CO to form CO_2. On the basis of DFT calculations, dissociative CO oxidation is favorable on the Pd−Au surface containing larger Pd ensembles; for the Pd−Au surface containing small Pd ensembles, associative CO oxidation and O_2 desorption are the two competing processes that are both favored over dissociative CO oxidation. In this study, an associative CO oxidation mechanism was not experimentally observed on the Pd−Au surface, which could be attributed to the fact that weakly bound O_2 desorbs readily by CO displacement at low temperatures. We hope the findings in this study will assist in the future design of Pd−Au bimetallic catalysts and their applications to associated reactions.

Chapter 6: Effect of Annealing in Oxygen on Alloy Structures of Pd−Au Bimetallic Model Catalysts

6.1 INTRODUCTION

Bimetallic catalysts have received substantial attention as their physicochemical properties often differ from those of their parent metals, which hold the promise of enhanced activity, selectivity and stability.[4-5] As one of the most studied bimetallic systems, Pd−Au catalysts have displayed promising performance for a broad range of catalytic reactions such as CO oxidation,[13-15] acetoxylation of ethylene to vinyl acetate,[16-17] selective oxidation of alcohols,[18-21] selective hydrogenation of unsaturated hydrocarbons,[22-25] hydrodechlorination (HDC) of chlorinated compounds,[26-28] hydrodesulfurization (HDS) of sulfur-containing molecules,[29-30] decomposition of liquid hydrocarbons for H_2 production,[31-32] and the direct synthesis of H_2O_2 from H_2 and O_2,[33-38] It has been suggested that the synergistic effects that are observed for Pd−Au bimetallic catalysts originate from the formation of alloy structures (homogeneous or core-shell) that could electronically modify the nature of the active sites.[21, 30, 38]

Recently it was reported that adequate calcination (i.e., annealing in air) can efficiently improve the catalytic performance of Pd−Au catalysts.[15, 30, 35-38, 200] Scanning transmission electron microscopy (STEM) imaging showed that calcination can modify the alloy structure of Pd−Au nanoparticles.[35-38, 200] The evolution of the alloy structure upon calcination appears to be a complex process as it depends on the calcination

temperature,[35-38, 200] type of support material used,[35-38] and method of catalyst preparation.[37-38] For instance, with TiO_2 as the support material, Pd−Au nanoparticles changed from a Pd-rich shell and Au-rich core structure to a homogeneous alloy when the calcination temperature was increased from 350 to 700 ^oC.[200] The structure of Pd−Au nanoparticles immobilized on carbon remained as a homogeneous alloy after calcination at 450 ^oC, whereas TiO_2- and Al_2O_3-supported Pd−Au nanoparticles transformed into a Pd-rich shell and Au-rich core structure.[35]

A molecular-level investigation of how the structure and composition of Pd−Au surfaces change in response to annealing in an oxygen ambient could enhance the fundamental understanding of the calcination effect on Pd−Au catalysts. In model catalyst studies, well-defined single-crystal surfaces are prepared under ultrahigh vacuum (UHV) conditions and characterized in-situ by surface science techniques, which enable surface characterization at the molecular level with minimal environmental interference.[4-11]

The evolution of the surface structure and composition of Pd−Au model catalysts upon annealing in UHV has been extensively studied.[43-45, 75-76, 88-89, 93-94, 118, 201-204] For example, using low-energy ion-scattering spectroscopy (LEISS), Koel et al.[88] have shown that annealing in UHV causes the diffusion of surface Pd atoms into the subsurface of the Au(111) single-crystal (i.e., alloying) at temperatures as low as 240 K. On the other hand, the intermixing of Au with Pd occurred at much higher temperatures (> 600 K) for an Au overlayer on the Pd(111) surface.[45, 118] In contrast to extensive studies of

annealing under UHV conditions, very little attention has been paid to experimental investigations with annealing Pd−Au model catalysts in an oxygen ambient. Recently the influence of adsorbed oxygen on the segregation of a Pd monomer in the Au(111) surface was studied theoretically.[205-206] By using density functional theory (DFT) analyses, Guesmi and co-workers[205] demonstrated that when oxygen atoms are present on the surface, the Pd monomer is energetically more favorable at the topmost layer of Au(111) surface than in the subsurface region.

In this study, we have prepared a variety of Pd−Au surfaces by annealing the Pd/Au(111) surface to various temperatures in the absence (UHV) and presence of oxygen (1×10^{-6} Torr of O_2). These annealed Pd/Au(111) surfaces were characterized and compared in order to study the influence of oxygen on the atomic structure of Pd−Au bimetallic surfaces. The composition of the near-surface region of annealed Pd/Au(111) surfaces was analyzed via Auger electron spectroscopy (AES). The effect of surface oxygen coverage on total system energy and surface Pd coverage of the 1 ML Pd/Au(111) surface was simulated using Basin hopping methods.[207] The surface structures on UHV-annealed and oxygen-annealed Pd−Au surfaces were further investigated by reflection-absorption infrared spectroscopy using CO as a probe molecule (CO-RAIRS). King−Wells measurements and temperature-programmed desorption (TPD) were conducted to study the interactions of oxygen with annealed Pd/Au(111) surfaces. Finally, the catalytic activities for CO oxidation on UHV-annealed and

oxygen-annealed Pd/Au(111) surfaces were compared via reactive molecular beam scattering (RMBS) experiments.

6.2 Experimental and Computational Methods

6.2.1 Model Catalyst Experiments

All experiments in this study were performed in an UHV chamber that has been described in detail previously.[84, 86] Briefly, the chamber is equipped with an Auger electron spectrometer (Physical Electronics 10-500), a quadrupole mass spectrometer (Extrel C-50), a Fourier transform infrared spectrometer (Bruker Tensor 27) combined with a mercury-cadmium-telluride (MCT) detector (Infrared Associates), as well as nozzles and apertures for generating two separate molecular beams.

The Au(111) single-crystal sample is a circular disk (Princeton Scientific, 12 mm in diameter × 2 mm thick) held in place by a Mo wire fitted around a groove cut into the side of the sample. This wire is also used to resistively heat the sample and to provide thermal contact between the sample and a liquid nitrogen bath for cooling. The temperature of the sample was measured with a K-type (Alumel−Chromel) thermocouple placed into a small hole in the edge of the disk-shaped sample. The Au(111) surface was periodically cleaned by Ar ion bombardment (2 keV), carried out at room temperature, followed by an anneal to 800 K. The cleanliness of the surface was verified by AES with a beam energy of 3 keV and emission current of 1.5 mA.

Pd−Au bimetallic model surfaces were prepared by depositing 1.5 monolayer (ML) of Pd atoms from a homemade thermal evaporator onto the Au(111) surface at 77 K followed by annealing in either UHV or in an ambient of O_2 at 1×10^{-6} Torr to a specified temperature for 10 min.[48-51] The growth of the Pd overlayer on the Au(111) surface at 77 K has been suggested to obey a layer-by-layer mechanism,[49] and upon annealing some of the surface Pd atoms can diffuse into the bulk of the Au(111) surface, forming a Pd−Au alloy at the surface.[17, 44, 88] The deposition rate of Pd was calibrated with a quartz crystal microbalance (QCM) controller (Maxtek Inc.) assuming a thickness of 1 ML Pd equals 0.274 nm.

CO-RAIRS was used to characterize the structure of annealed Pd/Au(111) surfaces.[48-49, 51] The Pd−Au surface was first heated to 500 K at 1 K/s to desorb any surface contaminants such as CO. After the sample had cooled to 77 K, an IR background scan was taken. A saturation coverage of CO was then delivered by a molecular beam of CO with the sample held at 77 K. The IR spectrum of saturated CO adsorbed on the surface was taken at 77 K. All spectra were averaged from 512 scans with a resolution of 4 cm^{-1}.

The adsorption of oxygen molecules on Pd−Au surfaces was investigated by King and Wells measurements.[51, 87, 116-117, 183] A neat O_2 molecular beam with a translational energy of ~0.1 eV was first impinged on the stainless steel inert flag to establish a baseline. The beam was then impinged on the annealed Pd/Au(111) surface at a surface

temperature of 77 K. The O_2 QMS signal ($m/z^+ = 32$) was monitored during these King−Wells measurements.

For O_2-TPD and CO-RMBS experiments, the Pd−Au bimetallic surface was generated by depositing 1.5 ML Pd atoms on the Au(111) surface followed by annealing to 500 K for 10 min in UHV or an oxygen ambient. In O_2-TPD measurements, oxygen was dosed by impinging an O_2 beam on the Pd−Au surface at 77 K until its saturation. The surface was then heated at a rate of 1 K/s while $m/z^+ = 32$ (O_2) was monitored by QMS. For CO-RMBS experiments, the Pd−Au surface was first saturated with oxygen at 77 K by backfilling the chamber with 1 langmuir (L; 1 L = 1 × 10−6 Torr-s) of O_2 through a leak valve. The oxygen-precovered Pd−Au surface was then heated to a specific temperature (77−250 K) prior to CO beam impingement. QMS signals of $m/z^+ = 32$ (O_2), 44 (CO_2) and 28 (CO) were monitored simultaneously during CO-RMBS experiments.

6.2.2 Basin Hopping Simulations

Basin hopping (BH) simulations were used to study the reorganization process of a Pd/Au(111) slab. The Pd/Au(111) slab was modeled as a five-layer 4 × 4 Au(111) slab with the bottom two layers fixed and the top layer initially replaced by a monolayer of Pd atoms. BH simulations on Pd/Au(111) slabs with 200 trials with the presence of different oxygen coverages (θ_O = 0, 0.25 and 0.5) were conducted at 500 K. For each

BH trail, one Pd atom was randomly selected to swap with one of its nearest-neighbor Au atoms. The acceptance probability (π) of each trial step is calculated by (eq. 6.1)

$$\pi = \min\ [1\ ,\ \exp(-\frac{E_i - E_{i-1}}{kT})] \qquad \text{(eq. 6.1)}$$

in which E_{i-1} and E_i are the energies of DFT optimized structures (in eV) before and after the ith swapping trial step, k is the Boltzmann constant (8.617×10^{-5} eV/K) and T is the absolute temperature (in K).

All DFT calculations were performed with the Vienna ab initio simulation package.[184-187] The interaction between the ionic core and the valence electrons was described by the project augmented wave method,[188] and the valence electrons were described with a plane-wave basis up to an energy cutoff of 220 eV.[189-190] The exchange correlation contribution to the total energy functional was determined using the Perdew-Burke-Ernzerhof (PBE) generalized gradient approximation functional.[191] The Brillouin zone was sampled using a $2 \times 2 \times 1$ Monkhorst-Pack k-point mesh.[194] The convergence criteria for the electronic structure and the atomic geometry were 10^{-4} eV and 0.05 eV/Å, respectively. A vacuum gap of 12 Å in the Z direction was used to avoid interactions from periodic images. Notably, values for the above computational parameters were chosen as a compromise of computational cost and proper physics.

6.3 Results and Discussion

6.3.1 AES Characterization of Pd/Au(111) Surfaces

We analyzed the composition in the near-surface region of annealed Pd/Au(111) surfaces by AES. Figures 6.1a and 6.1b show the AES spectra of the as-prepared Pd/Au(111) surface and those after annealing the surface to each specific temperature (i.e., 500, 550 and 600 K) in either UHV or 1×10^{-6} Torr of O_2, respectively.

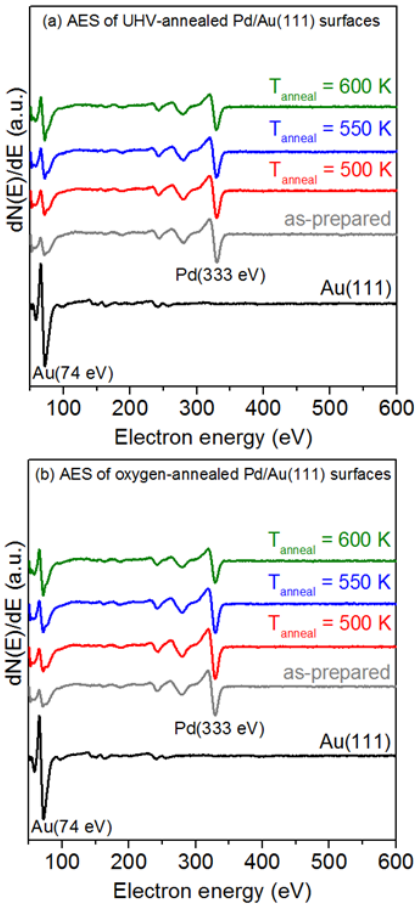

Figure 6.1. AES spectra of as-prepared 1.5 ML Pd/Au(111) surface and those after annealing the surface to a specific temperature in (a) UHV and (b) 1×10^{-6} Torr of O_2.

It is noted that the oxygen-annealed Pd/Au(111) surface typically showed a small oxygen signal in their first AES spectra after annealing in oxygen ambient (Figure 6.2). This oxygen signal was removed by simply heating to 500 K (Figure 6.2) to yield the oxygen-free AES spectra as shown in Figure 6.1b. We speculate that the presence of an oxygen signal on the oxygen-annealed surface was due to adsorption of background oxygen during sample cooling rather than formation of stable oxides on the Pd−Au surface. The adsorbed oxygen was weakly bound to the surface as indicated by desorption after mild heating.

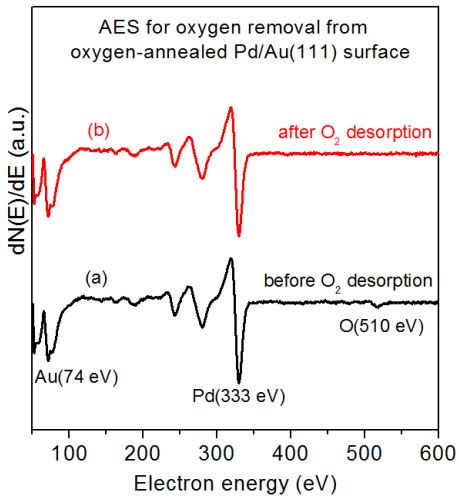

Figure 6.2. AES spectra of 1.5 ML Pd/Au(111) (a) immediately after annealed in 1 × 10^{-6} Torr of O_2 to 500 K for 10 min, and (b) after heating (a) surface to 500 K to desorb O_2.

The thermal stability of the Pd film deposited on the Au(111) surface in UHV has been thoroughly investigated.[44, 48, 88] Upon annealing under UHV conditions, alloying

occurs (i.e., Pd atoms from the topmost layer diffuse into the subsurface of Au(111) sample), which causes an increase in the Au LEISS signal intensity.[88] As shown in Figure 1, intensification of the Au AES signal intensity and attenuation of the Pd AES signal intensity were both observed when the Pd/Au(111) surface was annealed in either UHV or an oxygen ambient. These observations suggest that annealing the Pd/Au(111) surface in oxygen ambient also results in the interdiffusion of surface Pd atoms into the Au(111) sample, the same phenomena observed in the process of annealing in UHV.[44, 48, 88]

To further examine the influence of oxygen on the relative composition of Pd/Au(111) surfaces, the Pd(333 eV)/Au(74 eV) AES peak-to-peak ratios on the as-prepared surfaces and those annealed in UHV and oxygen were computed, as shown in Figure 6.3.

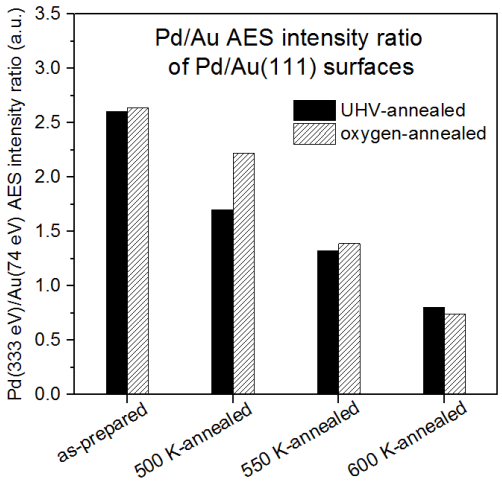

Figure 6.3. Pd(333 eV)/Au(74 eV) AES intensity ratio of as-prepared and annealed 1.5 ML Pd/Au(111) bimetallic surfaces.

With an annealing temperature of 500 K, the Pd/Au AES ratio on the oxygen-annealed Pd/Au(111) surface was significantly higher than that on the UHV-annealed surface, which suggests that the presence of oxygen can inhibit the diffusion of surface Pd atoms into the Au(111) subsurface. When Pd/Au(111) surfaces were annealed at higher temperatures (i.e., 550 and 600 K), the influence of adsorbed oxygen on the Pd/Au AES ratio became insignificant. We note that AES can detect not only the topmost layer of the surface but also the atoms in the near-surface region (the mean free path of electrons with energies between 10 and 1000 eV is of the order of a few atomic layers[208]). Accordingly, some Pd and Au atoms in the near-surface region that are not surface-accessible may also contribute to AES signals[203] on the annealed Pd/Au(111) surfaces.

6.3.2 Basin Hopping Simulations of Pd/Au(111) Surfaces

The influence of surface oxygen coverages on the total system energy and surface Pd coverage (θ_{Pd}) of the 1 ML Pd/Au(111) surface was investigated by Basin hopping simulations. The simulation results and top views for initial and final structures are depicted in Figure 6.4.

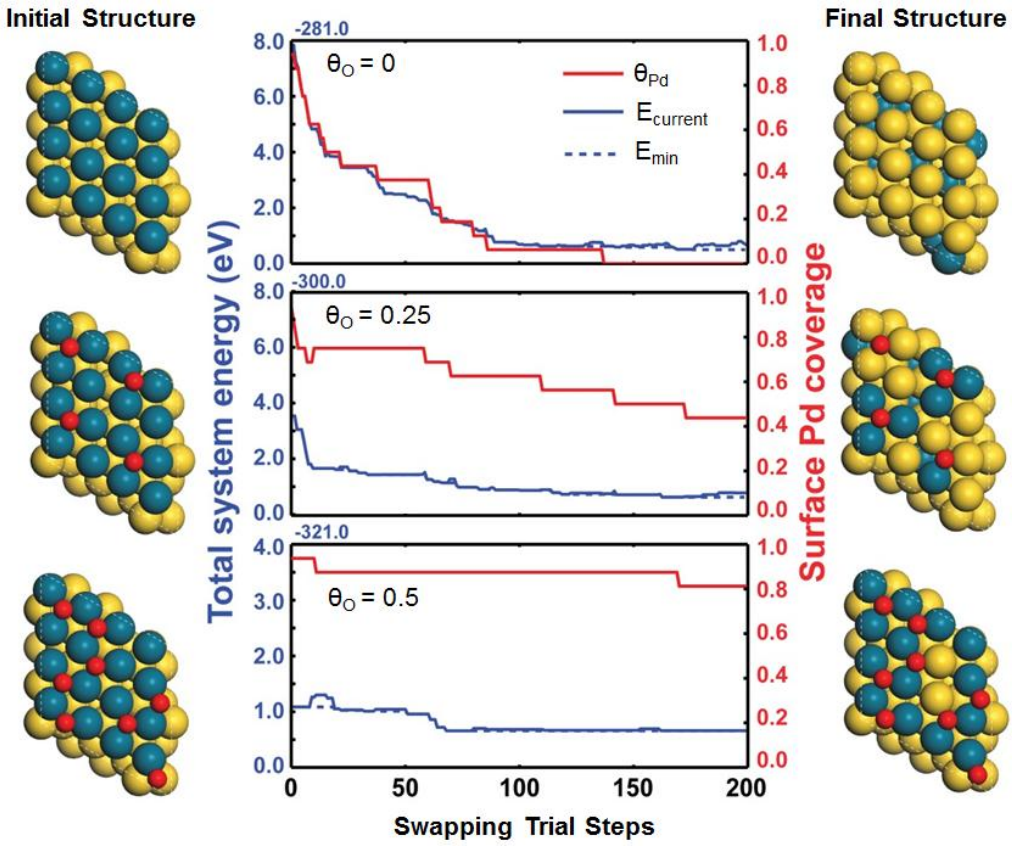

Figure 6.4. Basin hopping simulations for the total system energy and surface Pd coverage of the 1 ML Pd/Au(111) surface in the absence and presence of surface oxygen atoms. Blue solid and dashed lines represent the energy for current structure ($E_{current}$) and lowest energy visited so far (E_{min}), respectively. For convenience of comparison, the energy for surfaces with oxygen coverage of 0, 0.25 and 1 are referenced to -281, -300 and -321 eV, respectively. Red solid lines represent the surface Pd coverage. The top views for initial and final structures are included on left and right sides, respectively.

When oxygen atoms are absent from the surface ($\theta_O = 0$), the mixing of surface Pd atoms into the Au(111) subsurface is energetically favorable and the surface Pd coverage decreases sharply as simulation progresses. These results are consistent with

our AES observations (Figures 6.1 and 6.3) and previous studies using AES and LEISS characterizations[88] and STM imaging.[76, 204] For surfaces partially covered with oxygen atoms, the total system energy does not decrease as significantly during the simulation process. After 200 swapping steps, the decreases in total system energy are ~7.2, 2.8 and 0.3 eV for surfaces with oxygen coverages of 0, 0.25 and 0.5, respectively. These results suggest that the presence of surface oxygen atoms can stabilize the Pd/Au(111) system and the system is more energetically stable when more oxygen atoms are present on the surface.

Our Basin hopping simulations also show that the surface Pd coverage decreases more quickly in terms of number of swapping steps on the surface lacking oxygen than on the surfaces containing oxygen. The surface Pd coverage on the oxygen-free surface ($\theta_O = 0$) decreases to zero after 135 swapping steps, while the surface Pd coverages only decrease to 0.43 and 0.8 after 200 swapping steps on the oxygen-covered surfaces with $\theta_O = 0.25$ and 0.5, respectively. These simulation results suggest that oxygen atoms on the Pd/Au(111) can prevent the interdiffusion of Pd atoms into the Au slab, which supports our earlier interpretation from AES spectra (Figures 6.1 and 6.3) that surface oxygen atoms can inhibit the diffusion of surface Pd atoms into the Au(111) subsurface. These observations are also conceptually consistent with previous DFT studies,[205-206] in which the effect of oxygen on the segregation energy for Pd−Au surfaces was investigated using Pd monomer-Au(111) models.

The inhibition effect due to surface oxygen atoms likely results from the different strength between O−Pd bond and O−Au bond; because O binds to Pd more strongly than to Au, the swapping between surface Pd that bonds with oxygen and subsurface Au requires extra energy to overcome the energy difference between O-Pd and O-Au interaction. It is also worth noting that in the real case, the surface oxygen atoms that bond with Pd atoms could recombinatively desorb from the Pd−Au surface after Pd atoms are exchanged by Au atoms. This possible oxygen desorption was not included in our simulations in this study (it would further lower the surface Pd coverage if oxygen desorption is considered as a possibility).

6.3.3 CO-RAIRS Characterization of Pd/Au(111) Surfaces

The Pd/Au(111) surfaces annealed in UHV and oxygen were further characterized by CO-RAIRS. CO-RAIRS has long been used to study the properties and structures of model catalyst surfaces.[90, 209] The information regarding the adsorption site and surface morphology can be inferred from the observed CO stretching frequencies (νCO) as a result of varying degrees of π-antibonding back-donation from the surface electrons.[90, 209]

Figure 6.5 shows the RAIRS spectra of saturated CO on UHV-annealed and oxygen-annealed 1.5 ML Pd/Au(111) surfaces.

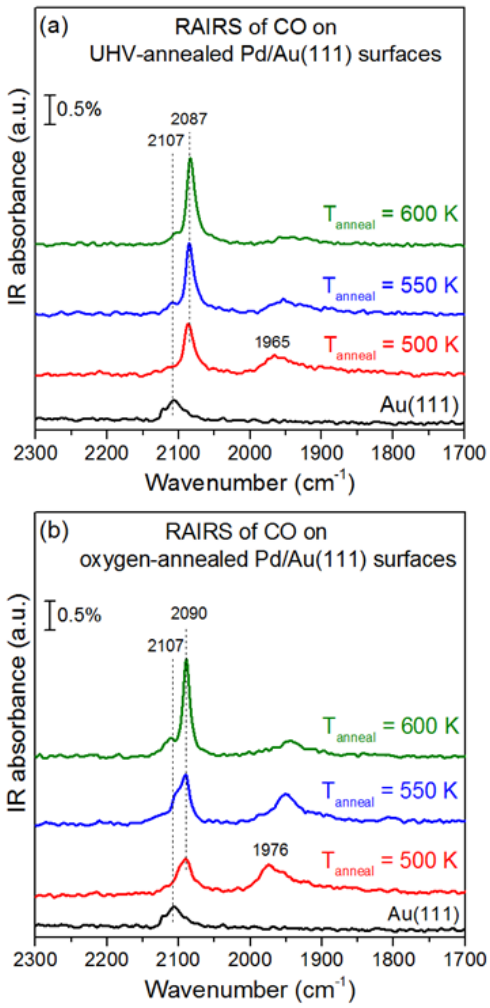

Figure 6.5. RAIRS spectra of saturated CO on 1.5 ML Pd/Au(111) surfaces annealed in (a) UHV and (b) 1×10^{-6} Torr of O_2 with various temperatures. These spectra were taken at a surface temperature of 77 K.

According to previously reported literature,[89, 93, 210] the assignment for the IR features of CO adsorbed on Pd−Au model surfaces has been established as follows:[39] ν_{CO} at 1900−2000, 2160−2085 and >2100 cm^{-1} corresponds to bridged CO on contiguous Pd

sites, atop CO on isolated Pd sites and atop CO on Au sites, respectively. As shown in Figure 6.5a, the Pd/Au(111) surface annealed in UHV at 500 K displayed two main IR bands at ~2087 and 1965 cm^{-1}, which can be attributed to CO adsorbed on isolated and contiguous Pd sites, respectively. These two IR bands shifted to higher frequencies at ~2090 cm^{-1} and 1976 cm^{-1} on the Pd/Au(111) surface annealed in oxygen at 500 K (Figure 6.5b). When the annealing temperature was gradually increased, the intensity of IR feature due to contiguous Pd sites attenuated and that due to isolated Pd sites intensified on both UHV-annealed and oxygen-annealed surfaces. It is found that with the same annealing temperature, the IR feature associated with contiguous Pd sites is consistently larger on oxygen-annealed surfaces than that on UHV-annealed surfaces. These observations suggest that a higher number of contiguous Pd atoms are present on oxygen-annealed surfaces in comparison to that on UHV-annealed surfaces.

It is noted that although CO-RAIRS can provide qualitative information such as surface morphology and adsorption sites of Pd−Au model surfaces, quantitative analysis using CO-RAIRS is quite difficult when contiguous Pd sites are present on the surface,[50] likely due to the vibrational coupling effect that attenuates the IR intensity at high surface CO coverages.[93]

6.3.4 Oxygen Adsorption and Desorption on Pd/Au(111) Surfaces

As mentioned earlier, Pd−Au catalysts have displayed promising performance in a number of catalytic reactions involving oxygen as a reactant.[13-21, 33-38] Accordingly, it is of interest to investigate the interaction of oxygen with the annealed Pd/Au(111) surfaces in this study. King−Wells measurements have been employed to study the adsorption of oxygen molecules on UHV-annealed Pd/Au(111) surfaces.[51] By analyzing the O_2 QMS signals from the inert flag and sample surface during the King−Wells measurement, (semi-)quantitative information such as the initial sticking probability and uptake for oxygen molecules on the surface can be determined.[51]

Figure 6.6 shows the O_2 QMS signal during a series of King−Wells measurements in which an O_2 beam was impinged onto annealed 1.5 ML Pd/Au(111) surfaces. In these measurements, the O2 molecular beam was first impinged onto the inert flag for 5 s (from 10 to 15 s) to establish a baseline signal (all O2 molecules scattering from the inert flag), and then impinged onto the annealed Pd/Au(111) surfaces that were held at 77 K for 30 s (from 15 to 45 s). The same measurements were carried out on the clean (Pd-free) Au(111) surface for comparison.

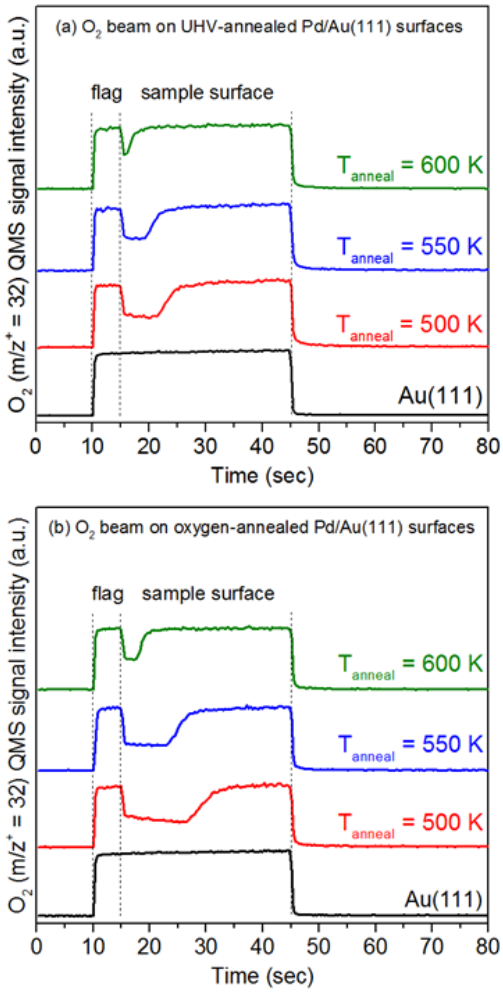

Figure 6.6. O_2 (m/z^+ = 32) QMS signals detected during King–Wells measurements. The 1.5 ML Pd/Au(111) surfaces were annealed to a specific temperature in (a) UHV and (b) 1×10^{-6} Torr of O_2. For these measurements, an O_2 beam was impinged on the surface at 77 K.

A constant O_2 QMS signal was detected when the O_2 beam was impinged on the inert flag and Au(111) surface, indicating that oxygen was not adsorbed on the Au(111) surface under this condition. The intensity of the O_2 QMS signal upon impingement of

the beam onto each annealed Pd/Au(111) surface is initially lower than that from impingement onto the inert flag due to the adsorption of oxygen on the surface. We attributed this observed adsorption to be molecular in nature[51] since oxygen molecularly adsorbs on the Pd(111) surface at 80 K,[167] and the dissociation of oxygen admolecules occurs at higher temperatures between ~180−200 K.[166-168] The initial sticking probability for oxygen molecules on each surface can be estimated from the O_2 QMS signal intensities from the inert flag and sample surface (Figure 6.7).

The initial sticking probability of O_2 (S_{O_2}) on the surface can be calculated by (eq. 6.2)

$$S_{O_2} = \frac{I_{inert\ flag} - I_{sample,\ initial}}{I_{inert\ flag}} \qquad \text{(eq. 6.2)}$$

where $I_{inert\ flag}$ is the intensity of O_2 QMS signal from impingement of the O_2 beam onto the inert flag, and $I_{sample,\ initial}$ is the initial intensity of O_2 QMS signal from impingement of the O_2 beam onto the sample.

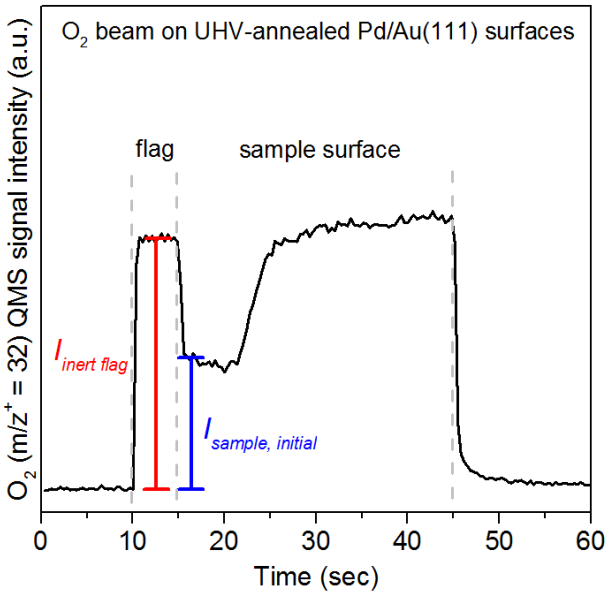

Figure 6.7. Calculation of initial sticking probability of O_2 on the annealed Pd/Au(111) surface in the King−Wells measurement at 77 K. The 1.5 ML Pd/Au(111) surface annealed at 500 K in UHV was used as an example surface.

The initial sticking probability for the oxygen-annealed Pd/Au(111) surfaces is ~0.48−0.52, which is slightly higher than that for the UHV-annealed surface (~0.43−0.45). It has been reported that the presence of contiguous Pd sites on Pd−Au surfaces is crucial for adsorption of oxygen molecules and that surfaces with only isolated Pd sites do not readily uptake O_2.[51] Accordingly, we speculate that the higher initial sticking probability observed here is due to a higher number of contiguous Pd sites present on oxygen-annealed Pd/Au(111) surfaces as compared to those on UHV-annealed surfaces.

The oxygen uptake on each surface during the King−Wells measurements can be computed using the O_2 QMS signals from the inert flag and sample surface (Figure 6.8). For convenience of comparison, the oxygen take on each surface in expressed as the relative oxygen uptake, which is relative to the oxygen uptake on the Pd/Au(111) surface annealed in UHV at 500 K (Figure 6.9).

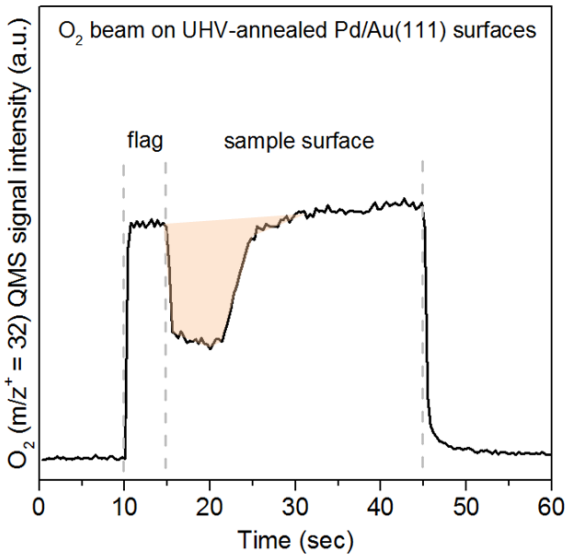

Figure 6.8. Calculation of O_2 uptake on oxygen-annealed 1.5 ML Pd/Au(111) surfaces during the King−Wells measurement at 77 K. The 1.5 ML Pd/Au(111) surface annealed at 500 K in UHV was used as an example surface. The O_2 uptake on the surface is proportional to the shaded area indicated in the figure.

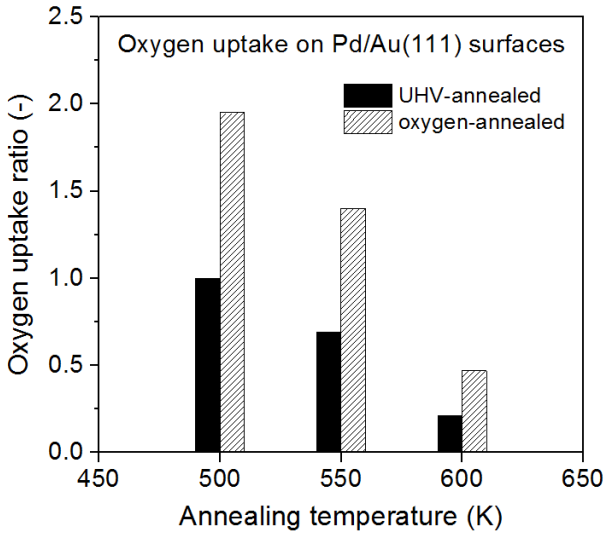

Figure 6.9. (a) O_2 ($m/z^+ = 32$) and (b) CO_2 ($m/z^+ = 44$) QMS signals during CO-RMBS on the oxygen-presaturated Pd/Au(111) bimetallic surface at various surface temperatures.

As expected, when the annealing temperature was increased, the relative oxygen uptake on UHV-annealed and oxygen-annealed surfaces was both decreased due to diffusion of surface Pd atoms into the Au(111) subsurface during annealing. For UHV-annealed surfaces, the oxygen uptake on the surface annealed at 500 K dropped to its 69% and 21% when surfaces annealed at 550 and 600 K, respectively. The decrease in oxygen uptake is found to be smaller on oxygen-annealed surfaces; the oxygen uptake on the surface annealed at 500 K reduced to 77% and 31% for annealing at 550 at 600 K, respectively. With the same annealing temperature, the oxygen uptake is consistently larger on oxygen-annealed surfaces than that on UHV-annealed surfaces. Since the oxygen adsorption sites on Pd/Au(111) surfaces consist of surface Pd atoms,[51] these

observations support that oxygen-annealed Pd/Au(111) surfaces contain more surface Pd atoms than UHV-annealed Pd/Au(111) surfaces, which are consistent with AES spectra (Figures 6.1 and 6.3) and Basin hopping simulations (Figure 6.4). It is noted that despite their similar Pd/Au AES ratios (Figure 6.3), the Pd/Au(111) surfaces annealed in UHV and oxygen at temperatures of 550 and 600 K display a significant difference in their oxygen uptake. This is explained as due to some of the Pd atoms residing in the subsurface region which will be detected by AES but unable to adsorb molecular oxygen. These results provide strong evidence that the presence of oxygen can keep Pd atoms stay on the topmost layer on Pd/Au(111) surfaces during annealing.

Figure 6.10 shows the TPD spectra of saturated O_2 from UHV-annealed and oxygen-annealed Pd/Au(111) surfaces. The Pd−Au surfaces were generated by depositing 1.5 ML Pd on the Au(111) surface at 77 K followed by annealing at 500 K in either UHV or 1×10^{-6} Torr of O_2. The surfaces were saturated with oxygen at 77 K by impinging a molecule beam of O_2 onto the surface prior to heating. To more clearly visualize desorption features, the O_2-TPD spectra were plotted within the temperature range between 77 and 300 K (no oxygen was observed when the temperature was higher than 300 K).

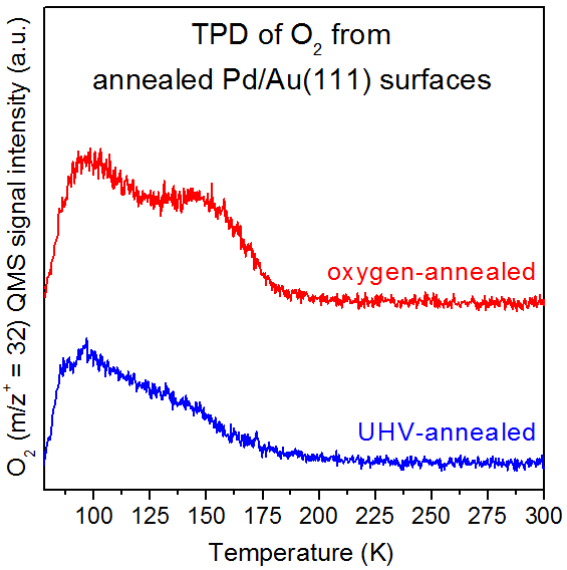

Figure 6.10. O_2 (m/z^+ = 32) QMS signals detected during O_2-TPD measurements. The 1.5 ML Pd/Au(111) surfaces was annealed at 500 K in (a) UHV and (b) 1×10^{-6} Torr of O_2. A saturation coverage of oxygen was dosed by impingement of O_2 beam at 77 K. The heating rate is 1 K/s.

The interaction of oxygen has been studied on the UHV-annealed Pd/Au(111) surfaces by O_2-TPD.[51] According to the desorption temperature, it was shown that with the exposure to O_2 at 77 K the oxygen admolecules on the UHV-annealed Pd/Au(111) surface desorbed molecularly (< ~220 K) without detectable dissociation upon heating.[51] In Figure 6.10, the oxygen desorption peak from the UHV-annealed and oxygen-annealed Pd/Au(111) surfaces both ended at ~200 K, which result from the desorption of molecularly adsorbed oxygen. The UHV-annealed surface displayed a broad O_2-TPD peak with a peak at ~97 K and a small shoulder at 140 K. This broad feature has been

attributed to the relatively high degree of surface heterogeneity in comparison to that of the Pd(111) surface.[51] It is noted that compared to the UHV-annealed surface, the shoulder of desorption peak (at ~148 K) became much more significant on the oxygen-annealed surface. High-resolution electron energy loss spectroscopy (HREELS) showed[166, 168] that oxygen molecules chemisorbed on the Pd(111) surface exist in three molecular states (one superoxo- and two peroxo-like species) with different vibrational frequencies of O−O stretching due to varying degrees of electron transfer from the surface into the oxygen molecule. Corresponding to these molecular states, three desorption features with peak temperatures of ~125, 150 and 200 K were observed.[167] Accordingly, the intensification of the desorption feature at ~148 K on the oxygen-annealed surface (Figure 6.10) suggests that some oxygen admolecules may exist in different molecular states that bind more strongly to the surface. Weaver and co-workers[211] have studied the O_2-TPD from the PdO(101) surface. In their O_2-TPD spectra, two main TPD peaks centered at 117 and 227 K as well as smaller features at 275 and 315 K were observed due to desorption of molecularly chemisorbed O_2.[211] The absence of a O_2-TPD feature at temperatures above 200 K in Figure 6.10 suggests that no oxide such as PdO formed after annealing the Pd/Au(111) surface in oxygen ambient, which is consistent with our observations from AES spectra (Figure 6.2).

6.3.5 Reaction of Oxygen and CO on Pd/Au(111) Surfaces

CO oxidation was employed to assess the catalytic activities of UHV-annealed and oxygen-annealed Pd/Au(111) surfaces by monitoring CO_2 production during CO-RMBS. As shown in Figure 6.11, CO-RMBS experiments were conducted by impinging a molecular beam of CO onto the inert flag for 5 s (from 10 to 15 s), and then onto the molecular oxygen-precovered Pd−Au surface for 60 s (from 15 to 75 s). For these measurements, the Pd−Au surface was generated by depositing 1.5 ML Pd onto the Au(111) surface at 77 K followed by annealing at 500 K in either UHV or 1×10^{-6} Torr of O_2. The surface was presaturated with molecular oxygen at 77 K and then heated to 250 K prior to CO beam impingement.

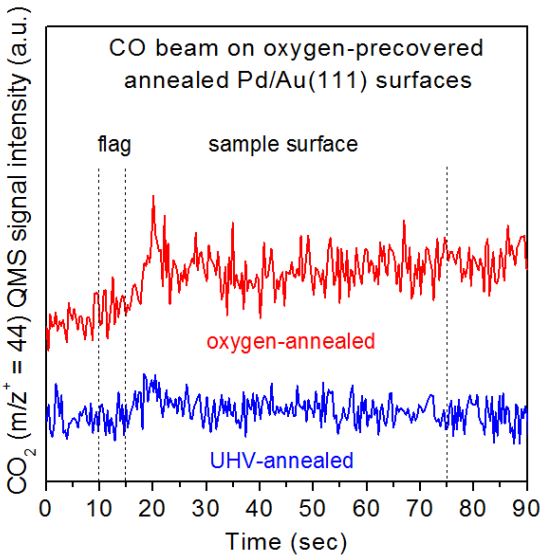

Figure 6.11. CO_2 ($m/z^+ = 44$) QMS signals detected during CO-RMBS experiments. The 1.5 ML Pd/Au(111) surfaces were annealed at 500 K in UHV and 1×10^{-6} Torr of O_2. The surface was presaturated with molecular oxygen at 77 K and then heated to 250 K prior to CO beam impingement.

Upon CO beam impingement at 250 K, CO_2 evolution was both detected from both UHV-annealed and oxygen-annealed Pd/Au(111) surfaces. A time delay for emergence of CO_2 signals has been attributed to the site blocking from oxygen and hydrogen impurities (from adsorption of background gas that is intrinsically present in our UHV chamber) on the Pd−Au surface.[51] The CO_2 peak observed from oxygen-annealed Pd/Au(111) surface was larger than that from UHV-annealed surface, indicative of a higher yield of CO_2. These observations demonstrate that the oxygen-annealed Pd/Au(111) surface is more active for CO oxidation than the UHV-annealed Pd/Au(111) surface. It is noted that the CO_2 production from the annealed Pd/Au(111) surface at 250 K is likely due to the reaction of CO with atomic oxygen since the desorption of molecular oxygen had completed at a temperature of ~220 K.[51] Accordingly, the higher activity for CO_2 production suggests that the dissociation of oxygen admolecules into oxygen adatoms is more facile on the oxygen-annealed surface than on the UHV-annealed surface. The relative ease of dissociation of oxygen admolecules could originate from the stronger interaction between O_2 and the oxygen-annealed Pd/Au(111) surface observed in TPD spectra (Figure 6.10).

6.4 CONCLUSIONS

In this study, we have conducted a model catalyst study that combines experimental and theoretical methods to investigate the effect of annealing in oxygen on the alloy structure and composition of Pd−Au bimetallic surfaces. Results based on AES, Basin hopping simulations and CO-RAIRS show that the presence of oxygen can inhibit the diffusion of surface Pd atoms into the Au(111) subsurface during annealing, resulting in a higher amount of Pd atoms present on the surface. Compared to the UHV-annealed Pd/Au(111) surface, the oxygen-annealed Pd/Au(111) surface exhibited a higher oxygen uptake during King−Wells measurements and stronger interactions with oxygen molecules in O_2-TPD experiments. CO-RMBS tests reveal that the oxygen-annealed Pd/Au(111) surface was more active than the UHV-annealed Pd/Au(111) surface for catalyzing CO oxidation to form CO_2. This enhanced activity on the oxygen-annealed surface is likely due to the higher oxygen uptake and a relatively more facile dissociation of oxygen admolecules. These results may enhance the fundamental understanding of Pd−Au alloy formation during calcination, and in turn aid the rational design of improved Pd−Au catalysts.

Chapter 7: Concluding Remarks and Future Research

7.1 Overview of Completed Work

In this dissertation, we performed five model catalyst studies with an attempt to enhance the understanding of the catalytic chemistry of Pd−Au bimetallic surfaces. The main findings in each chapter are summarized as follows:

In Chapter 2,[48] we demonstrate that Pd−Au bimetallic surfaces generated from annealing Pd/Au(111) in UHV readily dissociate H_2 and yet also weakly bind H adatoms, properties that could be beneficial for catalytic reactions involving hydrogen. The presence of contiguous Pd sites is vital for the dissociative adsorption of H_2 at 77 K. The H adatom binds to Pd−Au alloy sites more strongly than to Au(111) but more weakly than to Pd(111) as indicated by its desorption temperature (~200 K). With hydrogen exposure at slightly higher temperatures (i.e., 100−150 K), extension of a low-temperature desorption feature was observed, suggestive of the formation of subsurface H atoms (or H absorption). Experiments using deuterium indicate that H−D exchange over the Pd−Au bimetallic surface obeys Langmuir-Hinshelwood kinetics and that H/D adatoms are mobile on the surface at low temperatures.

In Chapter 3,[49] we show that CO adsorbs competitively on the hydrogen-precovered Pd−Au surface, causing surface H adatoms to diffuse away from stronger-binding sites (e.g., Pd(111)-like islands) to weaker-binding sites (e.g., Pd−Au alloy sites

and subsurface), as evidenced by a shift of the H_2 desorption feature to lower temperatures in TPD measurements. Evolution of H_2 was observed when a CO molecular beam was impinged onto the H-precovered Pd−Au surface, providing direct evidence that CO induces recombinative desorption of H adatoms. The presence of H adatoms on the Pd−Au surface was found to decrease the initial sticking probability of CO during MBS experiments but had little influence on CO desorption in subsequent TPD measurements.

In Chapter 4,[50] we tried to unravel the factors governing the catalytic properties of Pd−Au bimetallic surfaces for selective hydrogen production via HCOOH decomposition. Our results show that Pd atoms at the Pd−Au surface are responsible for activating HCOOH molecules; however, the selectivity of the reaction is dictated by the identity of the surface metal atoms adjacent to the Pd atoms. Pd atoms that reside at Pd−Au interface sites tend to favor dehydrogenation of HCOOH, whereas Pd atoms in Pd(111)-like sites, which lack neighboring Au atoms, favor dehydration of HCOOH. These observations suggest that the reactivity and selectivity of HCOOH decomposition on Pd−Au catalysts can be tailored by controlling the arrangement of surface Pd and Au atoms.

In Chapter 5,[51] we studied oxygen activation and reaction with CO on Pd−Au surfaces. Our results reveal that the presence of contiguous Pd sites is crucial for adsorption of oxygen molecules on Pd/Au(111) surfaces at 77 K. Upon heating, oxygen

admolecules desorbed molecularly without detectable dissociation. At lower temperatures (77−150 K), oxygen admolecules were readily displaced by CO due to competitive adsorption. Oxygen admolecules can be thermally activated at higher temperatures (180−250 K) to react with CO to form CO_2. DFT calculations show that the Pd−Au surface containing larger Pd ensembles favors dissociative CO oxidation, whereas associative CO oxidation and O_2 desorption are the two main competing processes for the Pd−Au surface containing small Pd ensembles. An associative CO oxidation pathway was not experimentally observed, which is likely due to facile CO-induced O_2 desorption.

In Chapter 6, we investigated the effect of annealing in oxygen on alloy structures of Pd−Au surfaces by comparing the physicochemical properties of Pd/Au(111) surfaces that were annealed in UHV versus an oxygen ambient. Our results reveal that the presence of oxygen can inhibit the diffusion of surface Pd atoms into the subsurface of the Au(111) sample. Pd/Au(111) surfaces annealed in an oxygen ambient possess more contiguous Pd sites than surfaces annealed under UHV conditions. The oxygen-annealed Pd/Au(111) surface exhibited a higher activity for CO oxidation. This enhanced activity likely results from the higher oxygen uptake and relatively facile dissociation of oxygen admolecules due to stronger adsorbate-surface interactions.

7.2 ONGOING AND FUTURE RESEARCH

In the following sections, several potential directions for the future research are described. Some of these directions are associated with the change of reactants or sample surfaces, which can be considered as short-term projects; while some of them are probably long-term projects as they will require the significant modifications on the apparatus.

7.2.1 Interactions with Alcohols

In this dissertation, we have studied the interactions between Pd−Au surfaces and small molecules including H_2, CO, O_2 and HCOOH. It is of research interest to study other organic molecules, particularly alcohols. Pd−Au alloys have displayed promising applications that convert alcohols into other fine chemicals (e.g., selective oxidation of alcohols into corresponding aldehydes or acids)[18-21, 57-58, 212-215] or electric energy (e.g., direct alcohol fuel cells).[101, 216]

The surface chemistry of alcohols on Pd−Au model catalysts are a relatively new research field and not well-studied yet. Lee and co-workers[46] reported that pure gold surfaces were catalytically inert towards crotyl alcohol. As compared to pure Pd surfaces, Pd−Au alloy surfaces exhibited high selectivity toward crotoaldehyde production with reduced activity for decomposition.[46] Very recently our group have studied the thermal desorption of ethanol and oxygen that coadsorbed on the annealed Pd/Au(111) surface. Our preliminary results suggest that acetaldehyde was produced

via partial oxidation from ethanol during TPD. Further investigations are undergoing to explore the possible mechanisms and the correlation between surface structures and activity/selectivity.

7.2.2 Utilization of Au/Pd(111) as Model Surfaces

In this dissertation, Pd−Au model surfaces were prepared by depositing Pd atoms onto the Au(111) surface followed by annealing to various temperatures. Our results show that the Au(111) surface is very inert and the Pd atoms on the surface are the active component. Indeed, Pd is more active than Au for many reactions, particularly when they are in the bulk form such as single crystals. Accordingly, utilization of Pd single-crystal surface as a substrate for Au deposition followed by annealing in UHV to generate Pd−Au model surfaces could be a useful approach to investigate the change in activity or selectivity of Pd modified by the addition of Au.

To date, several research groups have employed Au-decorated Pd single-crystal surfaces to study the catalytic reactions (e.g., CO oxidation,[47] coupling of acetylene to benzene,[45] and selective oxidation of crotyl alcohol to crotonaldehyde[46]), or surface interactions (e.g., ethylene,[217] acetic acid[218] and vinyl acetate[219]). Nevertheless, we believe that still many important reactions such as selective oxidation of alcohols (e.g., methanol, ethanol, glycerol etc.) and selective decomposition of carboxylic acid (e.g., formic acid) are worth investigations on the Au-decorated Pd single-crystal surfaces.

7.2.3 Bridging the Material Gap

Although the use of metal single crystals as sample surfaces has been proved useful for modeling the surface reaction on the high-surface-area catalyst, recently many researchers are striving to improve the molecular-level understanding of reaction mechanisms by employing more complicated model catalysts, for example, metal nanoparticles supported on the metal-oxide single-crystal, e.g., $Au/TiO_2(110)$[220-222], and metal-oxide nanoparticles supported on metal single-crystal (i.e., "inverse model catalysts"), e.g., CeOx/Au(111) and TiOx/Au(111)[223] and FeOx/Au(111).[224] Compared to metal/oxide model catalysts, inverse model catalyst (oxide/metal) is more attractive for investigating the role of the oxide in a catalytic process.[225]

The further approach would be the direct use of high-surface-area catalysts as the sample surface and combine it with surface-science techniques as characterization/testing tools. In this case, the method to mount the sample (namely, the design of sample holder) in the chamber is critical. One alternative that has been reported by Yates and co-workers[226] is the use of tungsten-mesh to secure the pressed Au/TiO_2 sample for IR measurements (Figure 7.1). In this design, IR spectra can be obtained using the transmission mode and tungsten-mesh allows ~70% IR transmission.[226]

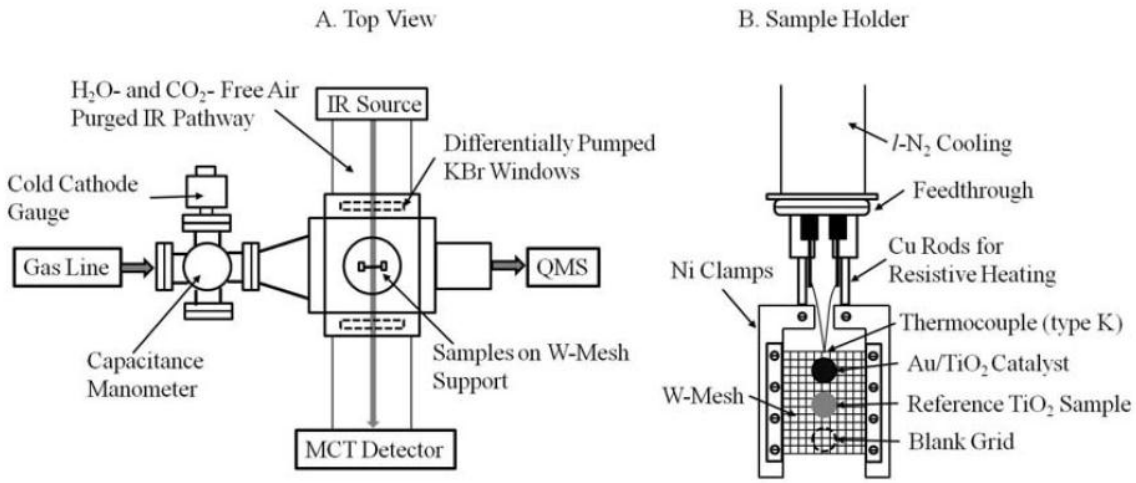

Figure 7.1. Schematic drawings of the high vacuum system for transmission IR studies. A.Top view of the IR cell. B. A closeup view of the sample holder.[226]

7.2.4 Bridging the Pressure Gap

In most of surface science studies, a (ultra)high vacuum environment is required to maintain a clean surface during measurements and to allow the use of surface-science spectroscopies that cannot operate at elevated pressures. This high vacuum is many orders of magnitude below the operating pressures used in practical catalytic processes. One approach to bridge this pressure gap is to combine an elevated pressure reactor (for kinetics study) with an UHV surface analysis chamber (for surface characterization before and after kinetic study).[227] For example, we have modified our UHV chamber to study the kinetics and deactivation mechanism of water-gas shift reaction on the Pt(111) surface at elevated pressure.[86]

Recently, some spectroscopic techniques have been developed to permit in-situ characterizations on model catalysts under reactive conditions at elevated pressures. For example, Goodman and co-workers have used polarization-modulation infrared reflection absorption spectroscopy (PM-IRAS) to study CO oxidation[39-40] and CO/NO reaction[41] on AuPd(100) model surfaces. Using ambient pressure X-ray photoelectron spectroscopy (APXPS), Somorjai group[228] characterized the restructuring of core-shell structures of Rh-Pd and Pt-Pd bimetallic nanoparticles that were deposited on oxidized surface of Si wafer in oxidizing and reducing environments.

Bibliography

1. Bartholomew, C. H.; R.J., F., *Fundamentals of Industrial Catalytic Processes*. New York:Wiley & Sons. 2nd ed.: 2006.

2. Gao, F.; Goodman, D. W., Model Catalysts: Simulating the Complexities of Heterogeneous Catalysts. *Annu. Rev. Phys. Chem.* **2012,** *63*, 265-286.

3. Chorkendorff, I.; Niemantsverdriet, J. W., *Concepts of Modern Catalysis and Kinetics*. Wiley-VCH. 2nd ed.: 2007.

4. Chen, J. G.; Menning, C. A.; Zellner, M. B., Monolayer Bimetallic Surfaces: Experimental and Theoretical Studies of Trends in Electronic and Chemical Properties. *Surf. Sci. Rep.* **2008,** *63*, 201-254.

5. Gao, F.; Goodman, D. W., Pd−Au Bimetallic Catalysts: Understanding Alloy Effects from Planar Models and (Supported) Nanoparticles. *Chem. Soc. Rev.* **2012,** *41*, 8009-8020.

6. Campbell, C. T., Bimetallic Surface Chemistry. *Annu. Rev. Phys. Chem.* **1990,** *41*, 775-837.

7. Somorjai, G. A., Modern Surface Science and Surface Technologies: An Introduction. *Chem. Rev.* **1996,** *96*, 1223-1235.

8. Weaver, J. F.; Carlsson, A. F.; Madix, R. J., The Adsorption and Reaction of Low Molecular Weight Alkanes on Metallic Single Crystal Surfaces. *Surf. Sci. Rep.* **2003,** *50*, 107-199.

9. Libuda, J.; Freund, H. J., Molecular Beam Experiments on Model Catalysts. *Surf. Sci. Rep.* **2005,** *57*, 157-298.

10. Gong, J. L., Structure and Surface Chemistry of Gold-Based Model Catalysts. *Chem. Rev.* **2012,** *112*, 2987-3054.

11. Pan, M.; Brush, A. J.; Pozun, Z. D.; Ham, H. C.; Yu, W.-Y.; Henkelman, G.; Hwang, G. S.; Mullins, C. B., Model Studies of Heterogeneous Catalytic Hydrogenation Reactions with Gold. *Chem. Soc. Rev.* **2013,** *42*, 5002-5013.

12. http://www.nobelprize.org/nobel_prizes/chemistry/laureates/2007/advanced-chemistryprize2007.pdf.

13. Gao, F.; Wang, Y. L.; Goodman, D. W., Reaction Kinetics and Polarization-Modulation Infrared Reflection Absorption Spectroscopy (PM-IRAS) Investigation of CO Oxidation over Supported Pd−Au Alloy Catalysts. *J. Phys. Chem. C* **2010,** *114*, 4036-4043.

14. Xu, J.; White, T.; Li, P.; He, C. H.; Yu, J. G.; Yuan, W. K.; Han, Y. F., Biphasic Pd−Au Alloy Catalyst for Low-Temperature CO Oxidation. *J. Am. Chem. Soc.* **2010,** *132*, 10398-10406.

15. Suo, Z. H.; Ma, C. Y.; Jin, M. S.; He, T.; An, L. D., The Active Phase of Au-Pd/Al_2O_3 for CO Oxidation. *Catal. Commun.* **2008,** *9*, 2187-2190.

16. Han, Y. F.; Wang, J. H.; Kumar, D.; Yan, Z.; Goodman, D. W., A Kinetic Study of Vinyl Acetate Synthesis over Pd-Based Catalysts: Kinetics of Vinyl Acetate Synthesis over Pd−Au/SiO_2 and Pd/SiO_2 Catalysts. *J. Catal.* **2005,** *232*, 467-475.

17. Chen, M. S.; Kumar, D.; Yi, C. W.; Goodman, D. W., The Promotional Effect of Gold in Catalysis by Palladium-Gold. *Science* **2005,** *310*, 291-293.

18. Enache, D. I.; Edwards, J. K.; Landon, P.; Solsona-Espriu, B.; Carley, A. F.; Herzing, A. A.; Watanabe, M.; Kiely, C. J.; Knight, D. W.; Hutchings, G. J., Solvent-Free Oxidation of Primary Alcohols to Aldehydes Using Au-Pd/TiO_2 Catalysts. *Science* **2006,** *311*, 362-365.

19. Wang, D.; Villa, A.; Porta, F.; Su, D. S.; Prati, L., Single-Phase Bimetallic System for the Selective Oxidation of Glycerol to Glycerate. *Chem. Commun.* **2006**, 1956-1958.

20. Dimitratos, N.; Lopez-Sanchez, J. A.; Anthonykutty, J. M.; Brett, G.; Carley, A. F.; Tiruvalam, R. C.; Herzing, A. A.; Kiely, C. J.; Knight, D. W.; Hutchings, G. J., Oxidation of Glycerol Using Gold-Palladium Alloy-Supported Nanocrystals. *Phys. Chem. Chem. Phys.* **2009,** *11*, 4952-4961.

21. Villa, A.; Wang, D.; Su, D. S.; Veith, G. M.; Prati, L., Using Supported Au Nanoparticles as Starting Material for Preparing Uniform Au/Pd Bimetallic Catalysts. *Phys. Chem. Chem. Phys.* **2010,** *12*, 2183-2189.

22. Hugon, A.; Delannoy, L.; Krafft, J.-M.; Louis, C., Selective Hydrogenation of 1,3-Butadiene in the Presence of an Excess of Alkenes over Supported Bimetallic Gold-Palladium Catalysts. *J. Phys. Chem. C* **2010,** *114*, 10823-10835.

23. Liu, R. X.; Yu, Y. C.; Yoshida, K.; Li, G. M.; Jiang, H. X.; Zhang, M. H.; Zhao, F. Y.; Fujita, S.; Arai, M., Physically and Chemically Mixed TiO_2-Supported Pd and Au Catalysts: Unexpected Synergistic Effects on Selective Hydrogenation of Citral in Supercritical CO_2. *J. Catal.* **2010,** *269*, 191-200.

24. Yang, X.; Chen, D.; Liao, S.; Song, H.; Li, Y.; Fu, Z.; Su, Y., High-Performance Pd–Au Bimetallic Catalyst with Mesoporous Silica Nanoparticles as Support and Its Catalysis of Cinnamaldehyde Hydrogenation. *J. Catal.* **2012,** *291*, 36-43.

25. El Kolli, N.; Delannoy, L.; Louis, C., Bimetallic Au-Pd Catalysts for Selective Hydrogenation of Butadiene: Influence of the Preparation Method on Catalytic Properties. *J. Catal.* **2013,** *297*, 79-92.

26. Nutt, M. O.; Hughes, J. B.; Wong, M. S., Designing Pd-on-Au Bimetallic Nanoparticle Catalysts for Trichloroethene Hydrodechlorination. *Environ. Sci. Technol.* **2005,** *39*, 1346-1353.

27. Fang, Y. L.; Heck, K. N.; Alvarez, P. J. J.; Wong, M. S., Kinetics Analysis of Palladium/Gold Nanoparticles as Colloidal Hydrodechlorination Catalysts. *ACS Catal.* **2011,** *1*, 128-138.

28. Fang, Y. L.; Miller, J. T.; Guo, N.; Heck, K. N.; Alvarez, P. J. J.; Wong, M. S., Structural analysis of palladium-decorated gold nanoparticles as colloidal bimetallic catalysts. *Catal. Today* **2011,** *160*, 96-102.

29. Venezia, A. M.; La Parola, V.; Deganello, G.; Pawelec, B.; Fierro, J. L. G., Synergetic Effect of Gold in Au/Pd Catalysts during Hydrodesulfurization Reactions of Model Compounds. *J. Catal.* **2003,** *215*, 317-325.

30. Suo, Z.; Ma, C.; Liao, W.; Jin, M.; Lv, H., Structure and Activity of Au-Pd/SiO_2 Bimetallic Catalyst for Thiophene Hydrodesulfurization. *Fuel Process. Technol.* **2011,** *92*, 1549-1553.

31. Zhou, X. C.; Huang, Y. J.; Xing, W.; Liu, C. P.; Liao, J. H.; Lu, T. H., High-Quality Hydrogen from the Catalyzed Decomposition of Formic Acid by Pd−Au/C and Pd-Ag/C. *Chem. Commun.* **2008**, 3540-3542.

32. Metin, O.; Sun, X. L.; Sun, S. H., Monodisperse Gold-Palladium Alloy Nanoparticles and their Composition-Controlled Catalysis in Formic Acid Dehydrogenation under Mild Conditions. *Nanoscale* **2013,** *5*, 910-912.

33. Landon, P.; Collier, P. J.; Carley, A. F.; Chadwick, D.; Papworth, A. J.; Burrows, A.; Kiely, C. J.; Hutchings, G. J., Direct Synthesis of Hydrogen Peroxide from H_2 and O_2 Using Pd and Au Catalysts. *Phys. Chem. Chem. Phys.* **2003,** *5*, 1917-1923.

34. Edwards, J. K.; Solsona, B.; Edwin, N. N.; Carley, A. F.; Herzing, A. A.; Kiely, C. J.; Hutchings, G. J., Switching Off Hydrogen Peroxide Hydrogenation in the Direct Synthesis Process. *Science* **2009,** *323*, 1037-1041.

35. Edwards, J. K.; Carley, A. F.; Herzing, A. A.; Kiely, C. J.; Hutchings, G. J., Direct Synthesis of Hydrogen Peroxide from H_2 and O_2 Using Supported Au-Pd Catalysts. *Faraday Discuss.* **2008,** *138*, 225-239.

36. Edwards, J. K.; Pritchard, J.; Piccinini, M.; Shaw, G.; He, Q.; Carley, A. F.; Kiely, C. J.; Hutchings, G. J., The Effect of Heat Treatment on the Performance and Structure of Carbon-Supported Au-Pd Catalysts for the Direct Synthesis of Hydrogen Peroxide. *J. Catal.* **2012,** *292*, 227-238.

37. Edwards, J. K.; Hutchings, G. J., Palladium and Gold-Palladium Catalysts for the Direct Synthesis of Hydrogen Peroxide. *Angew. Chem.-Int. Edit.* **2008,** *47*, 9192-9198.

38. Edwards, J. K.; Freakley, S. J.; Carley, A. F.; Kiely, C. J.; Hutchings, G. J., Strategies for Designing Supported Gold-Palladium Bimetallic Catalysts for the Direct Synthesis of Hydrogen Peroxide. *Accounts Chem. Res.* **2014,** *47*, 845-854.

39. Gao, F.; Wang, Y. L.; Goodman, D. W., CO Oxidation over AuPd(100) from Ultrahigh Vacuum to Near-Atmospheric Pressures: The Critical Role of Contiguous Pd Atoms. *J. Am. Chem. Soc.* **2009,** *131*, 5734-5735.

40. Gao, F.; Wang, Y. L.; Goodman, D. W., CO Oxidation over AuPd(100) from Ultrahigh Vacuum to Near-Atmospheric Pressures: CO Adsorption-Induced Surface Segregation and Reaction Kinetics. *J. Phys. Chem. C* **2009,** *113*, 14993-15000.

41. Gao, F.; Wang, Y.; Goodman, D. W., CO/NO and CO/NO/O_2 Reactions over A Au-Pd Single Crystal Catalyst. **2009,** *268*, 115-121.

42. Piednoir, A.; Languille, M. A.; Piccolo, L.; Valcarcel, A.; Aires, F.; Bertolini, J. C., Pd(111) versus Pd−Au(111) in Carbon Monoxide Oxidation under Elevated Pressures. *Catal. Lett.* **2007,** *114*, 110-114.

43. Ormerod, R. M.; Baddeley, C. J.; Lambert, R. M., Geometrical and Electronic Effects in the Conversion of Acetylene to Benzene on Au(111)/Pd and Au/Pd Surface Alloys. *Surf. Sci.* **1991,** *259*, L709-L713.

44. Baddeley, C. J.; Ormerod, R. M.; Stephenson, A. W.; Lambert, R. M., Surface Structure and Reactivity in the Cyclization of Acetylene to Benzene with Pd Overlayers and Pd/Au Surface Alloys on Au{111}. *J. Phys. Chem.* **1995,** *99*, 5146-5151.

45. Baddeley, C. J.; Tikhov, M.; Hardacre, C.; Lomas, J. R.; Lambert, R. M., Ensemble Effects in the Coupling of Acetylene to Benzene on A Bimetallic Surface: A Study with Pd{111}/Au. *J. Phys. Chem.* **1996,** *100*, 2189-2194.

46. Lee, A. F.; Hackett, S. F. J.; Hutchings, G. J.; Lizzit, S.; Naughton, J.; Wilson, K., In Situ X-ray Studies of Crotyl Alcohol Selective Oxidation over Au/Pd(111) Surface Alloys. *Catal. Today* **2009,** *145*, 251-257.

47. Li, Z. J.; Gao, F.; Tysoe, W. T., Carbon Monoxide Oxidation over Au/Pd(100) Model Alloy Catalysts. *J. Phys. Chem. C* **2010,** *114*, 16909-16916.

48. Yu, W.-Y.; Mullen, G. M.; Mullins, C. B., Hydrogen Adsorption and Absorption with Pd−Au Bimetallic Surfaces. *J. Phys. Chem. C* **2013,** *117*, 19535–19543.

49. Yu, W.-Y.; Mullen, G. M.; Mullins, C. B., Interactions of Hydrogen and Carbon Monoxide on Pd−Au Bimetallic Surfaces. *J. Phys. Chem. C* **2014,** *118*, 2129-2137.

50. Yu, W.-Y.; Mullen, G. M.; Flaherty, D. W.; Mullins, C. B., Selective Hydrogen Production from Formic Acid Decomposition on Pd−Au Bimetallic Surfaces. *J. Am. Chem. Soc.* **2014,** *136*, 11070–11078.

51. Yu, W.-Y.; Zhang, L.; Mullen, G. M.; Henkelman, G.; Mullins, C. B., Oxygen Activation and Reaction on Pd–Au Bimetallic Surfaces. *J. Phys. Chem. C* **2015,** *119*, 11754-11762.

52. Christmann, K., Interaction of Hydrogen with Solid Surfaces. *Surf. Sci. Rep.* **1988,** *9*, 1-163.

53. Behm, R. J., Interaction of Hydrogen with Bimetallic Surfaces. *Z. Phys. Chem.* **2009,** *223*, 9-36.

54. Greeley, J.; Mavrikakis, M., Surface and Subsurface Hydrogen: Adsorption Properties on Transition Metals and Near-Surface Alloys. *J. Phys. Chem. B* **2005,** *109*, 3460-3471.

55. Greeley, J.; Mavrikakis, M., Alloy Catalysts Designed from First Principles. *Nat. Mater.* **2004,** *3*, 810-815.

56. Lee, A. F.; Baddeley, C. J.; Hardacre, C.; Ormerod, R. M.; Lambert, R. M.; Schmid, G.; West, H., Structural and Catalytic Properties of Novel Au/Pd Bimetallic Colloid Particles - EXAFS, XRD, and Acetylene Coupling. *J. Phys. Chem.* **1995,** *99*, 6096-6102.

57. Ketchie, W. C.; Murayama, M.; Davis, R. J., Selective Oxidation of Glycerol over Carbon-Supported AuPd Catalysts. *J. Catal.* **2007,** *250*, 264-273.

58. Zhang, H. J.; Watanabe, T.; Okumura, M.; Haruta, M.; Toshima, N., Catalytically Highly Active Top Gold Atom on Palladium Nanocluster. *Nat. Mater.* **2012,** *11*, 49-52.

59. Hutchings, G. J., Nanocrystalline Gold and Gold Palladium Alloy Catalysts for Chemical Synthesis. *Chem. Commun.* **2008**, 1148-1164.

60. Huang, Y. J.; Zhou, X. C.; Yin, M.; Liu, C. P.; Xing, W., Novel PdAu@Au/C Core-Shell Catalyst: Superior Activity and Selectivity in Formic Acid Decomposition for Hydrogen Generation. *Chem. Mater.* **2010,** *22*, 5122-5128.

61. Gu, X. J.; Lu, Z. H.; Jiang, H. L.; Akita, T.; Xu, Q., Synergistic Catalysis of Metal-Organic Framework-Immobilized Au-Pd Nanoparticles in Dehydrogenation of Formic Acid for Chemical Hydrogen Storage. *J. Am. Chem. Soc.* **2011,** *133*, 11822-11825.

62. Conrad, H.; Ertl, G.; Latta, E. E., Adsorption of Hydrogen on Palladium Single Crystal Surfaces. *Surf. Sci.* **1974,** *41*, 435-446.

63. Behm, R. J.; Christmann, K.; Ertl, G., Adsorption of Hydrogen on Pd(100). *Surf. Sci.* **1980,** *99*, 320-340.

64. Behm, R. J.; Penka, V.; Cattania, M. G.; Christmann, K.; Ertl, G., Evidence for Subsurface Hydrogen on Pd(110) - An Intermediate between Chemisorbed and Dissolved Species. *J. Chem. Phys.* **1983,** *78*, 7486-7490.

65. Cattania, M. G.; Penka, V.; Behm, R. J.; Christmann, K.; Ertl, G., Interaction of Hydrogen with a Palladium(110) Surface. *Surf. Sci.* **1983,** *126*, 382-391.

66. Gdowski, G. E.; Felter, T. E.; Stulen, R. H., Effect of Surface Temperature on the Sorption of Hydrogen by Pd(111). *Surf. Sci.* **1987,** *181*, L147-L155.

67. Okuyama, H.; Siga, W.; Takagi, N.; Nishijima, M.; Aruga, T., Path and Mechanism of Hydrogen Absorption at Pd(100). *Surf. Sci.* **1998,** *401*, 344-354.

68. Sault, A. G.; Madix, R. J.; Campbell, C. T., Adsorption of Oxygen and Hydrogen on Au(110)-(1 × 2). *Surf. Sci.* **1986,** *169*, 347-356.

69. Pan, M.; Flaherty, D. W.; Mullins, C. B., Low-Temperature Hydrogenation of Acetaldehyde to Ethanol on H-Precovered Au(111). *J. Phys. Chem. Lett.* **2011,** *2*, 1363-1367.

70. Hammer, B.; Norskov, J. K., Why Gold Is the Noblest of All the Metals. *Nature* **1995,** *376*, 238-240.

71. Pan, M.; Brush, A. J.; Dong, G. B.; Mullins, C. B., Tunable Ether Production via Coupling of Aldehydes or Aldehyde/Alcohol over Hydrogen-Modified Gold Catalysts at Low Temperatures. *J. Phys. Chem. Lett.* **2012,** *3*, 2512-2516.

72. Pan, M.; Ham, H. C.; Yu, W.-Y.; Hwang, G. S.; Mullins, C. B., Highly Selective, Facile NO_2 Reduction to NO at Cryogenic Temperatures on Hydrogen Precovered Gold. *J. Am. Chem. Soc.* **2013,** *135*, 436-442.

73. Piccolo, L.; Piednoir, A.; Bertolini, J. C., Absorption and Oxidation of Hydrogen at Pd and Pd−Au (111) Surfaces. *Surf. Sci.* **2006,** *600*, 4211-4215.

74. Boscoboinik, J. A.; Calaza, F. C.; Garvey, M. T.; Tysoe, W. T., Identification of Adsorption Ensembles on Bimetallic Alloys. *J. Phys. Chem. C* **2010,** *114*, 1875-1880.

75. Tierney, H. L.; Baber, A. E.; Kitchin, J. R.; Sykes, E. C. H., Hydrogen Dissociation and Spillover on Individual Isolated Palladium Atoms. *Phys. Rev. Lett.* **2009,** *103*, 246102.

76. Baber, A. E.; Tierney, H. L.; Lawton, T. J.; Sykes, E. C. H., An Atomic-Scale View of Palladium Alloys and Their Ability to Dissociate Molecular Hydrogen. *ChemCatChem* **2011,** *3*, 607-614.

77. Ogura, S.; Okada, M.; Fukutani, K., Near-Surface Accumulation of Hydrogen and CO Blocking Effects on A Pd−Au Alloy. *J. Phys. Chem. C* **2013,** *117*, 9366-9371.

78. Roudgar, A.; Gross, A., Local Reactivity of Metal Overlayers: Density Functional Theory Calculations of Pd on Au. *Phys. Rev. B* **2003,** *67*, 033409.

79. Roudgar, A.; Gross, A., Local Reactivity of Thin Pd Overlayers on Au Single Crystals. *J. Electroanal. Chem.* **2003,** *548*, 121-130.

80. Roudgar, A.; Gross, A., Local Reactivity of Supported Metal Clusters: Pdn on Au(111). *Surf. Sci.* **2004,** *559*, L180-L186.

81. Venkatachalam, S.; Jacob, T., Hydrogen Adsorption on Pd-Containing Au(111) Bimetallic Surfaces. *Phys. Chem. Chem. Phys.* **2009,** *11*, 3263-3270.

82. Santana, J. A.; Rosch, N., Hydrogen Adsorption on and Spillover from Au- and Cu-Supported Pt_3 and Pd_3 Clusters: A Density Functional Study. *Phys. Chem. Chem. Phys.* **2012,** *14*, 16062–16069.

83. Mei, D. H.; Hansen, E. W.; Neurock, M., Ethylene Hydrogenation over Bimetallic Pd/Au(111) Surfaces: Application of Quantum Chemical Results and Dynamic Monte Carlo Simulation. *J. Phys. Chem. B* **2003,** *107*, 798-810.

84. Flaherty, D. W.; Hahn, N. T.; Ferrer, D.; Engstrom, T. R.; Tanaka, P. L.; Mullins, C. B., Growth and Characterization of High Surface Area Titanium Carbide. *J. Phys. Chem. C* **2009,** *113*, 12742-12752.

85. Flaherty, D. W.; Berglund, S. P.; Mullins, C. B., Selective Decomposition of Formic Acid on Molybdenum Carbide: A New Reaction Pathway. *J. Catal.* **2010,** *269*, 33-43.

86. Flaherty, D. W.; Yu, W.-Y.; Pozun, Z. D.; Henkelman, G.; Mullins, C. B., Mechanism for the Water-Gas Shift Reaction on Monofunctional Platinum and Cause of Catalyst Deactivation. *J. Catal.* **2011,** *282*, 278-288.

87. King, D. A.; Wells, M. G., Reaction Mechanism in Chemisorption Kinetics - Nitrogen on {100} Plane of Tungsten. *Proc. R. Soc. London, Ser. A* **1974,** *339*, 245-269.

88. Koel, B. E.; Sellidj, A.; Paffett, M. T., Ultrathin Films of Pd on Au(111) - Evidence for Surface Alloy Formation. *Phys. Rev. B* **1992,** *46*, 7846-7856.

89. Yi, C. W.; Luo, K.; Wei, T.; Goodman, D. W., The Composition and Structure of Pd−Au Surfaces. *J. Phys. Chem. B* **2005,** *109*, 18535-18540.

90. Trenary, M., Reflection Absorption Infrared Spectroscopy and the Structure of Molecular Adsorbates on Metal Surfaces. *Annu. Rev. Phys. Chem.* **2000,** *51*, 381-403.

91. Rodriguez, J. A.; Goodman, D. W., The Nature of the Metal-Metal Bond in Bimetallic Surfaces. *Science* **1992,** *257*, 897-903.

92. Meier, D. C.; Bukhtiyarov, V.; Goodman, D. W., CO Adsorption on Au(110)-(1 x 2): An IRAS Investigation. *J. Phys. Chem. B* **2003,** *107*, 12668-12671.

93. Wei, T.; Wang, J.; Goodman, D. W., Characterization and Chemical Properties of Pd−Au Alloy Surfaces. *J. Phys. Chem. C* **2007,** *111*, 8781-8788.

94. Sellidj, A.; Koel, B. E., Electronic and CO Chemisorption Properties of Ultrathin Pd Films Vapor-Deposited on Au(111). *Phys. Rev. B* **1994,** *49*, 8367-8376.

95. Ozensoy, E.; Goodman, D. W., Vibrational Spectroscopic Studies on CO Adsorption, NO Adsorption CO + NO Reaction on Pd Model Catalysts. *Phys. Chem. Chem. Phys*. **2004,** *6*, 3765-3778.

96. Maroun, F.; Ozanam, F.; Magnussen, O. M.; Behm, R. J., The Role of Atomic Ensembles in the Reactivity of Bimetallic Electrocatalysts. *Science* **2001,** *293*, 1811-1814.

97. Kyriakou, G.; Boucher, M. B.; Jewell, A. D.; Lewis, E. A.; Lawton, T. J.; Baber, A. E.; Tierney, H. L.; Flytzani-Stephanopoulos, M.; Sykes, E. C. H., Isolated Metal Atom Geometries as A Strategy for Selective Heterogeneous Hydrogenations. *Science* **2012,** *335*, 1209-1212.

98. Engel, T.; Kuipers, H., A Molecular-Beam Investigation of the Scattering, Adsorption and Absorption of H_2 and D_2 from/on/in Pd(111). *Surf. Sci.* **1979,** *90*, 162-180.

99. White, J. M., Surface Interactions in Nonreactive Coadsorption - H_2 and CO on Transition-Metal Surfaces. *J. Phys. Chem.* **1983,** *87*, 915-924.

100. Guo, X. C.; King, D. A., Coadsorption of Carbon Monoxide and Hydrogen on Metal Surfaces. In *Chapter 4, The Chemical Physics of Solid Surfaces*, Elsevier: 1993; Vol. 6, pp 113-155.

101. Ksar, F.; Ramos, L.; Keita, B.; Nadjo, L.; Beaunier, P.; Remita, H., Bimetallic Palladium-Gold Nanostructures: Application in Ethanol Oxidation. *Chem. Mater.* **2009,** *21*, 3677-3683.

102. Kiskinova, M. P.; Bliznakov, G. M., Adsorption and Coadsorption of Carbon Monoxide and Hydrogen on Pd(111). *Surf. Sci.* **1982,** *123*, 61-76.

103. Kok, G. A.; Noordermeer, A.; Nieuwenhuys, B. E., Decomposition of Methanol and the Interaction of Coadsorbed Hydrogen and Carbon Monoxide on A Pd(111) Surface. *Surf. Sci.* **1983,** *135*, 65-80.

104. Ratajczykowa, I., The Influence of CO on Hydrogen Sorption by Pd(111) Single Crystals. *Surf. Sci.* **1986,** *172*, 691-714.

105. Morkel, M.; Rupprechter, G.; Freund, H. J., Ultrahigh Vacuum and High-Pressure Coadsorption of CO and H_2 on Pd(111): A Combined SFG, TDS, and LEED Study. *J. Chem. Phys.* **2003,** *119*, 10853-10866.

106. Rupprechter, G.; Morkel, M.; Freund, H. J.; Hirschl, R., Sum Frequency Generation and Density Functional Studies of CO-H Interaction and Hydrogen Bulk Dissolution on Pd(111). *Surf. Sci.* **2004,** *554*, 43-59.

107. Rose, M. K.; Mitsui, T.; Dunphy, J.; Borg, A.; Ogletree, D. F.; Salmeron, M.; Sautet, P., Ordered Structures of CO on Pd(111) Studied by STM. *Surf. Sci.* **2002,** *512*, 48-60.

108. Cerda, J. I.; Santos, B.; Herranz, T.; Puerta, J. M.; de la Figuera, J.; McCarty, K. F., CO-Assisted Subsurface Hydrogen Trapping in Pd(111) Films. *J. Phys. Chem. Lett.* **2012,** *3*, 87-91.

109. Nyberg, C.; Westerlund, L.; Jonsson, L.; Andersson, S., Coadsorption of Hydrogen and Carbon Monoxide on Ni(100) and Pd(100) - Hydrogen Recombination, Dissolution and Desorption. *J. Electron Spectrosc. Relat. Phenom.* **1990,** *54*, 639-648.

110. Nyberg, C.; Westerlund, L., H and CO on Pd(100) - Coadsorption Induced Dissolution of Hydrogen. *Surf. Sci.* **1991,** *256*, 9-18.

111. Nyberg, C.; Westerlund, L., Adsorption of CO on the Pd(100)p(1x1)H Surface at Low-Temperatures - Altered CO Coordination. *Chem. Phys. Lett.* **1991,** *185*, 445-448.

112. Conrad, H.; Ertl, G.; Latta, E. E., Coadsorption of Hydrogen and Carbon Monoxide on A Pd(110) Surface. *Surf. Sci.* **1974,** *35*, 363-368.

113. Noordermeer, A.; Kok, G. A.; Nieuwenhuys, B. E., A Comparative Study of the Behavior of the PdAg(111) and Pd(111) Surfaces towards the Interaction with Hydrogen and Carbon Monoxide. *Surf. Sci.* **1986,** *165*, 375-392.

114. Noordermeer, A.; Kok, G. A.; Nieuwenhuys, B. E., Comparison between the Adsorption Properties of Pd(111) and PdCu(111) Surfaces for Carbon Monoxide and Hydrogen. *Surf. Sci* **1986,** *172*, 349-362.

115. Marcinkowski, M. D. J., April D.; Stamatakis, Michail; Boucher, Matthew B.; Lewis, Emily A.; Murphy, Colin J.; Kyriakou, Georgios; Sykes, E. Charles H., Controlling A Spillover Pathway with the Molecular Cork Effect. *Nat. Mater* **2013,** *12*, 523-528.

116. Wheeler, M. C.; Seets, D. C.; Mullins, C. B., Kinetics and Dynamics of the Initial Dissociative Chemisorption of Oxygen on Ru(001). *J. Chem. Phys.* **1996,** *105*, 1572-1583.

117. Davis, J. E.; Karseboom, S. G.; Nolan, P. D.; Mullins, C. B., Kinetics and Dynamics of the Initial Adsorption of Nitric Oxide on Ir(111). *J. Chem. Phys.* **1996,** *105*, 8362-8375.

118. Li, Z.; Gao, F.; Wang, Y.; Calaza, F.; Burkholder, L.; Tysoe, W. T., Formation and Characterization of Au/Pd Surface Alloys on Pd(111). *Surf. Sci.* **2007,** *601*, 1898-1908.

119. Guo, X. C.; Yates, J. T., Dependence of Effective Desorption Kinetic Parameters on Surface Coverage and Adsorption Temperature - CO on Pd(111). *J. Chem. Phys.* **1989,** *90*, 6761-6766.

120. Enthaler, S., Carbon Dioxide - The Hydrogen-Storage Material of the Future? *ChemSusChem* **2008,** *1*, 801-804.

121. Joo, F., Breakthroughs in Hydrogen Storage - Formic Acid as A Sustainable Storage Material for Hydrogen. *ChemSusChem* **2008,** *1*, 805-808.

122. Enthaler, S.; von Langermann, J.; Schmidt, T., Carbon Dioxide and Formic Acid - the Couple for Environmental-Friendly Hydrogen Storage? *Energy Environ. Sci.* **2010,** *3*, 1207-1217.

123. Loges, B.; Boddien, A.; Gartner, F.; Junge, H.; Beller, M., Catalytic Generation of Hydrogen from Formic Acid and Its Derivatives: Useful Hydrogen Storage Materials. *Top. Catal.* **2010,** *53*, 902-914.

124. Johnson, T. C.; Morris, D. J.; Wills, M., Hydrogen Generation from Formic Acid and Alcohols Using Homogeneous Catalysts. *Chem. Soc. Rev.* **2010,** *39*, 81-88.

125. Boddien, A.; Loges, B.; Gartner, F.; Torborg, C.; Fumino, K.; Junge, H.; Ludwig, R.; Beller, M., Iron-Catalyzed Hydrogen Production from Formic Acid. *J. Am. Chem. Soc.* **2010,** *132*, 8924-8934.

126. Boddien, A.; Gartner, F.; Jackstell, R.; Junge, H.; Spannenberg, A.; Baumann, W.; Ludwig, R.; Beller, M., ortho-Metalation of Iron(0) Tribenzylphosphine Complexes: Homogeneous Catalysts for the Generation of Hydrogen from Formic Acid. *Angew. Chem.-Int. Edit.* **2010,** *49*, 8993-8996.

127. Boddien, A.; Mellmann, D.; Gartner, F.; Jackstell, R.; Junge, H.; Dyson, P. J.; Laurenczy, G.; Ludwig, R.; Beller, M., Efficient Dehydrogenation of Formic Acid Using An Iron Catalyst. *Science* **2011,** *333*, 1733-1736.

128. Hull, J. F.; Himeda, Y.; Wang, W. H.; Hashiguchi, B.; Periana, R.; Szalda, D. J.; Muckerman, J. T.; Fujita, E., Reversible Hydrogen Storage Using CO_2 and A Proton-Switchable Iridium Catalyst in Aqueous Media under Mild Temperatures and Pressures. *Nat. Chem.* **2012,** *4*, 383-388.

129. Boddien, A.; Junge, H., Catalysis: Acidic Ideas for Hydrogen Storage. *Nat. Nanotechnol.* **2011,** *6*, 265-266.

130. Tedsree, K.; Li, T.; Jones, S.; Chan, C. W. A.; Yu, K. M. K.; Bagot, P. A. J.; Marquis, E. A.; Smith, G. D. W.; Tsang, S. C. E., Hydrogen Production from Formic Acid Decomposition at Room Temperature Using A Ag-Pd Core-Shell Nanocatalyst. *Nat. Nanotechnol.* **2011,** *6*, 302-307.

131. Zhou, X. C.; Huang, Y. J.; Liu, C. P.; Liao, J. H.; Lu, T. H.; Xing, W., Available Hydrogen from Formic Acid Decomposed by Rare Earth Elements Promoted Pd−Au/C Catalysts at Low Temperature. *ChemSusChem* **2010,** *3*, 1379-1382.

132. Yadav, M.; Singh, A. K.; Tsumori, N.; Xu, Q., Palladium Silica Nanosphere-Catalyzed Decomposition of Formic Acid for Chemical Hydrogen Storage. *J. Mater. Chem.* **2012,** *22*, 19146-19150.

133. Bulushev, D. A.; Beloshapkin, S.; Ross, J. R. H., Hydrogen from Formic Acid Decomposition over Pd and Au Catalysts. *Catal. Today* **2010,** *154*, 7-12.

134. Bulushev, D. A.; Jia, L. J.; Beloshapkin, S.; Ross, J. R. H., Improved Hydrogen Production from Formic Acid on A Pd/C Catalyst Doped by Potassium. *Chem. Commun.* **2012,** *48*, 4184-4186.

135. Bulushev, D. A.; Beloshapkin, S.; Plyusnin, P. E.; Shubin, Y. V.; Bukhtiyarov, V. I.; Korenev, S. V.; Ross, J. R. H., Vapour Phase Formic Acid Decomposition over PdAu/gamma-Al_2O_3 Catalysts: Effect of Composition of Metallic Particles. *J. Catal.* **2013,** *299*, 171-180.

136. Zhao, Y.; Deng, L.; Tang, S. Y.; Lai, D. M.; Liao, B.; Fu, Y.; Guo, Q. X., Selective Decomposition of Formic Acid over Immobilized Catalysts. *Energy Fuels* **2011,** *25*, 3693-3697.

137. O'Neill, B. J.; Gürbüz, E. I.; Dumesic, J. A., Reaction Kinetics Studies of the Conversions of Formic Acid and Butyl Formate over Carbon-Supported Palladium in the Liquid Phase. *J. Catal.* **2012,** *290*, 193-201.

138. Wang, Z. L.; Yan, J. M.; Wang, H. L.; Ping, Y.; Jiang, Q., Au@Pd Core-Shell Nanoclusters Growing on Nitrogen-Doped Mildly Reduced Graphene Oxide with Enhanced Catalytic Performance for Hydrogen Generation from Formic Acid. *J. Mater. Chem. A* **2013,** *1*, 12721-12725.

139. Yuan, D. W.; Liu, Z. R., Atomic Ensemble Effects on Formic Acid Oxidation on PdAu Electrode Studied by First-Principles Calculations. *J. Power Sources* **2013,** *224*, 241-249.

140. Christmann, K., Introduction to Surface Physical Chemistry In *Topics in Physical Chemistry*, Springer: New York: 1991; pp 152-166.

141. Masel, R. I., Principles of Adsorption and Reaction on Solid Surfaces. In *Wiley Series in Chemical Engineering*, John Wiley & Sons, Inc.: New York: 1996; pp 507-515.

142. Attard, G.; Barnes, C., Surfaces. In *Oxford Chemistry Primers 59*, Oxford University Press: Oxford: 1998; pp 71-75.

143. Kleyn, A. W., Molecular Beams and Chemical Dynamics at Surfaces. *Chem. Soc. Rev.* **2003,** *32*, 87-95.

144. Li, Z.; Gao, F.; Furlong, O.; Tysoe, W. T., Adsorption of Carbon Monoxide Au/Pd(100) Alloys in Ultrahigh Vacuum: Identification of Adsorption Sites. *Surf. Sci.* **2010,** *604*, 136-143.

145. Mullins, C. B.; Weinberg, W. H., Trapping of Molecular Ethane on the Ir(110)-(1x2) Surface. *J. Chem. Phys.* **1990,** *92*, 3986-3988.

146. Rettner, C. T.; Mullins, C. B.; Bethune, D. S.; Auerbach, D. J.; Schweizer, E. K.; Weinberg, W. H., Molecular Beam Studies of Trapping Dynamics. *J. Vac. Sci. Technol. A* **1990,** *8*, 2699-2704.

147. Mullins, C. B.; Rettner, C. T.; Auerbach, D. J.; Weinberg, W. H., Variation of the Trapping Probability of Ar on Pt(111) with Kinetic Energy and Angle of Incidence: The Changing Role of Parallel Momentum with Surface Temperature. *Chem. Phys. Lett.* **1989,** *163*, 111-115.

148. Sitz, G. O.; Mullins, C. B., Molecular Dynamics Simulations of the Influence of Surface Temperature on the Trapping of Methane on Iridium Single-Crystalline Surfaces. *J. Phys. Chem. B* **2002,** *106*, 8349-8353.

149. Liu, P.; Norskov, J. K., Ligand and Ensemble Effects in Adsorption on Alloy Surfaces. *Phys. Chem. Chem. Phys.* **2001,** *3*, 3814-3818.

150. Ham, H. C.; Hwang, G. S.; Han, J.; Nam, S. W.; Lim, T. H., Geometric Parameter Effects on Ensemble Contributions to Catalysis: H_2O_2 Formation from H_2 and O_2 on AuPd Alloys. A First Principles Study. *J. Phys. Chem. C* **2010,** *114*, 14922-14928.

151. Madix, R. J., Reaction Kinetics and Mechanism on Metal Single Crystal Surfaces. *Adv. Catal.* **1980,** *29*, 1-53.

152. Barteau, M. A., Linear Free Energy Relationships for C_1-Oxygenate Decomposition on Transition Metal Surfaces. *Catal. Lett.* **1991,** *8*, 175-184.

153. Columbia, M. R.; Thiel, P. A., The Interaction of Formic Acid with Transition Metal Surfaces, Studied in Ultrahigh Vacuum. *J. Electroanal. Chem.* **1994,** *369*, 1-14.

154. Davis, J. L.; Barteau, M. A., Reactions of Carboxylic Acids on the Pd(111)-(2 x 2)O Surface - Multiple Roles of Surface Oxygen Atoms. *Surf. Sci.* **1991,** *256*, 50-66.

155. Jeroro, E.; Vohs, J. M., Reaction of Formic Acid on Zn-modified Pd(111). *Catal. Lett.* **2009,** *130*, 271-277.

156. Aas, N.; Li, Y. X.; Bowker, M., The Adsorption and Decomposition of Formic Acid on Clean and Oxygen-Dosed Pd(110). *J. Phys.-Condes. Matter* **1991,** *3*, S281-S286.

157. Sander, D.; Erley, W., The Decomposition of Formic Acid on Pd(100). *J. Vac. Sci. Technol. A* **1990,** *8*, 3357-3360.

158. Jorgensen, S. W.; Madix, R. J., Active Oxygen on Group VIII Metals - Activation of Formic Acid and Formaldehyde on Pd(100). *J. Am. Chem. Soc.* **1988,** *110*, 397-400.

159. Solymosi, F.; Kovacs, I., Adsorption and Reaction of HCOOH on K-Promoted Pd(100) Surfaces. *Surf. Sci.* **1991,** *259*, 95-108.

160. Senanayake, S. D.; Stacchiola, D.; Liu, P.; Mullins, C. B.; Hrbek, J.; Rodriguez, J. A., Interaction of CO with OH on Au(111): HCOO, CO3, and HOCO as Key Intermediates in the Water-Gas Shift Reaction. *J. Phys. Chem. C* **2009,** *113*, 19536-19544.

161. Farkas, A. P.; Solymosi, F., Activation and Reactions of CO_2 on a K-Promoted Au(111) Surface. *J. Phys. Chem. C* **2009,** *113*, 19930-19936.

162. Wambach, J.; Odorfer, G.; Freund, H. J.; Kuhlenbeck, H.; Neumann, M., Influence of Alkali Co-Adsorption on the Adsorption and Reaction of CO2 on Pd(111). *Surf. Sci.* **1989,** *209*, 159-172.

163. Larsen, R.; Ha, S.; Zakzeski, J.; Masel, R. I., Unusually Active Palladium-Based Catalysts for the Electrooxidation of Formic Acid. *J. Power Sources* **2006,** *157*, 78-84.

164. Conrad, H.; Ertl, G.; Kuppers, J.; Latta, E. E., Interaction of NO and O_2 with Pd(111) surfaces. II. **1977,** *65*, 245-260.

165. Matsushima, T., Dissociation of Oxygen Admolecules on Rh(111), Pt(111) and Pd(111) Surfaces at Low Temperatures. *Surf. Sci.* **1985,** *157*, 297-318.

166. Imbihl, R.; Demuth, J. E., Adsorption of Oxygen on A Pd(111) Surface Studied by High Resolution Electron Energy Loss Spectroscopy (EELS). *Surf. Sci.* **1986,** *173*, 395-410.

167. Guo, X. C.; Hoffman, A.; Yates, J. T., Adsorption Kinetics and Isotopic Equilibration of Oxygen Adsorbed on the Pd(111) Surface. *J. Chem. Phys.* **1989,** *90*, 5787-5792.

168. Kolasinski, K. W.; Cemic, F.; Hasselbrink, E., O_2/Pd(111) - Clarification of the Correspondence between Thermal-Desorption Features and Chemisorption States. *Chem. Phys. Lett.* **1994,** *219*, 113-117.

169. Rose, M. K.; Borg, A.; Dunphy, J. C.; Mitsui, T.; Ogletree, D. F.; Salmeron, M., Chemisorption and Dissociation of O_2 on Pd(111) Studied by STM. *Surf. Sci.* **2003,** *547*, 162-170.

170. Nolan, P. D.; Lutz, B. R.; Tanaka, P. L.; Mullins, C. B., Direct Verification of A High-Translational-Energy Molecular Precursor to Oxygen Dissociation on Pd(111). *Surf. Sci.* **1998,** *419*, L107-L113.

171. Min, B. K.; Friend, C. M., Heterogeneous Gold-Based Catalysis for Green Chemistry: Low-Temperature CO Oxidation and Propene Oxidation. *Chem. Rev.* **2007,** *107*, 2709-2724.

172. Zhang, J.; Jin, H. M.; Sullivan, M. B.; Chiang, F.; Lim, H.; Wu, P., Study of Pd−Au Bimetallic Catalysts for CO Oxidation Reaction by DFT Calculations. *Phys. Chem. Chem. Phys.* **2009,** *11*, 1441-1446.

173. Ham, H. C.; Hwang, G. S.; Han, J.; Nam, S. W.; Lim, T. H., On the Role of Pd Ensembles in Selective H_2O_2 Formation on PdAu Alloys. *J.Phys. Chem. C* **2009,** *113*, 12943-12945.

174. Ham, H. C.; Stephens, J. A.; Hwang, G. S.; Han, J.; Nam, S. W.; Lim, T. H., Pd Ensemble Effects on Oxygen Hydrogenation in AuPd Alloys: A Combined Density Functional Theory and Monte Carlo Study. *Catal. Today* **2011,** *165*, 138-144.

175. Ham, H. C.; Stephens, J. A.; Hwang, G. S.; Han, J.; Nam, S. W.; Lim, T. H., Role of Small Pd Ensembles in Boosting CO Oxidation in AuPd Alloys. *J. Phys. Chem. Lett.* **2012,** *3*, 566-570.

176. Garcia-Mota, M.; Lopez, N., The Role of Long-Lived Oxygen Precursors on AuM Alloys (M = Ni, Pd, Pt) in CO Oxidation. *Phys. Chem. Chem. Phys.* **2011,** *13*, 5790-5797.

177. Wang, T. Y.; Li, B. H.; Yang, J. H.; Chen, H.; Chen, L. A., First Principles Study of Oxygen Adsorption and Dissociation on the Pd/Au Surface Alloys. *Phys. Chem. Chem. Phys.* **2011,** *13*, 7081-7089.

178. Yuan, D. W.; Liu, Z. R.; Chen, J. H., Catalytic Activity of Pd Ensembles over Au(111) Surface for CO Oxidation: A First-Principles Study. *J. Chem. Phys.* **2011,** *134*, 054704.

179. Yuan, D. W.; Liu, Z. R.; Xu, S., First-Principles Investigations of O_2 Dissociation on Low-Coordinated Pd Ensembles over Stepped Au Surfaces. *Phys. Lett. A* **2012,** *376*, 3432-3438.

180. Yuan, D. W.; Liu, Z. R., Catalytic Activity of Pd Ensembles Incorporated into Au Nanocluster for CO oxidation: A First-Principles Study. *Phys. Lett. A* **2011,** *375*, 2405-2410.

181. Kim, H. Y.; Henkelman, G., CO Adsorption-Driven Surface Segregation of Pd on Au/Pd Bimetallic Surfaces: Role of Defects and Effect on CO Oxidation. *ACS Catal.* **2013,** *3*, 2541-2546.

182. Cheng, D. J.; Xu, H. X.; Fortunelli, A., Tuning the Catalytic Activity of Au-Pd Nanoalloys in CO Oxidation via Composition. *J. Catal.* **2014,** *314*, 47-55.

183. Davis, J. E.; Nolan, P. D.; Karseboom, S. G.; Mullins, C. B., Kinetics and Dynamics of the Dissociative Chemisorption of Oxygen on Ir(111). *J. Chem. Phys.* **1997,** *107*, 943-952.

184. Kresse, G.; Hafner, J., Ab Initio Molecular Dynamics for Liquid Metals. *Phys. Rev. B* **1993,** *47*, 558-561.

185. Kresse, G.; Hafner, J., Ab Initio Molecular-Dynamics Simulation of the Liquid-Metal–Amorphous-Semiconductor Transition in Germanium. *Phys. Rev. B* **1994,** *49*, 14251-14269.

186. Kresse, G.; Furthmuller, J., Efficient Iterative Schemes for Ab Initio Total-Energy Calculations Using A Plane-Wave Basis Set. *Phys. Rev. B* **1996,** *54*, 11169-11186.

187. Kresse, G.; Furthmuller, J., Efficiency of Ab-Initio Total Energy Calculations for Metals and Semiconductors Using A Plane-Wave Basis Set. *Comput. Mater. Sci.* **1996,** *6*, 15-50.

188. Blochl, P. E., Projector Augmented-Wave Method. *Phys. Rev. B* **1994,** *50*, 17953-17979.

189. Hohenberg, P.; Kohn, W., Inhomogeneous Electron Gas. *Phys. Rev. B* **1964,** *136*, B864-B871.

190. Kohn, W.; Sham, L. J., Self-Consistent Equations Including Exchange and Correlation Effects. *Phys. Rev.* **1965,** *140*, 1133-1138.

191. Perdew, J. P.; Burke, K.; Ernzerhof, M., Generalized Gradient Approximation Made Simple. *Phys. Rev. Lett.* **1996,** *77*, 3865-3868.

192. Henkelman, G.; Uberuaga, B. P.; Jonsson, H., A Climbing Image Nudged Elastic Band Method for Finding Saddle Points and Minimum Energy Paths. *J. Chem. Phys.* **2000,** *113*, 9901-9904.

193. Henkelman, G.; Jonsson, H., Improved Tangent Estimate in the Nudged Elastic Band Method for Finding Minimum Energy Paths and Saddle Points. *J. Chem. Phys.* **2000,** *113*, 9978-9985.

194. Monkhorst, H. J.; Pack, J. D., Special Points for Brillouin-Zone Integrations. *Phys. Rev. B* **1976,** *13*, 5188-5192.

195. Campbell, C. T.; Arnadottir, L.; Sellers, J. R. V., Kinetic Prefactors of Reactions on Solid Surfaces. *Z. Phys. Chem.* **2013,** *227*, 1435-1454.

196. Kolasinski, K. W.; Cemic, F.; Demeijere, A.; Hasselbrink, E., Interactions in Co-Adsorbed CO+O_2/Pd(111) Layers. *Surf. Sci.* **1995,** *334*, 19-28.

197. Engel, T.; Ertl, G., Surface Residence Times and Reaction Mechanism in Catalytic Oxidation of CO on Pd(111) *Chem. Phys. Lett.* **1978,** *54*, 95-98.

198. Conrad, H.; Ertl, G.; Kuppers, J., Interactions between Oxygen and Carbon Monoxide on A Pd(111) Surface. *Surf. Sci.* **1978,** *76*, 323-342.

199. Engel, T.; Ertl, G., A Molecular Beam Investigation of Catalytic Oxidation of CO on Pd(111). *J. Chem. Phys.* **1978,** *69*, 1267-1281.

200. Cybula, A.; Priebe, J. B.; Pohl, M. M.; Sobczak, J. W.; Schneider, M.; Zielhiska-Jurek, A.; Bruckner, A.; Zaleska, A., The Effect of Calcination Temperature on Structure and Photocatalytic Properties of Au/Pd Nanoparticles Supported on TiO2. *Appl. Catal. B-Environ.* **2014,** *152*, 202-211.

201. Baddeley, C. J.; Barnes, C. J.; Wander, A.; Ormerod, R. M.; King, D. A.; Lambert, R. M., Surface Crystallography of Three Catalytically Important Structures in the Au{111}-Pd System. *Surf. Sci.* **1994,** *314*, 1-12.

202. Piccolo, L.; Piednoir, A.; Bertolini, J. C., Pd−Au Single-Crystal Surfaces: Segregation Properties and Catalytic Activity in the Selective Hydrogenation of 1,3-Butadiene. *Surf. Sci.* **2005,** *592*, 169-181.

203. Li, Z. J.; Furlong, O.; Calaza, F.; Burkholder, L.; Poon, H. C.; Saldin, D.; Tysoe, W. T., Surface Segregation of Gold for Au/Pd(111) Alloys Measured by Low-Energy Electron Diffraction and Low-Energy Ion Scattering. *Surf. Sci.* **2008,** *602*, 1084-1091.

204. Baber, A. E.; Tierney, H. L.; Sykes, E. C. H., Atomic-Scale Geometry and Electronic Structure of Catalytically Important Pd/Au Alloys. *ACS Nano* **2010,** *4*, 1637-1645.

205. Guesmi, H.; Louis, C.; Delannoy, L., Chemisorbed Atomic Oxygen Inducing Pd Segregation in PdAu(111) Alloy: Energetic and Electronic DFT Analysis. *Chem. Phys. Lett.* **2011,** *503*, 97-100.

206. Dhouib, A.; Guesmi, H., DFT Study of the M Segregation on MAu alloys (M = Ni, Pd, Pt) in Presence of Adsorbed Oxygen O and O_2. *Chem. Phys. Lett.* **2012,** *521*, 98-103.

207. Wales, D. J.; Doye, J. P. K., Global Optimization by Basin-Hopping and the Lowest Energy Structures of Lennard-Jones Clusters Containing Up to 110 Atoms. *J. Phys. Chem. A* **1997,** *101*, 5111-5116.

208. Ertl, G.; Kuppers, J., *Low Energy Electrons and Surface Chemistry*. VCH: 1985, ch. 1, pp. 6-8.

209. Wilson, E. L.; Brown, W. A., Low Pressure RAIRS Studies of Model Catalytic Systems. *J. Phys. Chem. C* **2010,** *114*, 6879-6893.

210. Luo, K.; Wei, T.; Yi, C. W.; Axnanda, S.; Goodman, A. W., Preparation and Characterization of Silica Supported Au-Pd model Catalysts. *J. Phys. Chem. B* **2005,** *109*, 23517-23522.

211. Hinojosa, J. A.; Kan, H. H.; Weaver, J. F., Molecular Chemisorption of O_2 on A PdO(101) Thin Film on Pd(111). *J. Phys. Chem. C* **2008,** *112*, 8324-8331.

212. Wang, D.; Villa, A.; Porta, F.; Prati, L.; Su, D. S., Bimetallic Gold/Palladium Catalysts: Correlation between Nanostructure and Synergistic Effects. *J. Phys. Chem. C* **2008,** *112*, 8617-8622.

213. Dimitratos, N.; Lopez-Sanchez, J. A.; Morgan, D.; Carley, A. F.; Tiruvalam, R.; Kiely, C. J.; Bethell, D.; Hutchings, G. J., Solvent-Free Oxidation of Benzyl Alcohol using Au-Pd Catalysts Prepared by Sol Immobilisation. *Phys. Chem. Chem. Phys.* **2009,** *11*, 5142-5153.

214. Nowicka, E.; Hofmann, J. P.; Parker, S. F.; Sankar, M.; Lari, G. M.; Kondrat, S. A.; Knight, D. W.; Bethell, D.; Weckhuysen, B. M.; Hutchings, G. J., In Situ Spectroscopic Investigation of Oxidative Dehydrogenation and Disproportionation of Benzyl Alcohol. *Phys. Chem. Chem. Phys.* **2013,** *15*, 12147-12155.

215. Pritchard, J.; Piccinini, M.; Tiruvalam, R.; He, Q.; Dimitratos, N.; Lopez-Sanchez, J. A.; Morgan, D. J.; Carley, A. F.; Edwards, J. K.; Kiely, C. J.; Hutchings, G. J., Effect of Heat Treatment on Au-Pd Catalysts Synthesized by Sol Immobilisation for the Direct Synthesis of Hydrogen Peroxide and Benzyl Alcohol Oxidation. *Catal. Sci. Technol.* **2013,** *3*, 308-317.

216. Chen, L. Y.; Chen, N.; Hou, Y.; Wang, Z. C.; Lv, S. H.; Fujita, T.; Jiang, J. H.; Hirata, A.; Chen, M. W., Geometrically Controlled Nanoporous PdAu Bimetallic Catalysts with Tunable Pd/Au Ratio for Direct Ethanol Fuel Cells. *ACS Catal.* **2013,** *3*, 1220-1230.

217. Calaza, F.; Gao, F.; Li, Z.; Tysoe, W. T., The Adsorption of Ethylene on Au/Pd(111) Alloy Surfaces. *Surf. Sci.* **2007,** *601*, 714-722.

218. Li, Z.; Calaza, F.; Gao, F.; Tysoe, W. T., The Adsorption of Acetic Acid on Au/Pd(111) Alloy Surfaces. *Surf. Sci.* **2007,** *601*, 1351-1357.

219. Calaza, F.; Li, Z.; Gao, F.; Boscoboinik, J.; Tysoe, W. T., The Adsorption and Reaction of Vinyl Acetate on Au/Pd(111) Alloy Surfaces. *Surf. Sci.* **2008,** *602*, 3523-3530.

220. Kim, T. S.; Stiehl, J. D.; Reeves, C. T.; Meyer, R. J.; Mullins, C. B., Cryogenic CO oxidation on TiO2-Supported Gold Nanoclusters Precovered with Atomic Oxygen. *J. Am. Chem. Soc.* **2003,** *125*, 2018-2019.

221. Stiehl, J. D.; Kim, T. S.; McClure, S. M.; Mullins, C. B., Evidence for Molecularly Chernisorbed Oxygen on TiO_2 Supported Gold Nanoclusters and Au(111). *J. Am. Chem. Soc.* **2004,** *126*, 1606-1607.

222. Stiehl, J. D.; Kim, T. S.; McClure, S. M.; Mullins, C. B., Reaction of CO with Molecularly Chemisorbed Oxygen on TiO_2-Supported Gold Nanoclusters. *J. Am. Chem. Soc.* **2004,** *126*, 13574-13575.

223. Rodriguez, J. A.; Ma, S.; Liu, P.; Hrbek, J.; Evans, J.; Perez, M., Activity of CeO_x and TiO_x Nanoparticles Grown on Au(111) in the Water-Gas Shift Reaction. *Science* **2007,** *318*, 1757-1760.

224. Yan, T.; Redman, D. W.; Yu, W. Y.; Flaherty, D. W.; Rodriguez, J. A.; Mullins, C. B., CO oxidation on inverse Fe_2O_3/Au(111) model catalysts. *J. Catal.* **2012,** *294*, 216-222.

225. Rodriguez, J. A.; Hrbek, J., Inverse Oxide/Metal Catalysts: A Versatile Approach for Activity Tests and Mechanistic Studies. *Surf. Sci.* **2010,** *604*, 241-244.

226. Green, I. X.; Tang, W. J.; Neurock, M.; Yates, J. T., Spectroscopic Observation of Dual Catalytic Sites during Oxidation of CO on a Au/TiO_2 Catalyst. *Science* **2011,** *333*, 736-739.

227. Goodman, D. W., Correlations between Surface Science Models and "Real-World" Catalysts. *J. Phys. Chem.* **1996,** *100*, 13090-13102.

228. Tao, F.; Grass, M. E.; Zhang, Y.; Butcher, D. R.; Renzas, J. R.; Liu, Z.; Chung, J. Y.; Mun, B. S.; Salmeron, M.; Somorjai, G. A., Reaction-Driven Restructuring of Rh-Pd and Pt-Pd Core-Shell Nanoparticles. *Science* **2008,** *322*, 932-934.

Vita

Wen-Yueh Yu was born in Taipei, Taiwan. He received the degrees of Bachelor of Science and Master of Science both in Chemical Engineering from National Taiwan University (NTU). During the years in NTU, he conducted undergraduate and graduate research by studying gold catalysis under the supervision of Prof. Ben-Zu Wan.

During the following years, he worked as a research assistant in Prof. Shu-Hua Chien group in Institute of Chemistry at Academia Sinica in Taiwan. His research centered at the preparation and applications of nanostructured materials and in-situ spectroscopic characterization techniques.

In 2009, he came to the University of Texas at Austin to pursue his Ph.D. in Chemical Engineering under the supervision of Professor C. Buddie Mullins. Currently he is studying the catalytic chemistry on Pd−Au bimetallic model surface with the aim of molecular-level understanding.

Email address: wenyueh@utexas.edu

This dissertation was typed by the author.